NPS-69-84-004

NAVAL POSTGRADUATE SCHOOL

Monterey, California

SURFACE DISTURBANCES DUE TO TRAILING VORTICES

by

T. SARPKAYA

D. O. HENDERSON

March 1984

Approved for public release; distribution unlimited.

Prepared for: Defense Advanced Research Projects Agency
1400 Wilson, Blvd., Arlington, VA 22209

NAVAL POSTGRADUATE SCHOOL
Monterey, California

Commodore R. H. Shumaker
Superintendent

D. A. Schrady
Provost

The work reported herein was supported by the Defense Advanced Research Projects Agency (DARPA).

This report was prepared by:

TURGUT SARPKAYA
Distinguished Professor of
Mechanical Engineering

Reviewed by:

Paul J. Marto, Chairman
Department of Mechanical
Engineering

Released by:

John N. Dyer
Dean of Science and Engineering

Unclassified

SECURITY CLASSIFICATION OF THIS PAGE (When Data Entered)

REPORT DOCUMENTATION PAGE

READ INSTRUCTIONS BEFORE COMPLETING FORM

REPORT NUMBER NPS-69-84-004	2. GOVT ACCESSION NO. AD-A142693
3. RECIPIENT'S CATALOG NUMBER	
4. TITLE (and Subtitle) Surface Disturbances due to Trailing Vortices	5. TYPE OF REPORT & PERIOD COVERED Progress Report 30 Dec. '83 - 30 March '84
	6. PERFORMING ORG. REPORT NUMBER
7. AUTHOR(s) Turgut Sarpkaya (Principal Investigator) Dwight O. Henderson, Jr.	8. CONTRACT OR GRANT NUMBER(s) ARPA Order 3925
9. PERFORMING ORGANIZATION NAME AND ADDRESS Naval Postgraduate School Monterey, California 93943	10. PROGRAM ELEMENT, PROJECT, TASK AREA & WORK UNIT NUMBERS
11. CONTROLLING OFFICE NAME AND ADDRESS Naval Postgraduate School Monterey, California 93943	12. REPORT DATE March 1984
	13. NUMBER OF PAGES 157
14. MONITORING AGENCY NAME & ADDRESS(if different from Controlling Office) Defense Advanced Research Projects Agency DARPA 1400 Wilson Blvd., Arlington, VA 22209 Attn: Dr. Arthur J. Bruckheim	15. SECURITY CLASS. (of this report) Unclassified
	15a. DECLASSIFICATION/DOWNGRADING SCHEDULE

16. DISTRIBUTION STATEMENT (of this Report)

Approved for public release; distribution unlimited.

17. DISTRIBUTION STATEMENT (of the abstract entered in Block 20, if different from Report)

18. SUPPLEMENTARY NOTES

19. KEY WORDS (Continue on reverse side if necessary and identify by block number)

Waves
Surface Disturbances
Trailing Vortices
Interfacial Disturbances

20. ABSTRACT (Continue on reverse side if necessary and identify by block number)

The characteristics of the surface signatures resulting from the interaction of the trailing vortices with the free surface have been investigated both theoretically and experimentally. The vortices were created through the use of three lifting surfaces of different shape and aspect ratio (two Delta wings and a rectangular foil). The surface disturbances have been classified into two groups (striations and scars) and the evolution of each type has been expressed in terms of the

DD FORM 1 JAN 73 1473 EDITION OF 1 NOV 65 IS OBSOLETE

S/N 0102-LF-014-6601

Unclassified

SECURITY CLASSIFICATION OF THIS PAGE (When Data Entered)

governing parameters such as the depth of generation of vortices, mutual induction velocity, and the initial vortex spacing. It has been shown that the surface signatures are a consequence of the strain field resulting from the nonuniform surface-velocity distribution and that they are not simple capillary-gravity waves. A turbulence model has been used to establish reasonable correlation between the theoretical and experimental results.

ABSTRACT

The characteristics of the surface signatures resulting from the interaction of the trailing vortices with the free surface have been investigated both theoretically and experimentally. The vortices were created through the use of three lifting surfaces of different shape and aspect ratio (two Delta wings and a rectangular foil). The surface disturbances have been classified into two groups (striations and scars) and the evolution of each type has been expressed in terms of the governing parameters such as the depth of generation of vortices, mutual induction velocity, and the initial vortex spacing. It has been shown that the surface signatures are a consequence of the strain field resulting from the nonuniform surface-velocity distribution and that they are not simple capillary-gravity waves. A turbulence model has been used to establish reasonable correlation between the theoretical and experimental results.

PREFACE

The work reported herein is part of a basic research on trailing vortices in stratified and unstratified fluids and was performed during the period 30 December 1983 to 30 March 1984. The principal investigator is Dr. Turgut Sarpkaya, Distinguished Professor of Mechanical Engineering at the Naval Postgraduate School. Sponsorship was provided by the Defense Advanced Research Projects Agency (DARPA) under ARPA Order 3925. The contract technical monitor was Dr. Arthur J. Bruckheim, Program Manager, Tactical Technology Office, DARPA.

TABLE OF CONTENTS

LIST OF FIGURES

TABLE OF SYMBOLS AND ABBREVIATIONS

A	Dissipation Parameter
AR	Aspect Ratio of the wing
a_o	ν_t/Γ_o
B	Wing Span
b_o	Initial Vortex Core Spacing
d_o	Initial Depth of the Vortex Pair
g	Gravitational Acceleration
h	Position of the Marker Particle
k	A Parameter
L	Length of the Striation
m	Semi-Major Axis of the Recirculation Cell
N	Brunt-Vaisala Frequency
n	Semi-Minor Axis of the Recirculation Cell
r	Radial Distance
r_e	Effective Core Radius
s	Position of the Scar Front
t	Time
U	Model Velocity
u	x-Component of Velocity
v	y-Component of Velocity
u_m	Maximum Surface Velocity at a Given Time
u_s	Velocity of the Scar Front
u_v	x-Component of the Velocity of the Vortex Core

v_v	y-Component of the Velocity of the Vortex Core
V_o	Initial Mutual Induction Velocity
$w(z)$	Complex Velocity Function
x	Horizontal Component of the Coordinate Axis (Parallel to the Line Joining the Vortex Cores)
y	Vertical Component of the Coordinate Axis
x_m	Horizontal Position of u_m
x_{sf}	Position of the Scar Front
x_v	Horizontal Position of the Vortex
y_v	Vertical Position of the Vortex from the Free Surface
z	Complex Variable
z_v	Complex Position of the Vortex
α	Model Angle of Attack
Γ	Circulation of the Vortex
Γ_o	Initial Circulation of the Vortex
γ	Inclination of the Trailing Vortex Relative to the Free Surface
η	x_v/b_o
Λ	u_s/u_m
λ	$(x_{sf} - x_m)/b_o$
ν	Kinematic Viscosity of Water
ν_t	Eddy Viscosity
ξ	Half-Width of the Surface Velocity Profile
ρ	Density of Water
ρ_o	Reference Density of Water in Stratified Medium
σ	Surface Tension

ACKNOWLEDGEMENTS

The writers wish to acknowledge the generous support of DARPA and the constructive comments and suggestions of Dr. Arthur J. Bruckheim, Program Manager, Tactical Technology Office, DARPA.

A special note of thanks is extended to Mr. Jack McKay for his most skillful work in the construction of the test models.

I. INTRODUCTION

Vortices and vortex wakes have become a major theme of aerodynamics research since the advent of the large aircraft and the understanding of their evolution required an examination of many fundamental problems in fluid mechanics. Much of the progress made during the past two decades was discussed at the Symposium on Aircraft Wake Turbulence and Its Detection [Ref. 1] and at the Aircraft Wake Vortices Conference [Ref. 2]. Comprehensive reviews of the entire subject have been given by Donaldson and Bilanin [Ref. 3], Widnall [Ref. 4] and Hallock and Eberle [Ref. 5].

These studies, as well as numerous others carried out since 1977, have uncovered a number of complex problems which must be resolved in order to achieve a better understanding of the important features of trailing vortices in homogeneous and stratified media. The principal ones are as follows [Ref. 6]:

(i) Roll-up process: The velocity and turbulence distributions at any station behind the wing depend on the wing section, wing-tip shape, Reynolds number, wing incidence, and the distance of the station from the wing [Ref. 7]. The distributions of the initial velocity and turbulence, which influence the roll-up and the decay process, cannot be changed independently. For example, a change in tip shape changes the core size, as well as the velocity and turbulence distributions. High levels of turbulence result in an increased diffusion of vorticity, which in turn increases the core size.

(ii) Probe sensitivity of the vortices: Flow visualization studies suggest that trailing vortices are extremely sensitive to disturbances created by even very small probes or bubbles. This forces one to use non-intrusive means of measurements such as an LDV. Even then, 'vortex wandering' [Ref. 8], which makes the vortices appear larger than normal in time-averaged velocity measurements (for vortices generated by a wing in a wind tunnel), or the unsteady nature of the flow (for vortices generated by a wing in a tow basin) makes the mean velocity profiles in the vortices difficult to determine.

(iii) Large-scale instabilities: The vortices are seldom observed to decay away owing to viscous and turbulent dissipation, but are almost always destroyed by either mutual induction instability (Crow instability [Ref. 9]) and/or vortex breakdown. The Crow instability grows exponentially, and results either in a linking of the vortex pair into a series of crude vortex rings or in a highly disorganized intermingling of the vortices. Vortex breakdown, whose mathematical details have not yet been adequately treated, rearranges the vortex structure and increases the core size, turbulence, and energy dissipation. Thus, it is very difficult to measure accurately the trajectories of the three-dimensional vortices from their creation to their ultimate demise.

(iv) Reynolds number: Even the highest Reynolds numbers, based on wing chord, reached in wind tunnels or towing basins, are an order of magnitude lower than what is possible for an aircraft. Thus, the scale effects are not easy to assess.

(v) Ambient conditions such as turbulence and stratification play major roles in the evolution of vortices. The quantification of these effects offers exceedingly complex difficulties. Finally,

(vi) Ground or free-surface effects: The Vortex pair may move towards a rigid boundary at which the no-slip condition must be satisfied or towards a free surface at which the zero-shear condition must be satisfied. In either case, the vortices come under the influence of their images and the mutual induction instability may occur not only between the two real vortices but also between a real vortex and its image. In general, one would expect mutual induction instability among four vortices (two real and two image vortices).

The phenomenon is further complicated by several additional facts. When the vortices are propelled towards a rigid surface, vorticity of opposite sign is generated on the no-slip boundary and swept towards the vortex pair. The total vorticity diminishes very quickly as vorticity from the two regions diffuses, the wall region serving as a strong sink for the vorticity associated with the original vortex [Ref. 10]. The development of a boundary layer along the rigid wall may give rise to flow separation for sufficiently high Reynolds numbers. With or without such a separation, however, the center of the vortex pair eventually moves away, or 'rebounds', from the wall [10-12].

For the case of a zero-stress boundary, the free surface still acts as a vorticity sink, but this is relatively weak due to the absence of intense oppositely-signed vorticity. Thus, in the absence of other impeding phenomena, one expects a mild interaction between the vortices and the free surface and a small rebound of the vortex center from the free surface. However, the ability of the free surface to deform under the influence of strain fields leads to a strong interaction between the vortices and the free surface.

When the vortex pair approaches the free surface (with or without mutual induction instability and/or vortex breakdown), the vortices (or the crude vortex rings) and their images give rise to distinct surface disturbances (waves of very small length). These waves or the local roughening of the free surface are visible because the particle motions they create as they propagate produce a straining field at the surface which modifies the physical characteristics of the sea surface (reflection, refraction and the scattering of sound, heat and light). In fact, in many photographs of the sea surface taken from aircraft or satellites using passive or active sensors, the differential roughening of the free surface can be seen clearly [Ref. 13]. It is important to note that the roughening of the sea surface is brought about not only by the proximity of vortices or vortex rings but also by internal waves [Ref. 13]. However, the character of the surface signature strongly depends on the manner it is generated and there is no difficulty in distinguishing the surface signature created by the vortices from that created by the internal waves.

The surface signatures produced by a pair of trailing vortices generally occur in the later stages of the vortex lifetimes, and as such are subject to the complex mechanisms previously cited. Thus, it is essential to achieve some understanding of the evolution of vortices in an infinite homogeneous or stratified medium prior to embarking on an investigation of the free-surface effects and surface signatures.

A number of experimental and analytical studies has been carried out at the Naval Postgraduate School by Sarpkaya and his students [Refs. 6, 14-16] in order to investigate the effects of the governing parameters,

with the exception of those due to surface-proximity, on the rise and demise of the trailing vortices in homogeneous and density stratified media. These studies have clearly identified the various demise mechanisms in both media and established basic relationships between the rise of vortices and the governing parameters in an effectively infinite medium. It is against this background that the present investigation of the free-surface effects and the evolution of surface signatures is undertaken.

II. EXPERIMENTAL EQUIPMENT AND PROCEDURES

A. EQUIPMENT

The equipment used to generate the trailing vortices has been extensively used at this facility over the past three years [Refs. 6, 14-16]. Only the salient features, most recent modifications and the adaptation for this work are briefly described in the following.

The system consists essentially of a towing basin. The auxiliary components of the basin are the plumbing for water and for water and brine mixture (to establish a density stratification), turbulence management system, top and bottom carriages, velocity measuring system, lighting system, and the models [Refs. 14-16].

A mirror, inclined 45 degrees from the horizontal, is attached to the top of the tank at the test section to allow viewing of the vortex pair and the surface disturbances from the top of the basin. As the shadows of the surface disturbances rather than the disturbances themselves were photographed (taking advantage of the differential roughening of the water surface and the change of its reflective properties), a single light was positioned along the axis of the basin at a distance far enough to reduce glare and parallax and near enough to produce sharp shadows of the surface disturbances. Sheets of plexiglas (painted flat black) were placed on the side walls of the test section to eliminate undesirable reflections (see Fig. 1).

The drains are provided at the bottom at each end of the basin. Two parallel rails are mounted along the bottom of the tank. A carriage

rides smoothly on these rails and provides the test body with a constant velocity through the use of an endless cable and a DC motor. The velocity of the model is measured and continuously monitored through the use of a magnetic linear displacement transducer. It yields a signal proportional to the velocity of the model with an error less than 1 percent.

The two rails, the carriage and the filling pipes are located on or near the bottom of the basin and under a turbulence management system. The system consists of one inch thick polyurethane foam sandwiched between two perforated aluminum plates.

B. MODELS

Three models were used in the experiments: A rectangular foil (NACA 0012) and two Delta-wings, one with sharp edges, and one with rounded edges. These are the same models which were used previously at this facility [Refs. 6, 14-16]. The interior of each model was hollowed and used as a dye reservoir to seed the vortex cores. The models are mounted on their bases by means of a thin streamlined aluminum bar with a cross section of a NACA 0006 foil and set at the desired angle of attack. As noted earlier, all models are pulled by means of a DC motor, pulley, and cable system at the desired speed (ranging from 1.0 to 5.0 feet/second).

C. TEST PROCEDURES

The model is placed in the basin and the basin is filled gradually with fresh water to the desired level. In the cases where dye was used to examine the vortex pair, the models were filled with dye prior to filling the tank. After removal of trapped air and after a sufficient period of waiting for the escape of dissolved air in the water and the

elimination of any internal currents in the basin, the model was set in motion at the desired speed.

The shadowgraph technique was used to determine the characteristics of the surface signatures. For this purpose, the instantaneous shape and position of the shadows of the surface signatures were projected on a line-engraved plexiglas, placed at the bottom of the test section, and recorded on high-speed Polaroid film through the use of the inclined mirror. Each picture included time accurate to 0.1 seconds (generated by an electronic timer and projected into the inclined mirror by a small magnifying mirror). Either prior to or after each experiment, a scale was placed on the surface of the water, and both the scale and its shadow were recorded on film. The relationship between the actual scale and its shadow was used to transform the measurements obtained from the shadows to those of the actual disturbances in order to account for the parallax, free surface magnification and light-source proximity effects. In this manner, the actual separation of the surface signatures was deduced from the photographs at suitable time intervals (determined from the times recorded on the films). All surface disturbances were recorded on film until they had completely dissipated. The results are nondimensionalized and plotted in various forms and compared with those obtained theoretically. Each experiment was repeated at least twice to ascertain that the results were reproducible.

III. ANALYSIS

A. DIMENSIONAL ANALYSIS

The dependent parameters of major importance are the instantaneous positions of the vortex pair (x,y) and the surface disturbances (s,0). They may be expressed as functions of the following parameters:

$$x = f(t, U, d_o, \rho_o, d\rho/dy, \nu, B, AR, \alpha, g, r_e) \quad (1)$$

$$y = f(t, U, d_o, \rho_o, d\rho/dy, \nu, B, AR, \alpha, g, r_e) \quad (2)$$

and

$$s = f(t, U, d_o, \rho_o, d\rho/dy, \nu, B, AR, \alpha, g, r_e, \ ) \quad (3)$$

in which t represents the time, U the velocity of the model, d_o the initial depth of the vortex pair, ρ_o the reference density of water, $d\rho/dy$ the linear density gradient, ν the kinematic viscosity of water, B the base width of the model, AR the aspect ratio of the model, α the angle of attack of the model, g the gravitational acceleration, σ the surface tension of water, and r_e an effective core radius, characterizing the effect of the wing-tip shape in addition to other wing parameters.

The height and width of the test section and the height of the model within it were not included in the foregoing because a detailed analysis, based on ideal vortices, has shown that the velocities induced by the bottom were negligible. Effects of surface tension on the instantaneous

position of the vortex pair is deemed neglible. It is for this reason that σ is not included in Eqs. (1) and (2).

A dimensional analysis of Eqs. (1) through (3) yields

$$x/B = f(Ut/B,\ d_o/B,\ NB/U,\ U^2/gB,\ UB/\nu,\ AR,\ \alpha,\ r_e/B) \tag{4}$$

$$y/B = f(Ut/B,\ d_o/B,\ NB/U,\ U^2/gB,\ UB/\nu,\ AR,\ \alpha,\ r_e/B) \tag{5}$$

and

$$s/B = f(Ut/B,\ d_o/B,\ NB/U,\ U^2/gB,\ UB/\nu,\ AR,\ \alpha,\ r_e/B,\ \rho_o BU^2/\sigma) \tag{6}$$

in which

$$N = (-g/\rho_o\ d\rho/dy)^{1/2} \tag{7}$$

and is known as the Brunt-Vaisala frequency.

Equations (4), (5) and (6) may be recast in terms of the initial separation b_o of the vortex pair, and the initial mutual induction velocity V_o of the vortices by noting that B/b_o and V_o/U are uniquely determined by AR and α for a given wing shape. Thus, one has

$$x/b_o = f(V_o t/b_o,\ d_o/b_o,\ Nb_o/V_o,\ V_o^2/gb_o,\ V_o b_o/\nu,\ r_e/b_o) \tag{8}$$

$$x/b_o = f(V_o t/b_o,\ d_o/b_o,\ Nb_o/V_o,\ V_o^2/gb_o,\ V_o b_o/\nu,\ r_e/b_o) \tag{9}$$

and

$$s/b_o = f(V_o t/b_o,\ d_o/b_o,\ Nb_o/V_o,\ V_o^2/gb_o,\ v_o b_o/\nu,\ r_e/b_o,\ \rho_o b_o V_o^2/\sigma) \tag{10}$$

Experiments have shown that [Ref. 6] the ratio of the initial vortex-core spacing to wing span, b_o/B, is 0.70 for the sharp-edged Delta wing

0.71 for the round-edged Delta wing, and nearly equal to $\pi/4$ for the rectangular wing (NACA 0012).

The previous measurements have also shown that the dimensinal parameters V_o^2/gb_o (a Froude number which ranged from 0.003 to 0.03) and $V_o b_o/\nu$ (a Reynolds number which ranged from 3500 to 10,500) are not important within the range of the parameters encountered in the present experiments. With the foregoing arguments and noting that in experiments in a homogeneous medium, N=0, Eqs. (8), (9) and (10) may be written as

$$x/b_o = f(V_o t/b_o,\ d_o/b_o,\ r_e/b_o) \tag{11}$$

$$y/b_o = f(V_o t/b_o, d_o/b_o,\ r_e/b_o) \tag{12}$$

and

$$s/b_o = f(v_o t/b_o,\ /b_o,\ r_e/b_o,\ \rho_o/b_o V_o^2/\sigma) \tag{13}$$

Whereas the parameters $V_o t/b_o$ and d_o/b_o may be changed independently, r_e/b_o is taken as nature provides it. The primary reason for this is that a century of theoretical and experimental aerodynamics research has been incapable of describing the details of the structure of the tip vortex to be used as initial conditions in a viscous solution. It is surprising, but true, that until recently the importance of the wing-tip shape and its influence upon both the initial tangential velocity profile and the initial turbulence in the vortex has not been fully appreciated. Here the said influence has been characterized in terms of an effective core radius with full awareness of its shortcomings.

In Eq. (13), the last term $\rho_o b_o V_o^2/\sigma$ represents the so-called Weber number. It expresses the ratio of the inertial force to the surface tension force and hence the effect of the surface tension on the characteristics of the surface disturbances. It is a well known fact that the capillary waves have a minimum length of 0.681 inches (1.73 cm), a minimum phase speed of 9.13 inches/second (23.2 cm/s), and a minimum group velocity (at which the energy is transmitted) of about 7 inches/second (17.8 cm/s) [Ref. 17]. The speed of the surface disturbances observed in the present investigation ranged from 0.5 inch/second (1.26 cm/s) to 4 inches/second (10 cm/s). Furthermore, the present investigation has conclusively shown that the surface signatures are not capillary waves but rather disturbances generated by and slaved to the vortices. Hence the effect of the Weber number on the speed and position of the surface signatures is considered negligible. The amplitude of the disturbances, which may be affected by the surface tension, has not been studied in the present investigation. The foregoing does not rule out the possibility that for larger vortex strengths the speed of the surface signatures may coincide or exceed that of the capillary waves.

B. AN INVISCID FLOW ANALYSIS OF THE MOTION OF TRAILING VORTICES

It is possible to analyze the interaction of a vortex pair with the free surface only when suitable assumptions are made regarding the vortices and the free surface conditions. One can assume a steady two-dimensional potential flow past a submerged line vortex and examine the behavior of the resulting waves. Such an analysis has been carried out

by Salvesen and von Kerczek [18] for the purpose of exploring the effect of higher order approximations on nonlinear problems. Their analysis is valid only for waves with very long lengths and, thus, is not of particular interest for the present study. Furthermore, it is noted that in the Salvesen-von Kerczek analysis the vortex is assumed to remain at rest in a steady stream of arbitrary velocity U. It is easy to show that such a situation is physically impossible and the vortex may be kept at rest only when the free stream has the proper velocity so as to cancel the mutual induction velocity of the vortex and its image.

A relatively simple alternative is to assume the free surface to be undeformable at first and calculate the resulting flow field due to the vortex pair and its image, and then examine the behavior of the free surface due to the velocities induced on it. For the case under consideration where the disturbances are of very small amplitude and wave length, the proposed method yields remarkably satisfactory results.

For an inviscid line-vortex pair approaching the free surface (assumed to be rigid), (see Fig. 2), the complex potential is given by

$$w(z) = -\frac{i\Gamma}{2\pi}\left[\ln(z-z_v) + \ln(z+z_v) - \ln(z-\bar{z}_v) - \ln(z+\bar{z}_v)\right] \qquad (14)$$

where Γ and z_v represent, respectively, the strength and position of the vortex.

The complex velocity anywhere in the field is obtained by differentiating Eq. (14) with respect to z

$$\frac{dw}{dz} = u - iv = -\frac{i\Gamma}{2\pi}\left(\frac{1}{z-z_v} + \frac{1}{z+z_v} - \frac{1}{z-\bar{z}_v} - \frac{1}{z+\bar{z}_v}\right) \qquad (15)$$

Substituting $z = x+iy$ and $z_v = x_v+iy_v$ in Eq. (15) and separating the real and imaginary parts, one has

$$u = \frac{dx}{dt} = \frac{\Gamma}{2\pi}\left(\frac{y-y_v}{(x+x_v)^2 + (y-y_v)^2} + \frac{y+y_v}{(x-x_v)^2 + (y+y_v)^2} \right.$$

$$\left. - \frac{y+y_v}{(x+x_v)^2 + (y+y_v)^2} - \frac{y-y_v}{(x-x_v)^2 + (y-y_v)^2} \right) \qquad (16a)$$

and

$$v = \frac{dy}{dt} = \frac{\Gamma}{2\pi}\left(\frac{x-x_v}{(x-x_v)^2 + (y-y_v)^2} + \frac{x+x_v}{(x+x_v)^2 + (y+y_v)^2} \right.$$

$$\left. - \frac{x-x_v}{(x-x_v)^2 + (y+y_v)^2} - \frac{x+x_v}{(x+x_v)^2 + (y-y_v)^2} \right) \qquad (16b)$$

since the initial mutual induction velocity is given by

$$\frac{\Gamma}{2\pi b_o} = V_o \qquad (17)$$

Eqs. (16a) and (16b) can be recast as

$$\frac{u}{V_o} = \frac{\frac{y}{b_o} - \frac{y_v}{b_o}}{\left(\frac{x}{b_o} + \frac{x_v}{b_o}\right)^2 + \left(\frac{y}{b_o} - \frac{y_v}{b_o}\right)^2} + \frac{\frac{y}{b_o} + \frac{y_v}{b_o}}{\left(\frac{x}{b_o} - \frac{x_v}{b_o}\right)^2 + \left(\frac{y}{b_o} + \frac{y_v}{b_o}\right)^2}$$

$$- \frac{\frac{y}{b_o} + \frac{y_v}{b_o}}{\left(\frac{x}{b_o} + \frac{x_v}{b_o}\right)^2 + \left(\frac{y}{b_o} + \frac{y_v}{b_o}\right)^2} - \frac{\frac{y}{b_o} - \frac{y_v}{b_o}}{\left(\frac{x}{b_o} - \frac{x_v}{b_o}\right)^2 + \left(\frac{y}{b_o} - \frac{y_v}{b_o}\right)^2} \qquad (18a)$$

and

$$\frac{v}{V_o} = \frac{\frac{x}{b_o} - \frac{x_v}{b_o}}{\left(\frac{x}{b_o} - \frac{x_v}{b_o}\right)^2 + \left(\frac{y}{b_o} - \frac{y_v}{b_o}\right)^2} + \frac{\frac{x}{b_o} + \frac{x_v}{b_o}}{\left(\frac{x}{b_o} + \frac{x_v}{b_o}\right)^2 + \left(\frac{y}{b_o} + \frac{y_v}{b_o}\right)^2}$$

$$- \frac{\frac{x}{b_o} - \frac{x_v}{b_o}}{\left(\frac{x}{b_o} - \frac{x_v}{b_o}\right)^2 + \left(\frac{y}{b_o} + \frac{y_v}{b_o}\right)^2} - \frac{\frac{y}{b_o} + \frac{y_v}{b_o}}{\left(\frac{x}{b_o} + \frac{x_v}{b_o}\right)^2 + \left(\frac{y}{b_o} - \frac{y_v}{b_o}\right)^2} \qquad (18b)$$

The velocity distribution on the free surface may be found by setting $y/b_o = 0$ and $v/V_o = 0$. Then, Eqs. (18a) and (18b) reduce to

$$\frac{u_s}{V_o} = 2 \frac{y_v}{b_o} \left(\frac{1}{\left(\frac{x}{b_o} - \frac{x_v}{b_o}\right)^2 + \left(\frac{y_v}{b_o}\right)^2} - \frac{1}{\left(\frac{x}{b_o} + \frac{x_v}{b_o}\right)^2 + \left(\frac{y_v}{b_o}\right)^2} \right) \qquad (19)$$

where u_s is the velocity at the free surface.

It is of special interest to know the position x_m of the maximum surface velocity u_{sm} relative to the position of the trailing vortex. The position of the vortex is given by [Ref. 19].

$$\frac{1}{(x_v/b_o)^2} + \frac{1}{(y_v/b_o)^2} = 4 + \frac{b_o^2}{d_o^2} \tag{20}$$

where it is seen that the relationship between x_v/b_o and y_v/b_o depends on d_o/b_o. Differentiating Eq. (19) with respect to x/b_o, setting it equal to zero, and, finally, combining it with Eq. (20), one has

$$\frac{x_m}{b_o} = \sqrt{\frac{k\eta^2(\eta^2-1)}{2(k\eta^2-1)} + \frac{\eta^2}{3(k\eta^2-1)}\sqrt{4k^2\eta^4 - 10k\eta^2 + 10}} \tag{21}$$

where $\eta = x_v/b_o$ and

$$k = 4 + (b_o/d_o)^2$$

The velocities at the center of a vortex, located at $x = x_v$ and $y = y_v$, may be obtained from Eqs. (18a) and (18b) by omitting the contribution of the vortex itself to the velocity at its center [i.e., by omitting the last term in Eq. (18a) and the first term in Eq. (18b)]. This procedure yields

$$\frac{u_v}{V_o} = \frac{\left(\frac{x_v}{b_o}\right)^2}{2\left(\frac{y_v}{b_o}\right)\left\{\left(\frac{x_v}{b_o}\right)^2 + \left(\frac{y_v}{b_o}\right)^2\right\}} \tag{22a}$$

and

$$\frac{v_v}{V_o} = \frac{-\left(\frac{y_v}{b_o}\right)^2}{2\left(\frac{x_v}{b_o}\right)\left\{\left(\frac{x_v}{b_o}\right)^2 + \left(\frac{y_v}{b_o}\right)^2\right\}} \tag{22b}$$

It is of particular interest to know the normalized positions of the vortex and of the maximum surface velocity as a function of the normalized time $V_o t/b_o$. Noting that

$$u_v = \frac{dx_v}{dt} \quad \text{and} \quad v_v = \frac{dy_v}{dt}$$

and combining with Eqs. (22a) and (22b) one can numerically evaluate the position of the vortex and of the maximum velocity as a function of the normalized time $V_o t/b_o$ and the initial depth of the vortex pair d_o/b_o. This enables one to determine first the surface velocity profile and then the position of the maximum velocity as functions of $V_o t/b_o$, d_o/b_o, and x/b_o. The computer programs for the calculation of u_s/V_o and x_m/b_o are given in Appendices A and B. The program for the simultaneous calculation of x_v/b_o, y_v/b_o, x_m/b_o, and u_m/V_o is presented in Apprendix C.

The position of a marker particle initially located at $(0, d_o)$ may be calculated as a function of time for various values of d_o/b_o. Noting that for a fluid particle on the vertical axis $x = 0$ and $u = 0$, Eq. (18b) may be written as

$$\frac{v}{V_o} = -2\left(\frac{x_v}{b_o}\right)\left(\frac{1}{\left(\frac{x_v}{b_o}\right)^2 + \left(\frac{y}{b_o} - \frac{y_v}{b_o}\right)^2} - \frac{1}{\left(\frac{x_v}{b_o}\right)^2 + \left(\frac{y}{b_o} + \frac{y_v}{b_o}\right)^2}\right) \qquad (23)$$

Writing $v = dy/dt$ and noting that $y = d_o$ at $t = 0$, a numerical integration scheme can be employed to calculate the position of the marker particle through the use of Eqs. (22) and (23) as a function of d_o/b_o and $V_o t/b_o$. The computer code presented in Appendix D enables one to perform the said calculations. The results obtained in this manner are discussed later.

Similarly, one can calculate the position of the top of the recirculation cell as a function of $V_o t/b_o$ and d_o/b_o by noting that the top of the recirculation cell is a stagnation point. The code for such a calculation is given in Appendix E.

IV. RESULTS

A. PHYSICAL CHARACTERISTICS OF THE SURFACE DISTURBANCES

The physical appearance of the surface signatures produced by a vortex pair approaching the free surface can be characterized in two distinct modes: "striations" and "scars".

The striations appear abruptly sometime after the passage of the lifting surface as ridges perpendicular to the path of the model (see (Fig. 3). They grow rapidly to a total length of about 2.6 b_o to 3.0 b_o, ($L/2/b_o$ = 1.3 to 1.5). The pure striation phase of the surface condition lasts for a time interval of $(V_o t/b_o)$ = 0.6 to 1.0. Shortly thereafter, two distinct signatures or 'scars' appear. They are nearly parallel to the model track and run along the tips of the striations (see Figs. 4 and 5). While the scars become the dominant features of the free surface, the striations remain in the signature band and stretch more or less randomly in the transverse direction.

The scars move side ways, i.e., the width of the signature band increases with time, at a more or less constant speed if unimpeded by other phenomena such as Crow instability or vortex breakdown (see Figs. 6 and 7). The lateral motion of the scars is nearly in phase with that of the vortices. As the scars and striations age, they attenuate, spread over a larger area, and eventually become indistinguishable. The foregoing takes place at relatively small depths (say for d_o/b_o less than about 4). For larger depths of submergence, the Crow instability sets in and amplifies rapidly during the later stages of the rise of vortices. In the absence of ambient

turbulence, as in the present case, the Crow instability is a consequence of the Helmholtz and Rayleigh instabilities which lead to the production of turbulence around the periphery of the vortex core and in the recirculation cell. The proximity of the free surface may impede the occurrence of the Crow instability due to the mutal interaction of the vortex pair with its image, i.e., the mutual interaction of four vortices. Leaving aside, for the time being, the exact nature of the Crow instability under the influence of the free surface, it is evident from Figs. 8 through 10 that the cause of the scars is in fact the vortices beneath the free surface. In other words, the scars and striations are not small amplitude surface waves propagating independently away from their generator but are local disturbances whose generation, growth and propagation are controlled by the vortices. Figures 8 through 10 are representative examples of the surface signatures which could have resulted only from the vortices which have undergone Crow instability. The simultaneous observations of the vortex core (i.e., the dye) and the surface signatures have shown that the signatures are trapped by and slaved to the vortices beneath the surface.

Figure 9 shows a succession of ring-shaped scars generated following the linking of the vortices. It is noted that while the inside of these relatively crude rings are covered with randomly distributed striations, the region outside the scars is disturbance free. Figure 10 shows scars similar to those discussed above for a different test run. It is clear from Fig. 9 that the linking does not necessarily occur simultaneously along the trail at equal intervals. As was shown in previous investigations [Ref. 6], the linking, like the Crow instability, is dependent on the ambient turbulence and one cannot expect the linking to take place

with perfect regularity. Figures 8 through 10 show the nearly perfect symmetry of the ring-shaped scars with respect to the axis of the channel. These figures also show a number of dark circular regions corresponding to local surface depressions. They result from the simple fact that when a vortex ring approaches the free surface it breaks and opens up like a horseshoe or a U-shaped magnet under the influence of its image. Then the U-shaped vortex immediately joins its mirror image at the free surface, forming a new ring (half real, half imaginary), in accordance with the well-known vortex theorems. The local surface depressions correspond to the points where the real and image vortex arms shake hands at the free surface. Figure 11 shows the scar and the striations generated by an inclined vortex ring just prior to the occurrence of the breaking-relinking phenomenon.

B. EXPERIMENTAL DATA

The experimental data evaluated in the manner described previously have been plotted in terms of the governing parameters. The relative horizontal half spacing s/b_o is shown as a function of the normalized time $V_o t/b_o$ in Figs. 12 through 16 for the Round-edged Delta wing (Delta-2R), in Figs. 17 through 20 for the sharp-edged Delta wing (Delta-2S, and in Figs. 21 through 25 for the rectangular wing (RP-2), for the d_o/b_o ratios noted in each figure. Each symbol in each figure represents one independent test run. At least two test runs were performed for a given set of initial conditions.

The characteristics of the data will be discussed through the use of two representative plots. Figure 14 shows the data obtained with Delta-2R

for $d_o/b_o = 4$. This figure reveals the following facts: (i) the surface signatures in the form of striations do not come into existence until a definite time of $V_o t/b_o$, ($V_o t/b_o = 3.3$ in Fig. 14); (ii) for small values of $V_o t/b_o$, corresponding to the striation phase, the data show larger scatter; (iii) the pure striation phase of the surface signatures ends (as determined from the pictures) after a time interval of $\Delta V_o t/b_o = 0.6$ to 1.0, (in Fig 14, $\Delta V_o t/b_o = 0.9$); (iv) there is a particular time interval where the data represent the scar-dominated surface signatures (from $V_o t/b_o = 4.3$ to 7 in Fig. 14); and, (v) the scatter in the latter region is not due to the shift of the data in the vertical direction from one run to the next but rather due to the random errors as noted from the figure.

Data for a larger d_o/b_o are shown in Fig. 16. In addition to all of the characteristics noted earlier, one observes that the data in Fig. 16 show larger scatter. This is primarily due to the occurrence of the Crow instability and the formation of the vortex rings. They give rise to sinusoidal and ring-shaped scars and render the accurate evaluation of s/b_o somewhat more difficult.

In the foregoing, all the data obtained with the three models at various depths have been presented (the tabulated data are given in Appendix F). It has been stated on the basis of observations and measurements that the surface signatures are slaved to the vortices. However, the fundamental question of what gives rise to the disturbances and how they are related to the velocity field generated by the vortices has not yet been discussed. It has been surmised that the position and the amplitude of the disturbances are directly related to the strain

field arising from the velocity field generated by the vortices. It is with this hypothesis in mind that the velocity distributions obtained from the inviscid flow analysis will be presented and subsequently related to the experimental data.

C. RESULTS OF THE INVISCID FLOW ANALYSIS

Figures 26 through 31 show the surface velocity profiles at various times for various depths, as obtained through the use of Eq. (19). Evidently, the maximum velocity becomes nearly constant for x/b_o larger than about 2. This correponds to the state where the vortex and its image are no longer affected by the other vortex of the pair and its image. In other words, the surface velocity for x/b_o larger than about 2 is dictated primarily by one of the trailing vortices and its image. It is exactly for the same reason that the shape of the velocity profile becomes increasingly more symmetrical about a vertical axis. Furthermore, it is noted for future reference that the half-width of the velocity profile at 40 percent of its maximum is $\xi/b_o = 0.66$.

Figure 32 is a plot fo the relative position of the maximum surface velocity as a function of the normalized time for various d_o/b_o values, as obtained through the use of Eq. (21). For a given d_o/b_o, the maximum surface velocity occurs first at a distance x_m which is larger than the initial vortex separation (e.g., at $x_m/b_o = 1.2$ for $d_o/b_o = 2$). As time increases and as the vortex pair rises, x_m/b_o decreases. Subsequently, x_m/b_o approaches a minimum and then increases, more or less uniformly. The foregoing results are predicated on the assumption that the flow is inviscid and there is no mutual induction instability.

Figures 33 through 38 show x_m/b_o and u_m/V_o as functions of $V_o t/b_o$ for various values of d_o/b_o. Also shown in these figures (with dashed lines) are the variations of x_v/b_o and y_v/b_o with the normalized time. These figures reveal several interesting facts which will be pointed out with reference to Fig. 33. First, it is noted that the vortices are closer to the vertical axis than the position of the maximum velocity, i.e., $x_v > x_m$. This rather surprising condition prevails for a time period dependent on d_o/b_o, as evidences from Figs. 34 through 38. Second, beyond a minimum $V_o t/b_o$, the position of the maximum velocity and the x-position of the vortex are indistinguishable. In other words, the maximum velocity arises only from the contributions of the vortex and its image directly above it. Finally, the amplitude of the surface velocity increases rapdily with time and reaches a nearly constant value when the x-positions of the vortex and the maximum velocity become nearly identical. Had the vortices migrated from an infinite depth towards the free surface, they could not have come a distance closer than $b_o/2$ to the free surface and the surface velocity would have been $u_s = 2(\Gamma/2\pi b_o/2)) = 4V_o$. In Fig. 33, u_m/V_o asymptotically reaches a value slightly larger than 4.0 because the vortices are generated at a relatively small depth. In fact, Eq. (20) for $x_v/b_o =$ reduces to

$$\frac{y_v}{b_o/2} = \frac{2}{\sqrt{4 + \left(\frac{b_o}{d_o}\right)^2}} \tag{24}$$

which shows that $y_v/b_o/2$ is smaller than 1.0 for vortices migrating upwards from a finite depth of d_o. For larger values of d_o/b_o (see e.g., Fig. 38) u_m/V_o asymptotically approaches 4.0.

Figure 39 shows the position of the marker particle, originally located at $(x,y,t) = (0,d_o,0)$, relative to the instantaneous position of the vortices. Note that at an arbitrary time t, the marker particle is located at $(0,y)$ and the vortices at (x_v,y_v). The relative position of the marker particle, as given by $(y_v-y)/b_o$, increases rapidly at first and then reaches a maximum value equal to the semi-minor axis of the recirculation cell (see insert in Fig. 39). For a vortex pair migrating in an infinite fluid, the semi-major and semi-minor axes are given by $m/b_o = 1.045$ and $n/b_o = 0.865$, respectively [Ref. 19]. For vortices migrating in a finite depth of fluid, the smaller the initial depth of the vortices, the smaller is n/b_o (see Fig. 39). Accordingly, m/b_o increases since the recirculation cell contains the same body of fluid (the effects of entrainment and detrainment through recirculation cell boundary will not be discussed here). Once the marker particle reaches the top of the recirculation cell, it continues to move with the recirculation cell, provided the latter is not deformed due to the free surface effects. Under these circumstances $(y_v-y)/b_o$ remains constant for a certain period of time (as seen from Fig. 39, particularly for larger values of d_o/b_o). As the recirculation cell begins to 'see' the free surface, it flattens against the free surface and thus $(y_v-y)/b_o$ decreases. Ultimately, the vortices reach their maximum elevation, as dictated by Eq. (21), and the marker particle nearly touches the free surface, as does the top of the recirculation cell.

So far the discussion has centered around the motion of a two-dimensional vortex pair. The trailing vortices are generated at a speed of U (model velocity) and rise, at least initially, with a mutual induction velocity V_o. Thus the vortex pair, as viewed from the side, is inclined at an angle of $\gamma = \arctan(V_o/U)$ relative to the horizontal. Consequently, the top of the recirculation cell does not arrive at the free surface at all points along the trailing vortex at the same instant. In fact, if one were to consider an imaginary point depicting the intersection of the top of the recirculation cell with the free surface, one would see it move at a speed of U in the direction of motion of the model.

Figure 40 shows the position of the marker particle relative to the initial position of the vortex pair for various d_o/b_o values. In other words, the marker particle located at $(0,d_o)$ at $t = 0$ moves to a point $(0,y)$ at time t. Thus, $h = d_o - y$ represents the migration of the marker particle from its original position. Since the marker particle very quickly reaches the top of the recirculation cell, Fig. 40 shows, for all intents and purposes, the position of the top of the cell relative to the initial position of the vortex pair.

D. ANALYSIS AND DATA

It has been hypothesized on the basis of the observations and measurements that the creation and propagation of the striations and scars are a consequence of the strain field arising from the nonuniform surface velocity distribution. The following is a critical examination of this hypothesis through the use of the experimental data and the inviscid flow analysis.

The variables of primary concern in the comparison of the theoretical and experimental results are the time of creation, the instantaneous shape and position, the rate of propagation, and the duration of the surface signatures.

The data obtained with all the models have shown that the striations always appear first when the vortex pair arrives at a particular depth from the free surface. The measurements and the calculations based on Eq. (26) and Eqs. (14) through (23) have shown that the said distance is $y_v/b_o = 1.0$. The pure striation phase lasts a time period of $\Delta V_o t/b_o = 0.6$ to 1.0. During this time interval, the amplitude of the surface velocity increases rapidly and nearly attains its maximum value (see Figs. 33 through 38). This rapid transition period culminates with the appearance of scars as shown in Figs. 4 and 5.

Figures 41 and 42 are two representative plots showing the position of the scar front, as deduced from the data, and the position of the maximum surface velocity, as given by Eq. (21), as a function of the normalized time. The conclusions to be arrived at on the basis of these two figures are uniformly valid for all the data obtained during this investigation.

It is noted from Figs. 41 and 42 that (i) the variation of x_{sf}/b_o with $V_o t/b_o$ is essentially linear, i.e., the scar front has a fairly constant velocity, (0.43 V_o in Fig. 41 and 0.53 V_o in Fig. 42); (ii) the position of the maximum velocity (based on the inviscid flow analysis) trails the scar front for a normalized time smaller than about 5.8 (in Fig. 41) and leads the scar front for larger times; (iii) the scars come into existence at a time when the vortex pair almost reaches its maximum

height and begins to move essentially in the lateral direction (see also Figs. 33 through 38); and finally, (iv) the scars cease to exist when the vortices completely dissipate. The normalized time of dissipation has been previously established [Refs. 6, 15 and 16].

The conclusions reached on the basis of Figs. 41, 42, and all others like them, point out one important fact: If the position of the scars is slaved to the vortices, as shown by numerous test runs, and if the vortices are observed to dissipate in a finite time, then an analysis based on constant vortex strength and inviscid flow assumption cannot adequately predict either the magnitude or the location of the maximum surface velocity or the positions of the vortices and the scars. Consequently, one must consider a circulation model which accounts for the dissipation of the vortex partly due to the mixing of the counter-sign vorticity in the overlapping regions of the vortex pair in the recirculation cell, partly due to turbulence, and partly due to the diffusion of vorticity generated beneath the free surface.

Squire [Ref. 20] suggested that a turbulent trailing vortex could be described by Lamb's solution [Ref. 19] if the kinematic viscosity ν in it were replaced by an eddy diffusivity ν_t as

$$\frac{\Gamma}{\Gamma_o} = (1-\exp(-\eta^2/4a_o)) \tag{25}$$

where $\eta^2 = r^2/t\Gamma_o$, r the radial distance from the vortex core and $a_o = \nu_t/\Gamma_o$ which is a function of the vortex Reynolds number, Γ_o/ν. For the experiments reported herein, the vortex Reynolds number is about 3×10^4

which corresponds to an a_o value of 2×10^{-3}, according to the data compiled and reported by Govindaraju and Saffman [Ref. 21]. Thus, Eq. (25) reduces to

$$\frac{\Gamma}{\Gamma_o} = 1 - \exp(-A/V_o t/b_o) \tag{26}$$

where $A = 20(r_e/b_o)^2$.

During the early stages of the motion of the vortex pair, the vortex core relaminarizes while the periphery of the core becomes increasingly more turbulent. Neither the distribution of vorticity nor the amount of circulation at a given r is measured or calculated to any degree of accuracy in spite of a century of aerodynamics research. Notwithstanding this fact, one can obtain some idea about the magnitude of A as follows. As the vortices begin to rise, the distribution of vorticity may be assumed to be Gaussian with an effective core radius smaller than $b_o/2$. It is noted that the vortices are still a distance b_o apart at this time. Thus, it is reasonable to assume $r_e = 0.4b_o$, (i.e., A = 3.2), for the vortices which have not yet had time to diffuse much as the time they come near the free surface (a) distance of about $b_o/2$, see Eq. (24). This is particularly true for vortices generated in shallower depths, (small d_o/b_o values). The majority of the dissipation for these vortices takes place when they begin to move sideways during which time they give rise to relatively strong scars and suffer from increased dissipation due to free surface proximity and core distortion.

The vortices migrating from larger depths have sufficient time for the spread of turbulence in their core, leading to a larger effective core

radius. Noting that the top of the recirculation cell is bounded by the free surface, the effective core radius is at least equal to $b_o/2$. However, as the recirculation cell flattens against the free surface and as the vortex core becomes more elliptical in shape, the effective core radius may acquire even larger values (say, $r_e = 0.6b_o$ for which $A = 7.2$). The majority of the dissipation for these vortices takes place before they come near the free surface. Thus, they move sideways at a slower speed, dissipate at a slower rate, and generate relatively weaker scars.

It is important to note that no simple expression, such as Eq. (25), based on the replacement of the molecular diffusivity by an approximate turbulence diffusivity, is likely to account for the entire spectrum of the complex phenomena ranging from turbulent diffusion to Crow instability to vortex linking. Thus, Eqs. (25) and (26) are not proposed here as definitive solutions, but rather as means of exploring the observed behavior of the vortices and its consequences. If the hypotheses made prove to be workable on the basis of these simple turbulence models, then one can explore in greater detail the phenomena controlling the mutual interaction of the vortices with the homogeneous and density stratified media and with the free surface.

With the objectives cited above, Eq. (26) has been incorporated into Eqs. (14) through (23) and the resulting expressions were used to plot Fig. 43 for various values of A. It is seen that the variation of A from 3 to ∞ does not materially affect x_m/b_o for normalized times smaller than that corresponding to the minimum x_m/b_o. The reason for this is that during the early stages of the rise of the vortices, the dissipation of vorticity is not significant, particularly for vortices migrating in

a shallow medium as in Fig. 43. For normalized times larger than that corresponding to the minimum x_m/b_o, the slope of each curve depends strongly on A. The reason for this is that the vortices come under the influence of the free surface and dissipate faster as noted earlier. The slope of each curve represents the lateral velocity of the point at which the maximum velocity occurs. Thus, it is clear that the velocity of the said point may be rendered identical to that of the scars by choosing judiciously the value of A.

Figures 44 through 46 show the effect of the variation of A on x_m/b_o, u_m/V_o, x_v/b_o, and y_v/b_o. These figures may be compared with Fig. 35, which corresponds to the case of $A = \infty$, (i.e., Γ = constant). It is noted that u_m/V_o is relatively smaller and begins to decrease after reaching a maximum (see Fig. 46) instead of asymptotically rising to a constant value (see Fig. 35).

One is now in a position to explore the consequences of the hypothesis that the scars are slaved to the vortices and that the strain field arising from the nonuniform velocity distribution is the cause of the scars. With this objective in mind, the representative data obtained with Delta-2R for $d_o/b_o = 4.0$ are compared with the corresponding analytical results in Fig. 43 and it is found that the mean slope of the experimental data (representing only the scars) matches reasonably well the slope of one of the analytical curves for which A = 6. Figure 47 shows the comparison of the said slopes. Even though the ability of the remainder of the data to yield similar correspondence remains yet to be seen, it is at once clear from Fig. 47 that the scar and the maximum-velocity point are in phase but are not spatially coincident. A simple calculation shows that

$\lambda = (x_{sf}-x_m)/b_o$, i.e., the vertical distance between the dashed line and the mean line going through the data, is about 0.66. In other words, the front of the scar is not at the point of maximum velocity, but at the point where the velocity is a certain fraction Λ of the maximum. From the velocity profiles similar to those shown in Fig. 28, it is determined that the velocity is 40 percent of the maximum, i.e., $\Lambda = 0.4$, for $\lambda = (x_{sf}-x_m)/b_o = 0.66$.

The foregoing results have been obtained on the basis of Figs. 43 and 47 alone. It will now be shown that the values of Λ and λ are nearly universal constants of the surface velocity profiles for x/b_o larger than about 1.5. For this purpose, let us consider Fig. 48 where u_s/V_o is shown as a function of x/b_o for various values of $V_o t/b_o$ for $d_o/b_o = 4$ and $A = 6$. This and all other similar figures for other relative depths show that (i) the amplitude of the maximum velocity rises sharply with increasing normalized time and then decreases gradually, as evidenced by the envelope of the maximum points, and (ii) the velocity profiles become almost symmetrical about a vertical axis passing through their maximum for x/b_o larger than about 1.5*.

A detailed analysis of those profiles which have become symmetrical has shown that they are also similar. In other words, all symmetrical profiles under consideration may be reduced to a single profile if the velocities are normalized by $u_m/2$ and the lateral distances ξ (half of

*The normalized times for x/b_o larger than about 1.5 also correspond to the scar-phase of the surface disturbances during which the vortices move laterally, more or less independent of the influence of their real counterpart.

the width of the velocity profile where $u = u_m/2$). From such a nearly universal profile it has been deduced that $\lambda = \xi = 0.66$ corresponds to $\Lambda = 0.4$.

Special experiments have been carried out in order to determine the relative positions of the scar front and the vortex axis (which corresponds to the position of the maximum velocity). Figure 49 shows the picture of the trailing vortices and the scars. The value of λ has been deduced from such figures and was found to be equal to 0.65 ∓ 0.05. This result compares exceedingly well with that cited above and provides indirect evidence of the assumptions made regarding the relationship between the vortices and the scars and between the vortex strengths and Squire's model. Obviously, additional evidence in the way of analysis and measurements is needed to strengthen the validity of all aspects of the hypothesis.

In the following, the entire scar data will be compared with the theoretical predictions, and then the dependence of A on d_o/b_o and the model shape will be discussed.

Figures 50 through 54 show the normalized position of the scar front, x_{sf}/b_o, as a function of $V_o t/b_o$ for the round-edged Delta model (Delta-2R) for various values of d_o/b_o. Also shown in these figures are the theoretically predicted scar fronts and the relative position of the maximum velocity. It should be emphasized that the data and the analysis presented in these figures pertain only to the scars. Similar data and comparisons are presented in Figs. 55 through 58 for the sharp-edged Delta model (Delta-2S), and in Figs. 59 through 63 for the rectangular wing (RP2).

In comparing the relative positions of the scar front with the predictions of the analytical model, it has been discovered that a single value of A cannot account for the changes brought about in the scar velocity with the depth of migration of the vortices. It has been emphasized earlier that the vortices which rise from relatively small depths create stronger scars, while the vortices migrating from greater depths give rise to weaker scars. It has also been noted that the scars generated by stronger vortices must move faster laterally because the surface velocity at $\lambda = 0.65$ is necessarily larger than that generated by weaker vortices. Consequently, one should expect smaller A values for larger scar-front velocities, and vice versa. Furthermore, as pointed out in Ref. [6] , all of the characteristics of a vortex depend both on the circumstances under which it is created and on the conditions to which it is subjected afterwards. This is particularly true for vortices which propagate in a turbulence free environment. Since the roll-up of the vortices varies from one model to another, and since the Helmholtz and Rayleigh instabilities depend upon the particular roll-up process, the initial turbulence resulting from them may vary significantly. This in turn, affects the vorticity distribution in the core and the subsequent evolution of the vortex, including the degree of its susceptability to Crow instability. In other words, one does expect variations in A from model to model for the same d_o/b_o.

Figure 64 shows the dependence of A on d_o/b_o and the model shape. As anticipated on the basis of heuristic reasoning, A increases with d_o/b_o and shows a variation of $\mp$ 0.5 about a mean value, for a given d_o/b_o.

Some of this variation could have been attributed to the errors in the execution of the experiments and in the evaluation of the experimental data, had it not been due to the fact that the values of A for a given model are quite consistent. It must also be noted that the values of A shown in Fig. 64 correspond to those calculated through the use of an effective core radius ranging from about $0.4b_o$ to $0.6b_o$. Thus, the variation of A from model to model for a given d_o/b_o may be due to the variations in the core radius. Experiments with additional models will have to be carried out to determine the dependence of A on the model shape or the roll-up process. Furthermore, experiments in an environment with prescribed ambient turbulence may shed further light on the variation of A with d_o/b_o and the model shape.

V. CONCLUSIONS

The investigation reported herein warranted the following conclusions:

1. The trailing vortices give rise to surface signatures in the form of striations and scars.

2. The striations come into existence when the vortex pair is at a distance equal to one initial vortex separation from the free surface. The duration of the pure striation phase is roughly equal to the time that the vortex pair would take to rise a distance of about one-half to one initial vortex separation.

3. The scars come into existence towards the end of the pure striation phase and when the vortices are at a distance of about one-half the initial vortex separation from the free surface.

4. The velocity of the scar front is essentially constant and depends only upon the initial position of the vortex pair relative to the free surface.

5. A theoretical model based partly on inviscid flow analysis and partly on an approximate turbulence model has shown that the instantaneous position as well as the velocity of propagation of the scars may be predicted with confidence. The single parameter expressing the relationship between the eddy viscosity and the turbulence prevailing in the vortex must be obtained experimentally.

6. A comparison of the characteristics of the surface signatures with those of capillary-gravity waves has shown that the signatures are

not capillary waves, but rather a consequence of the strain field arising from the nonuniform surface velocity distribution created by the vortices.

LIST OF REFERENCES

1. Olsen, J. H., Goldburg, A., and Rogers, M. (eds.), Aircraft Wake Turbulence and Its Detection, Plenum Press, New York, 1971.

2. Hallock, J. N. (ed.), Proceedings of the Aircraft Wake Vortices Conference, 1977, National Technical Information Services, Springfield, VA 22161.

3. Donaldson, C. duP. and Bilanin, A. J., Vortex Wakes of Conventional Aircraft, AGARDograph AGARD-AG-204, 1975.

4. Widnall, S. E., The Structure and Dynamics of Vortex Filaments, Annual Reviews of Fluid Mechanics, Vol. 7, 1975, pp. 141-165.

5. Hallock, J. N. and Eberle, W. R. (eds.), Aircraft Wake Vortices: A State-of-the-Art Review of the United States R & D Program, Transportation Systems Center, Cambridge, MA, Report No. FAA-RD-77-23, 1977.

6. Sarpkaya, T., Trailing Vortices in Homogeneous and Density-Stratified Media, Journal of Fluid Mechanics, Vol. 136, 1983, pp. 85-109.

7. Panton, R. L., Oberkampf, W. L., and Soskic, N., Flight Measurements of a Wing Tip Vortex, Journal of Aircraft, Vol. 17, 1980, pp. 250-259.

8. Baker, G. R., Barker, S. J., Bofah, K. K. and Saffman, P. G., Laser Anemometer Measurements of Trailing Vortices in Water, Journal of Fluid Mechanics, Vol. 65, 1974, pp. 325-336.

9. Crow, S. C., Stability Theory for a Pair of Trailing Vortices, AIAA Journal, Vol. 8, 1970, pp. 2172-2179.

10. Peace, A. J. and Riley, N., A Viscous Vortex Pair in Ground Effect, Journal of Fluid Mechanics, Vol. 129, 1983, pp. 409-426.

11. Parker, S. J. and Crow, S. C., The Motion of a Two-Dimensional Vortex Pair in Ground Effect, Journal of Fluid Mechanics, Vol. 82, 1977, pp. 659-671.

12. Tombach, I. H., Transport of a Vortex Wake in a Stably Stratified Atmosphere, Aircraft Wake Turbulence and Its Detection, Edited by J. H. Olsen et al., Plenum Press, New York, 1971, pp. 41-57.

13. Maxworthy, T., Solitary Waves on Density Interfaces, Waves on Fluid Interfaces, Edited by R. E. Meyer, Academic Press, New York, 1983, pp. 201-220.

14. Sarpkaya, T. and Johnson, S. K., Trailing Vortices in Stratified Fluids, NPS-69-82-003, June 1982, Monterey, CA.

15. Johnson, S. K., Trailing Vortices in Stratified Fluids, M.S. Thesis, Naval Postgraduate School, Monterey, CA, June 1982.

16. Turkmen, C., Trailing Vortices in Stratified and Unstratified Fluids, M.S. Thesis, Naval Postgraduate School, Monterey, CA, December 1982.

17. Neumann, G. and Pierson, W. J. Jr., Principles of Physical Oceanography, Prentice-Hall, Inc., Inglewood Cliffs, N. J., 1966, pp. 286-290.

18. Salvesen, N. and von Kerczek, C., Comparison of Numerical and Perturbation Solutions of Two-Dimensional Nonlinear Water-Wave Problems, Journal of Ship Research, Vol. 20, No. 3, September 1976, pp. 160-1970.

19. Lamb, H. (Sir), Hydrodynamics, Dover Publications, New York (6th ed.), 1945, pp. 221-224.

20. Squire, H. B., "The Growth of a Vortex in Turbulent Flow," British Aeronautical Research Council, Paper No. 16666, 1955.

21. Govindaraju, S. P. and Saffman, P. G., Flow in a Turbulent Vortex, The Physics of Fluids, Vol. 14, No. 10, 1971, pp. 2074-2080.

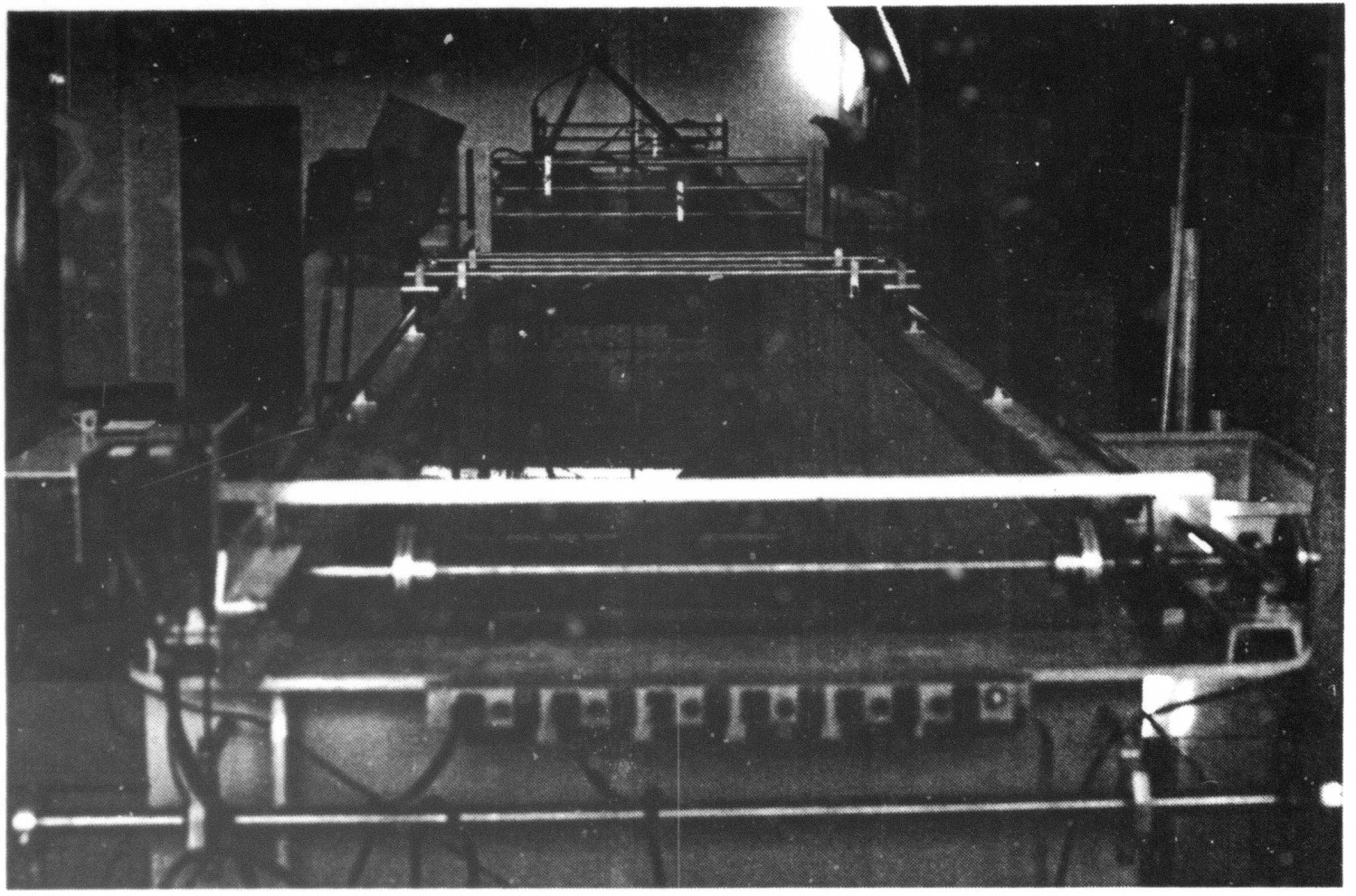

Figure 1. Water Basin

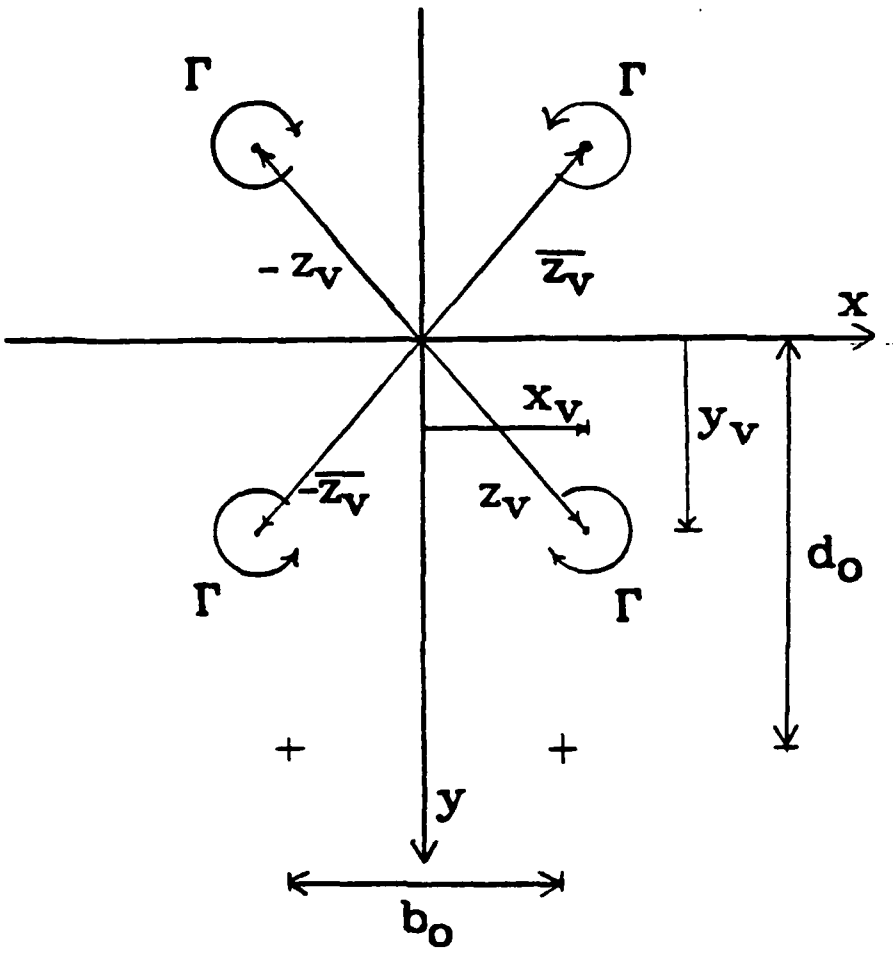

Figure 2. Coordinate Axes

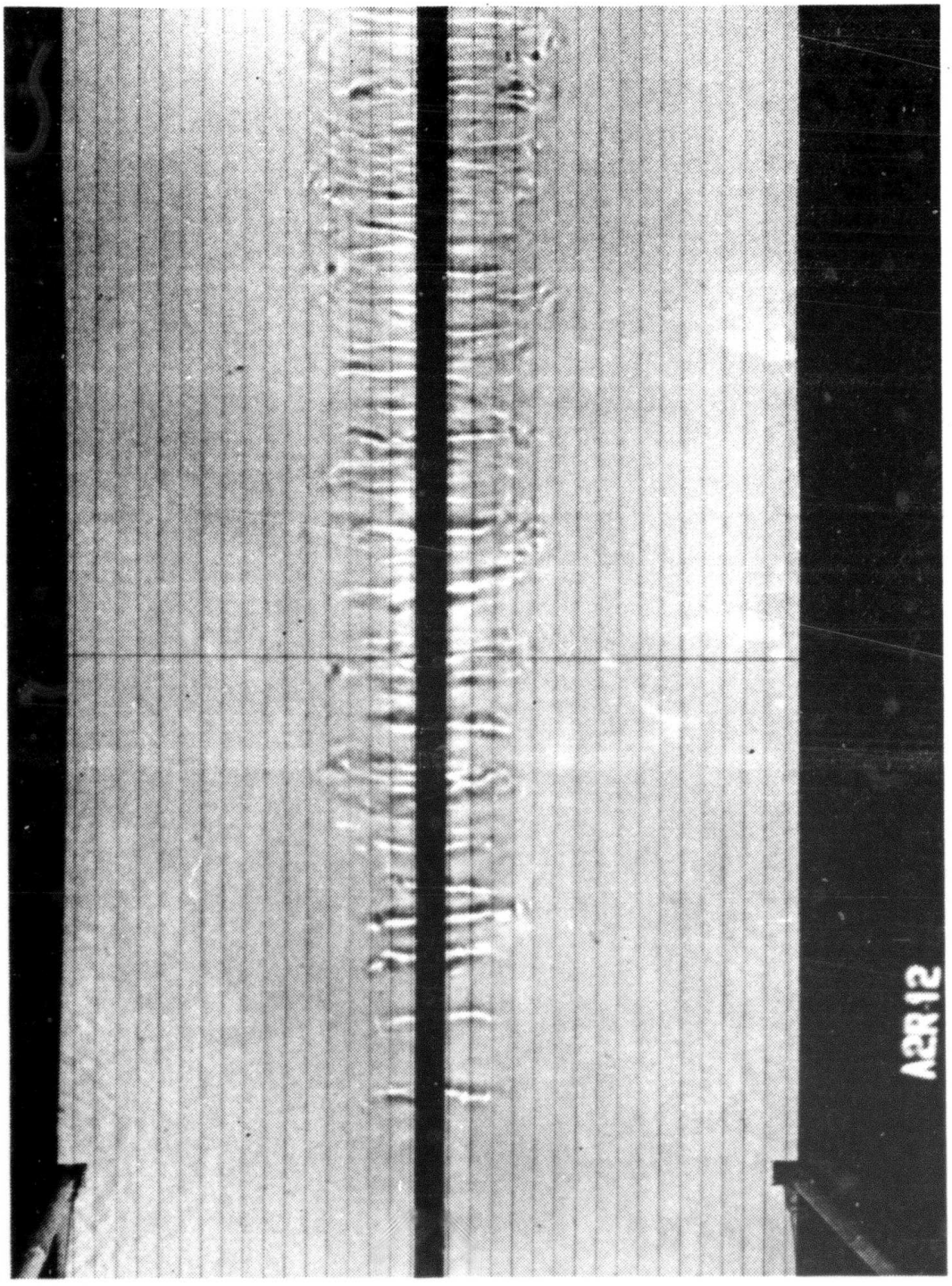

Figure 3. Striations

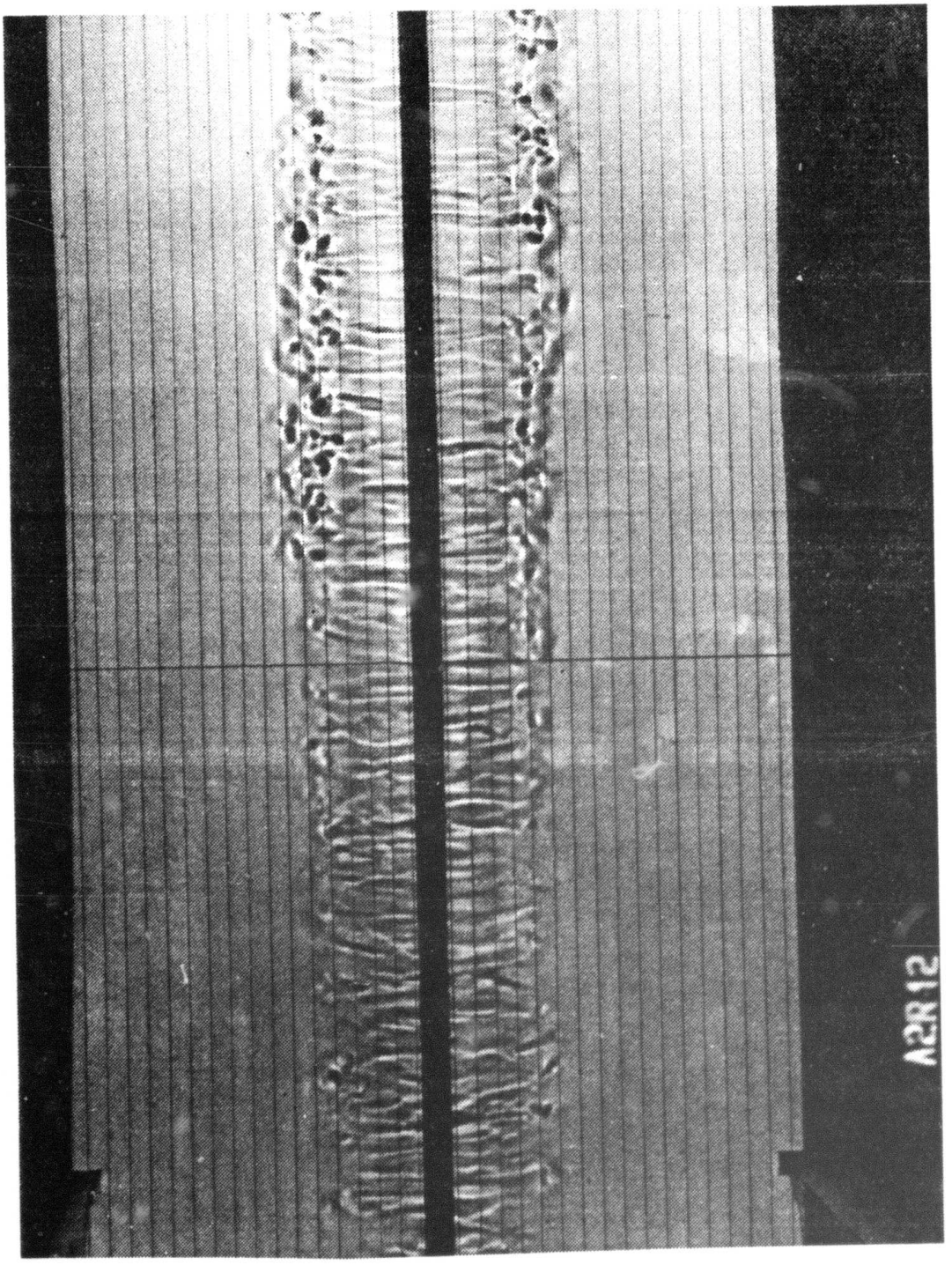

Figure 4. Striations and Scars (Example 1)

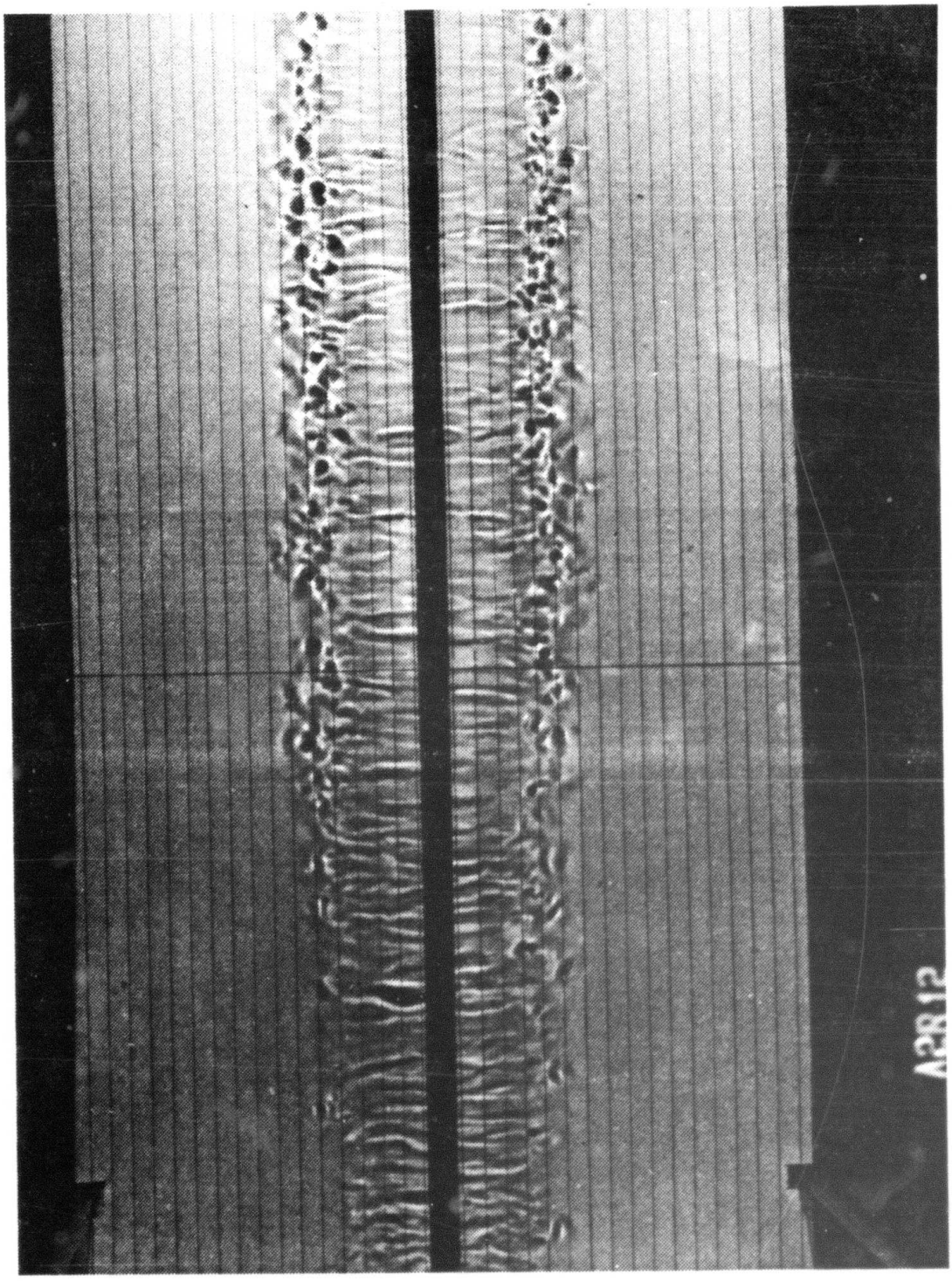

Figure 5. Striations and Scars (Example 2)

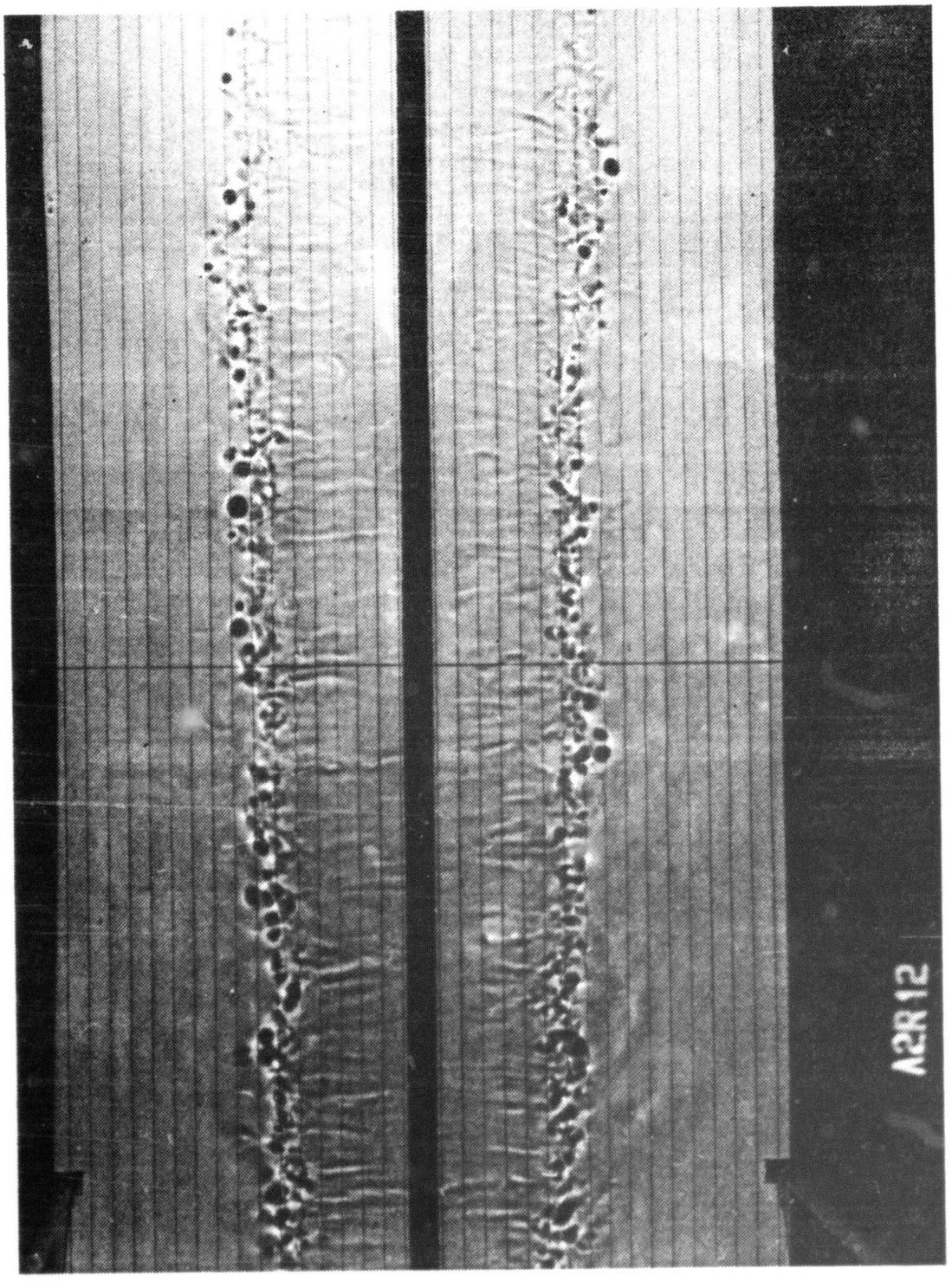

Figure 6. Scars (Example 1)

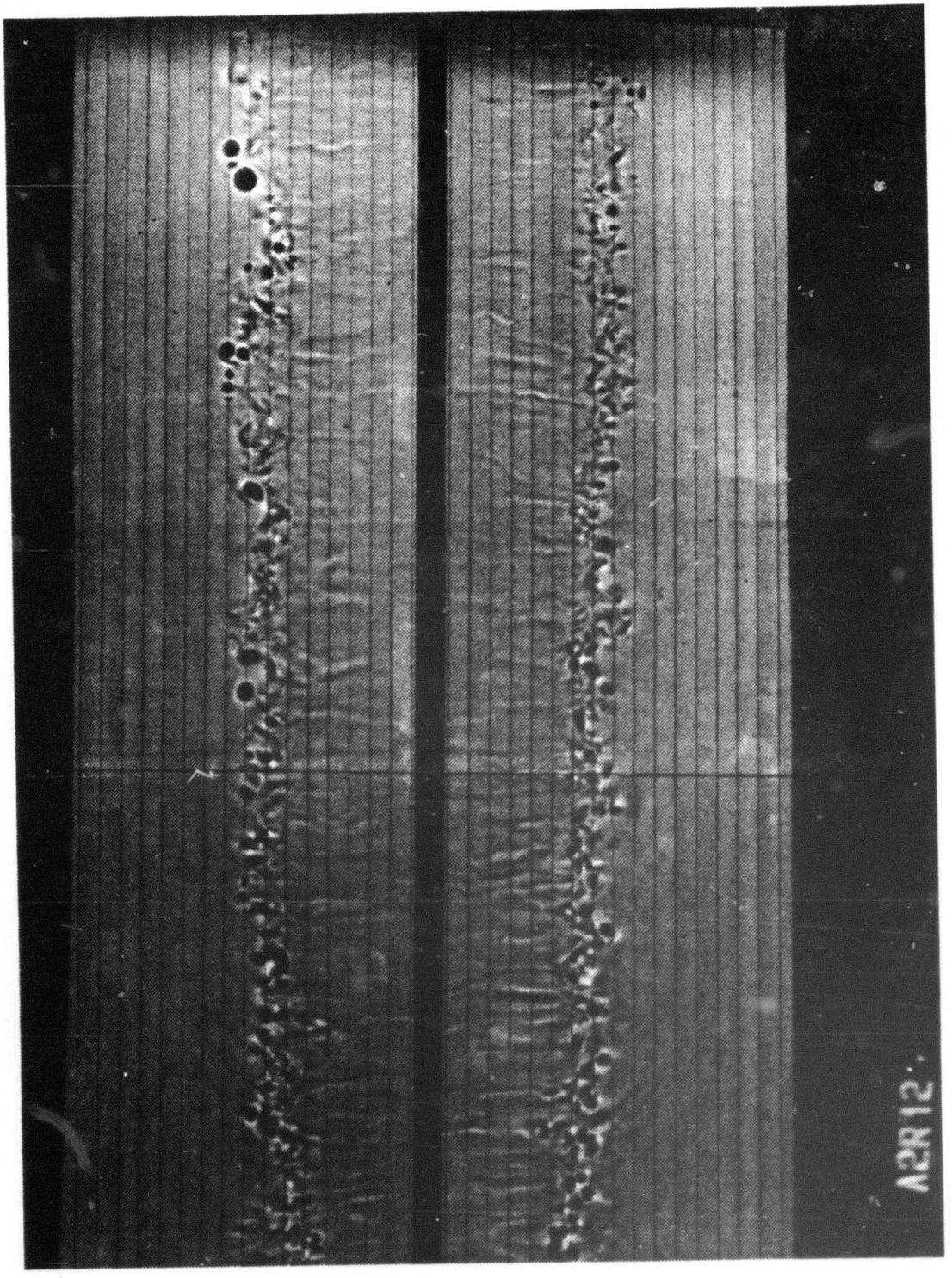

Figure 7. Scars (Example 2)

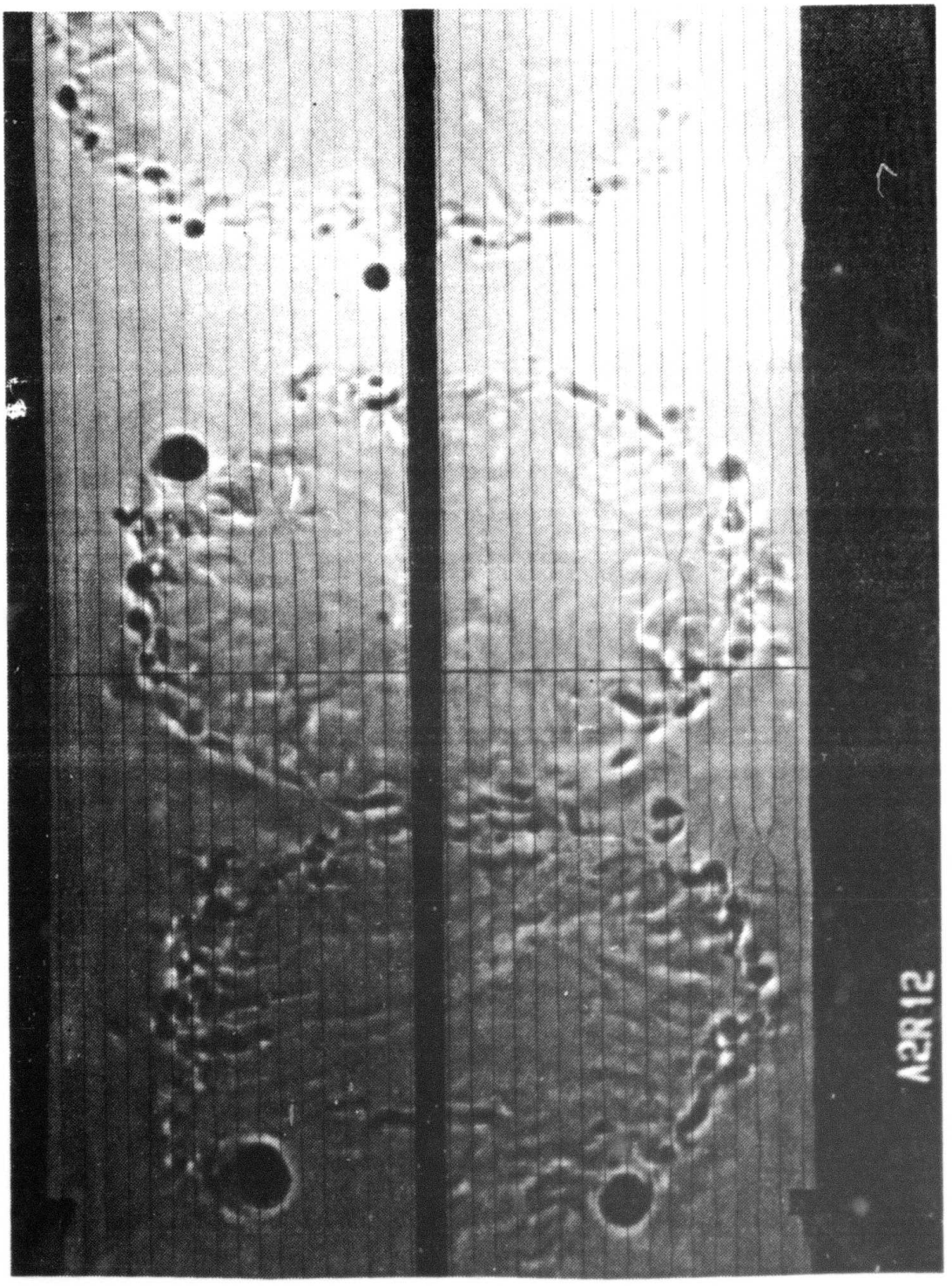

Figure 8. Crow Instability (Example 1)

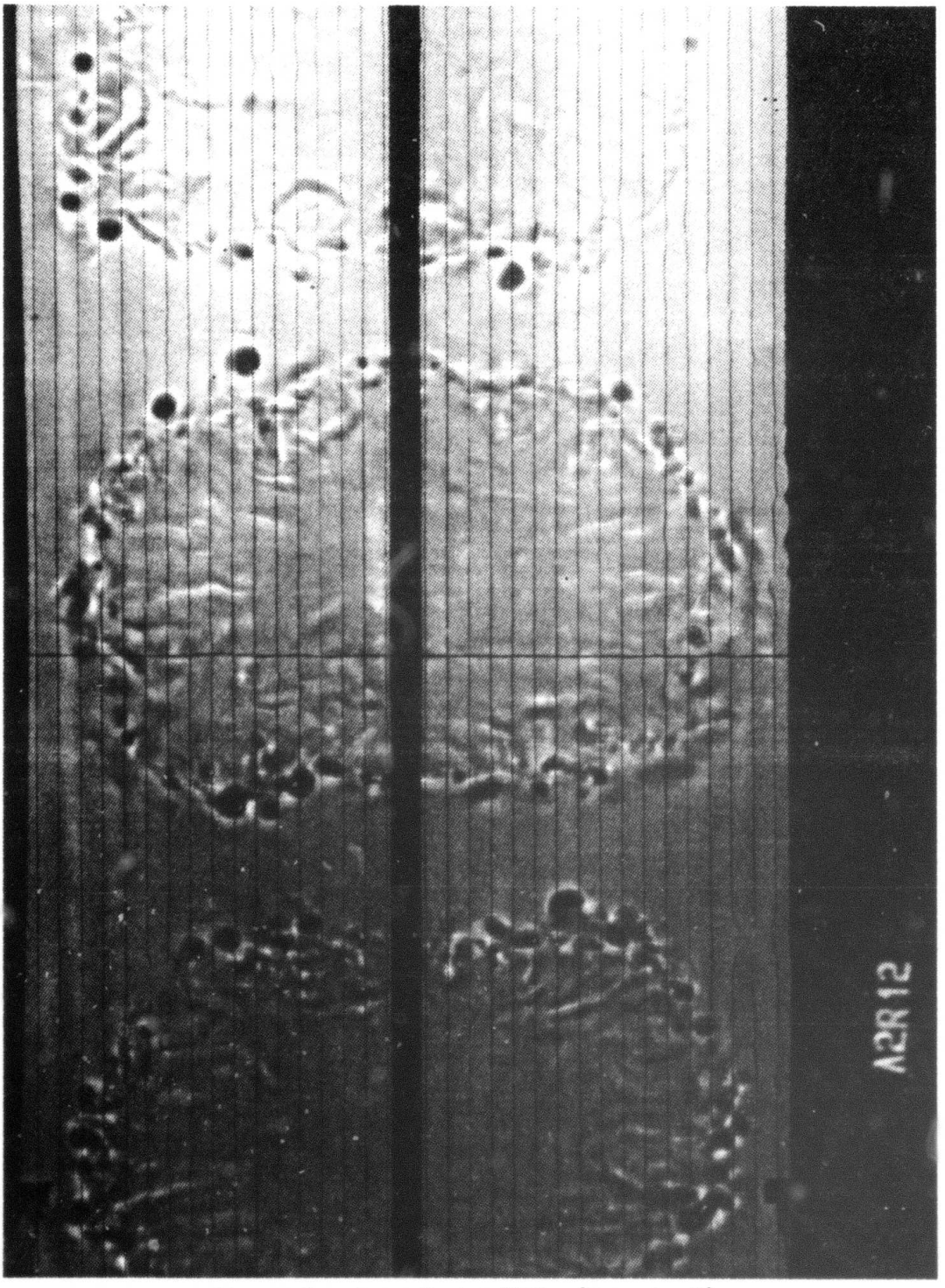

Figure 9. Crow Instability (Example 2)

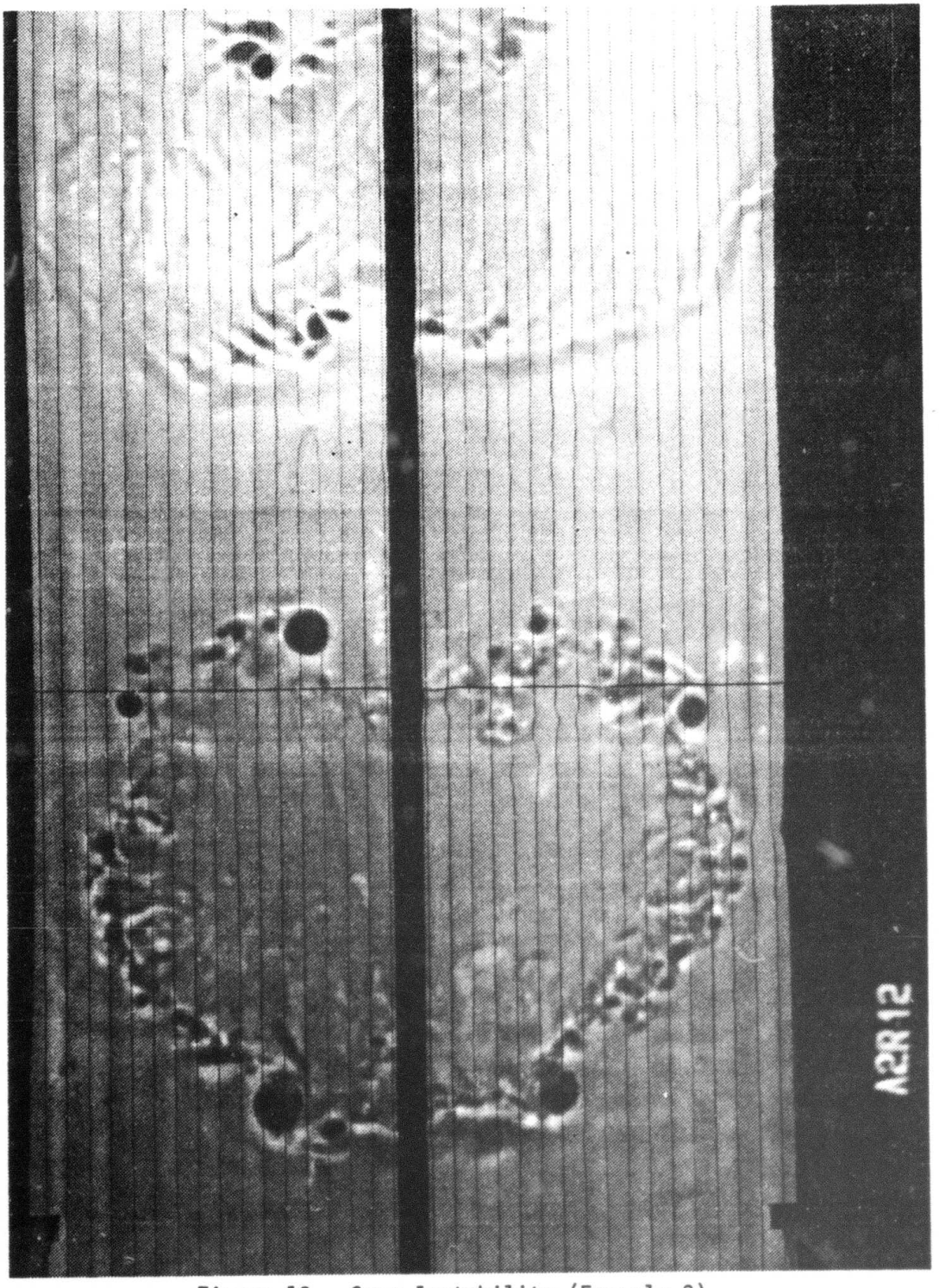

Figure 10. Crow Instability (Example 3)

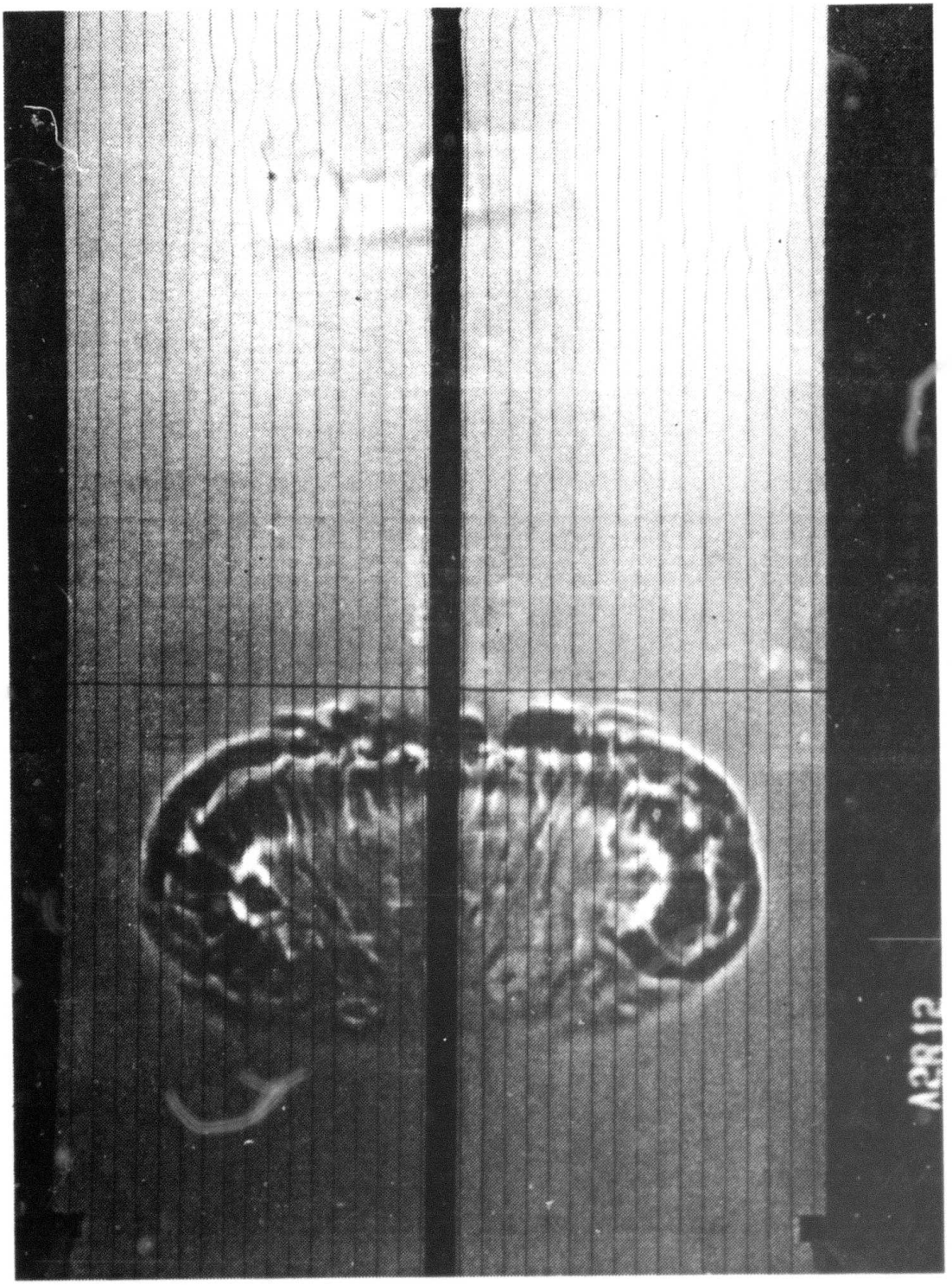

Figure 11. Vortex Ring Approaching Free Surface

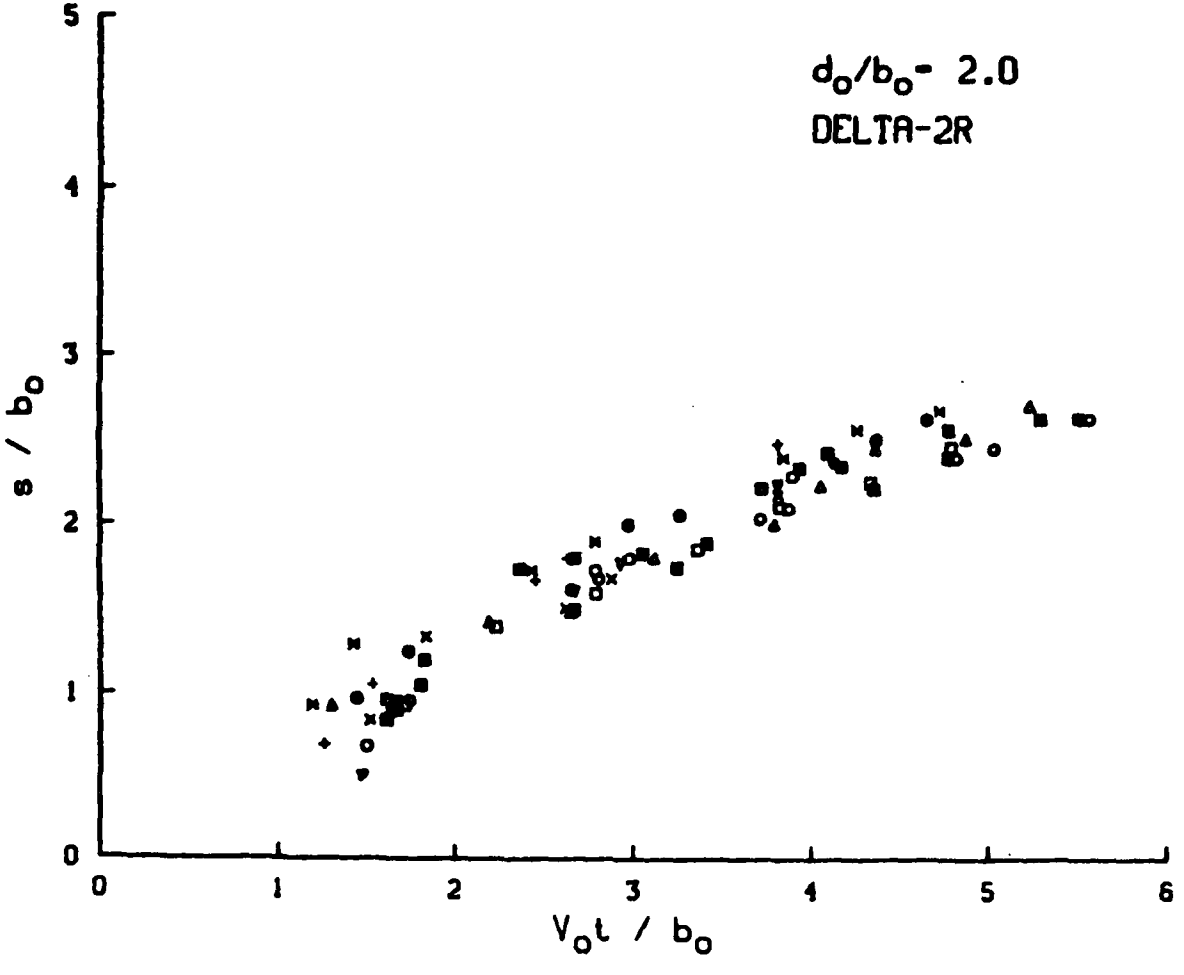

Figure 12. Surface Disturbance Position for Delta-2R, d_o/b_o = 2

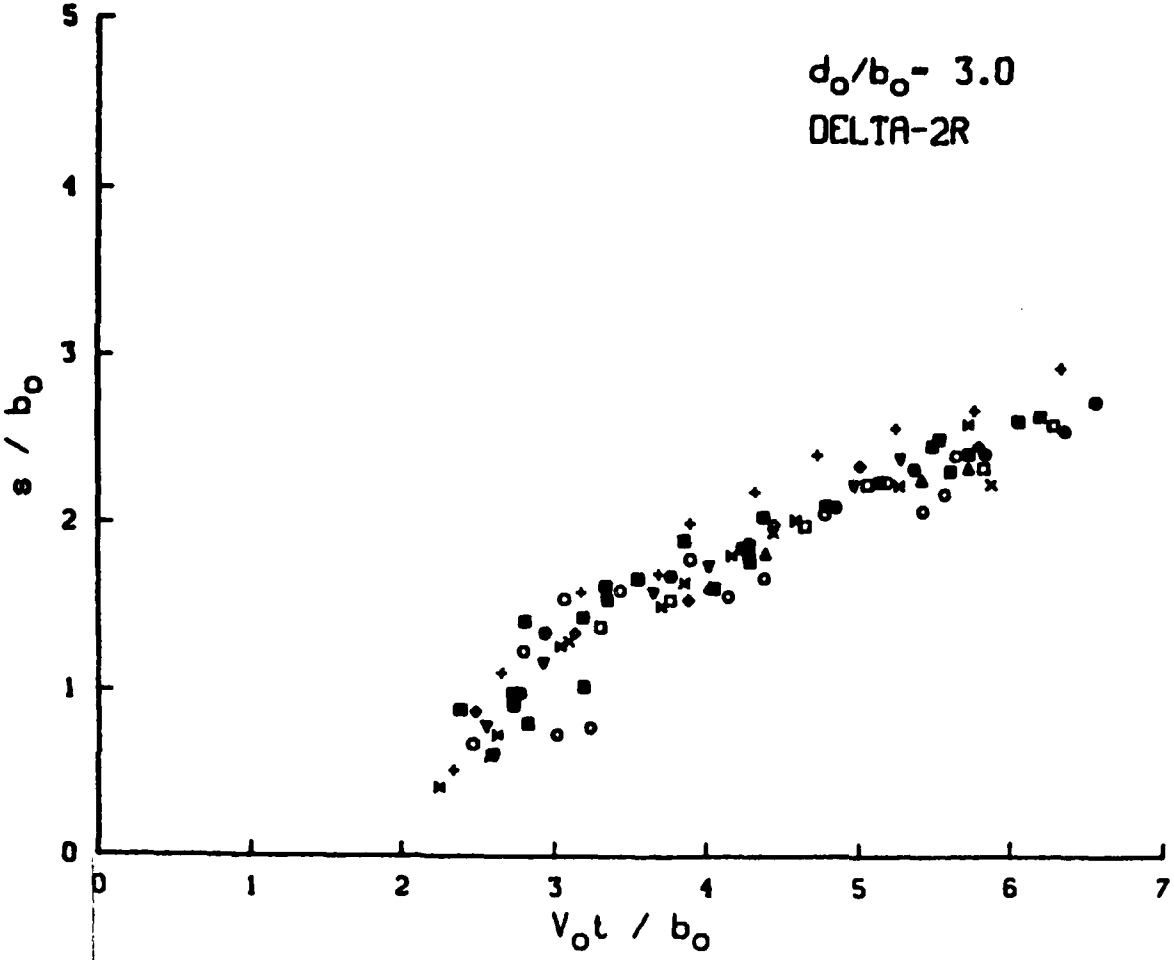

Figure 13. Surface Disturbance Position for Delta-2R, d_o/b_o = 3

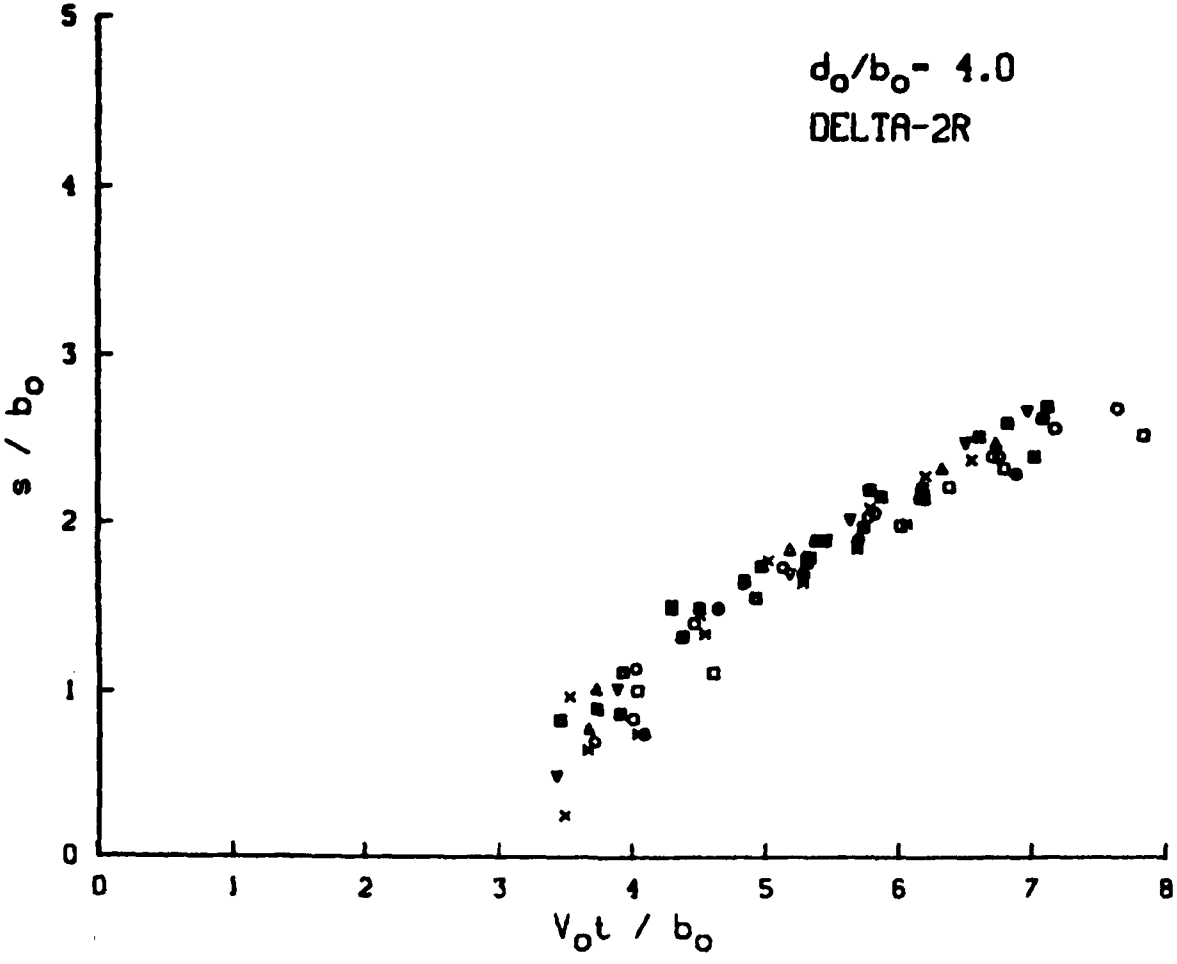

Figure 14. Surface Disturbance Position for Delta-2R, d_o/b_o = 4

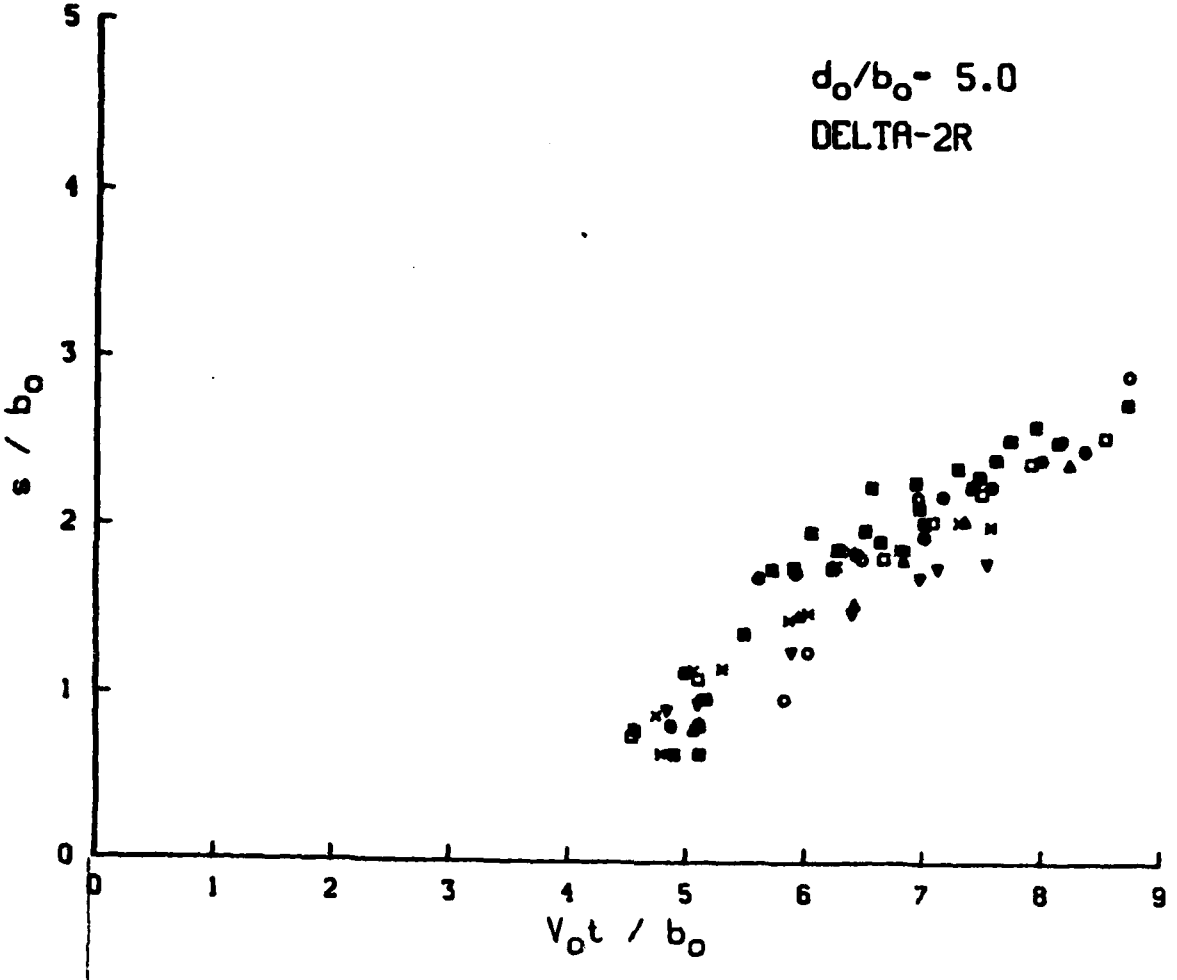

Figure 15. Surface Disturbance Position for Delta-2R, d_o/b_o = 5

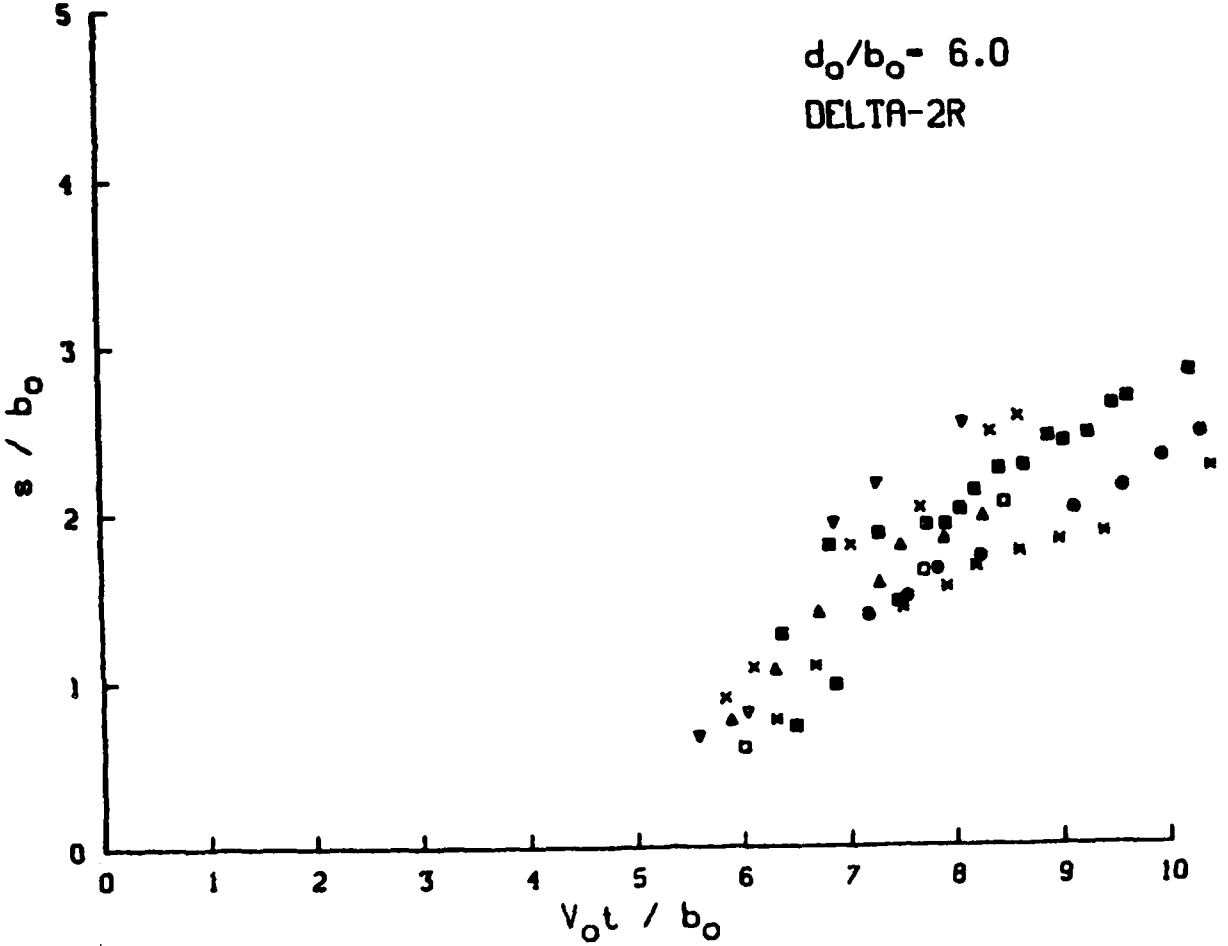

Figure 16. Surface Disturbance Position for Delta-2R, d_o/b_o = 6

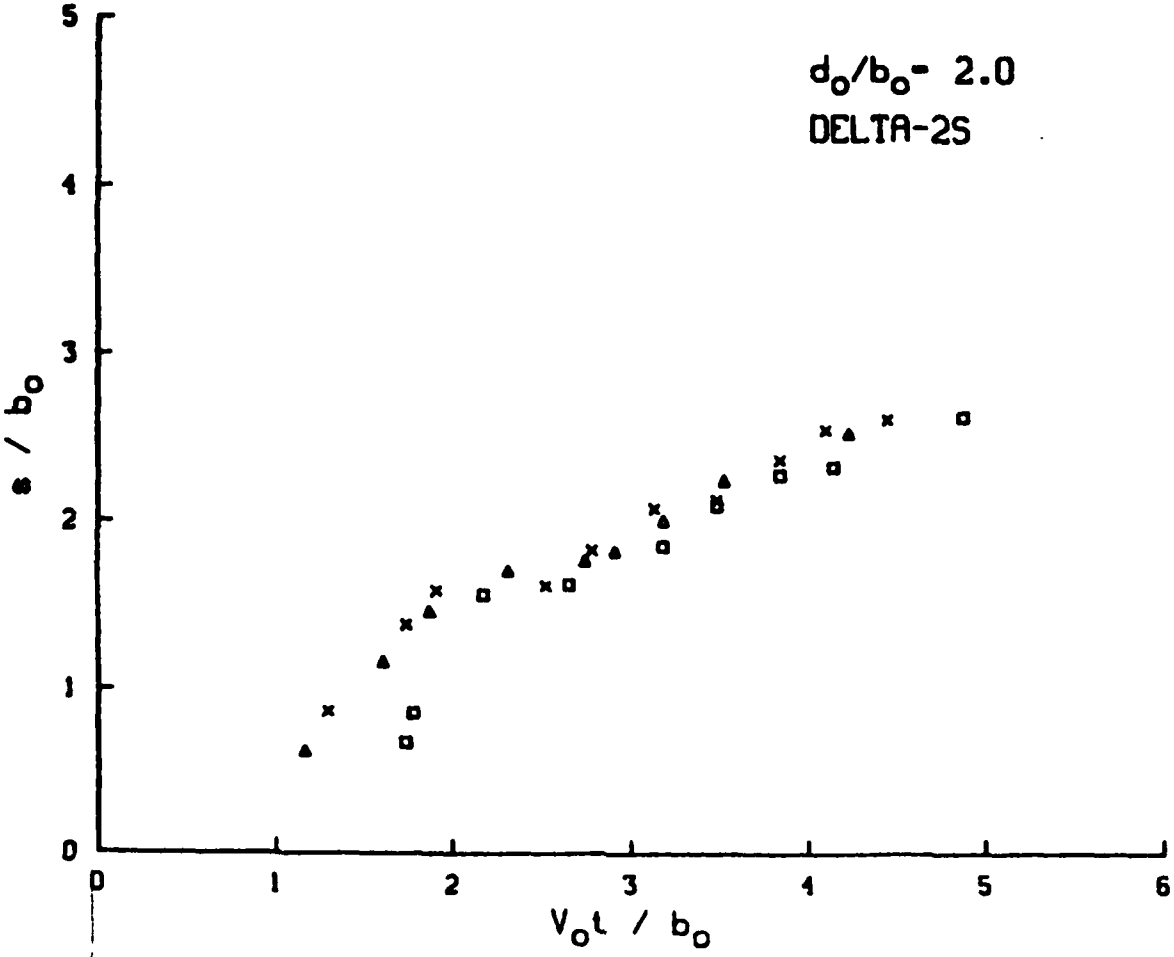

Figure 17. Surface Disturbance Position for Delta-2S, d_o/b_o = 2

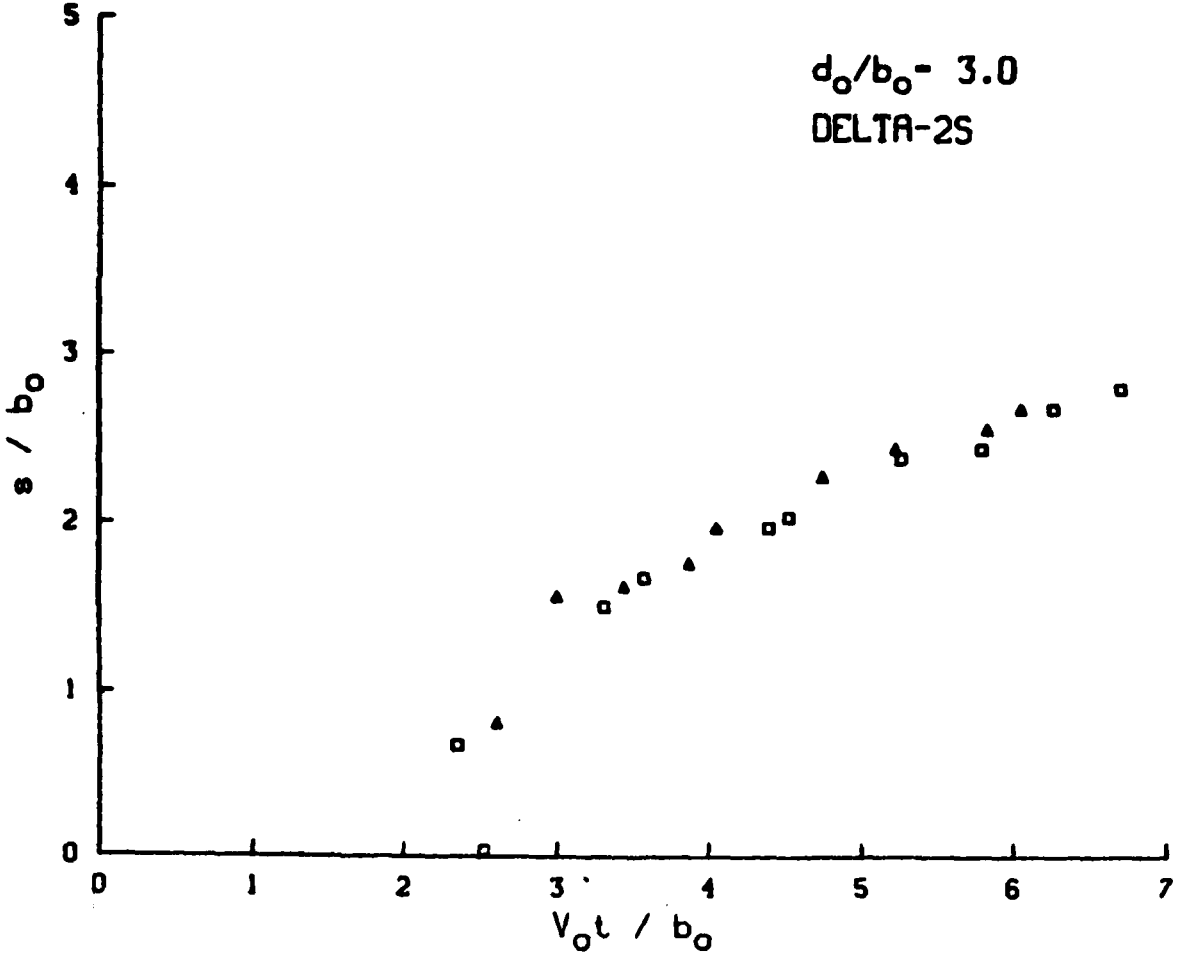

Figure 18. Surface Disturbance Position for Delta-2S, d_o/b_o = 3

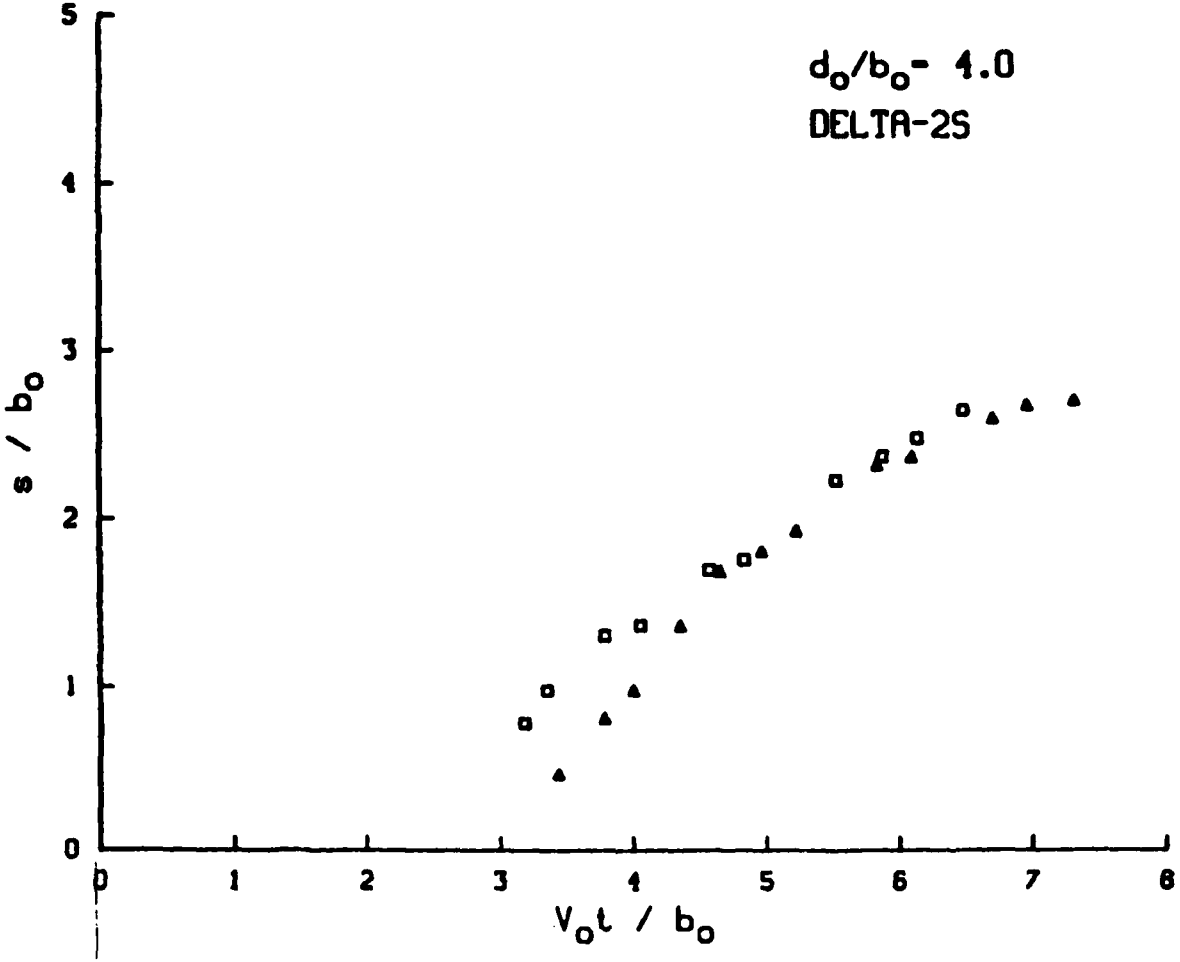

Figure 19. Surface Disturbance Position for Delta-2S, d_o/b_o = 4

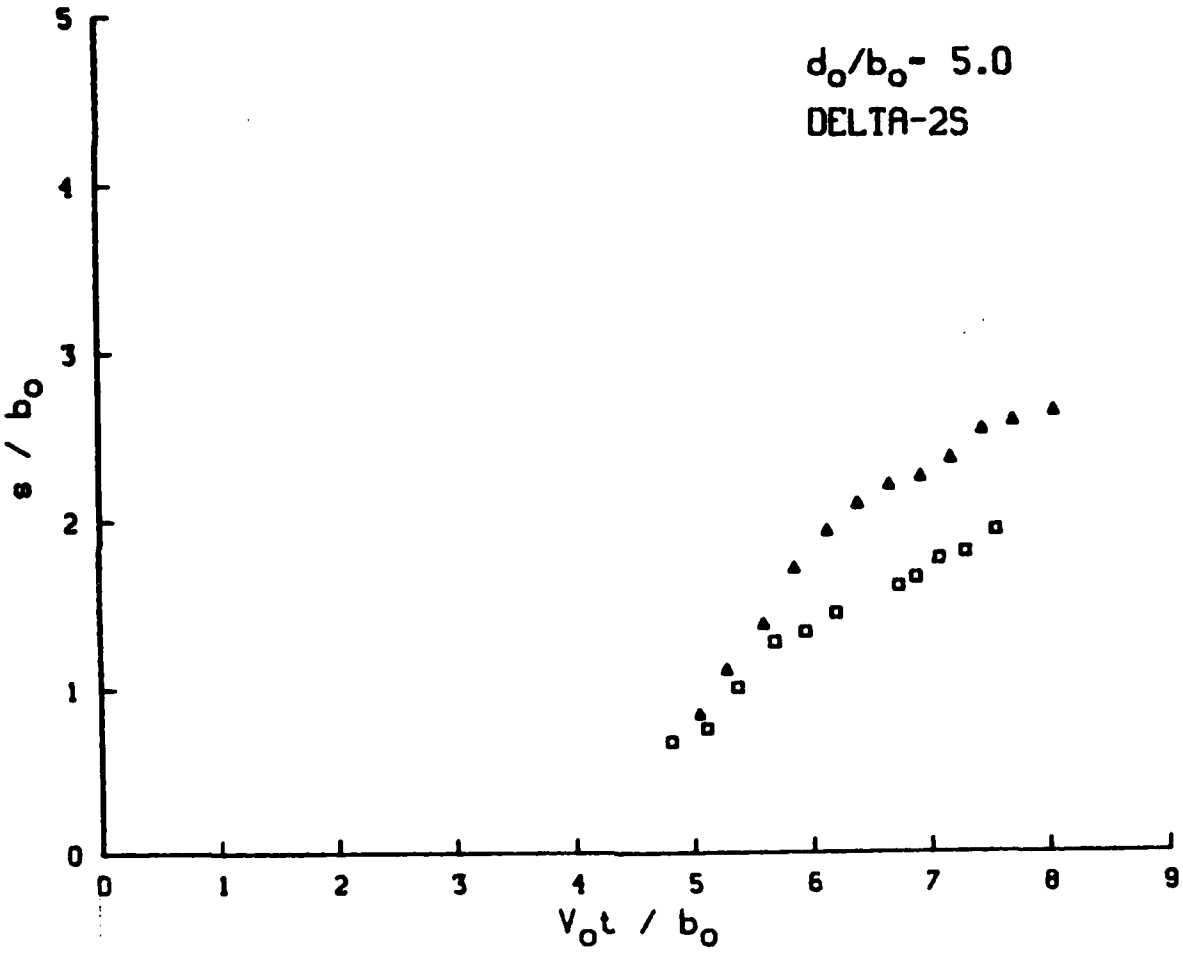

Figure 20. Surface Disturbance Position for Delta-2S, d_o/b_o = 5

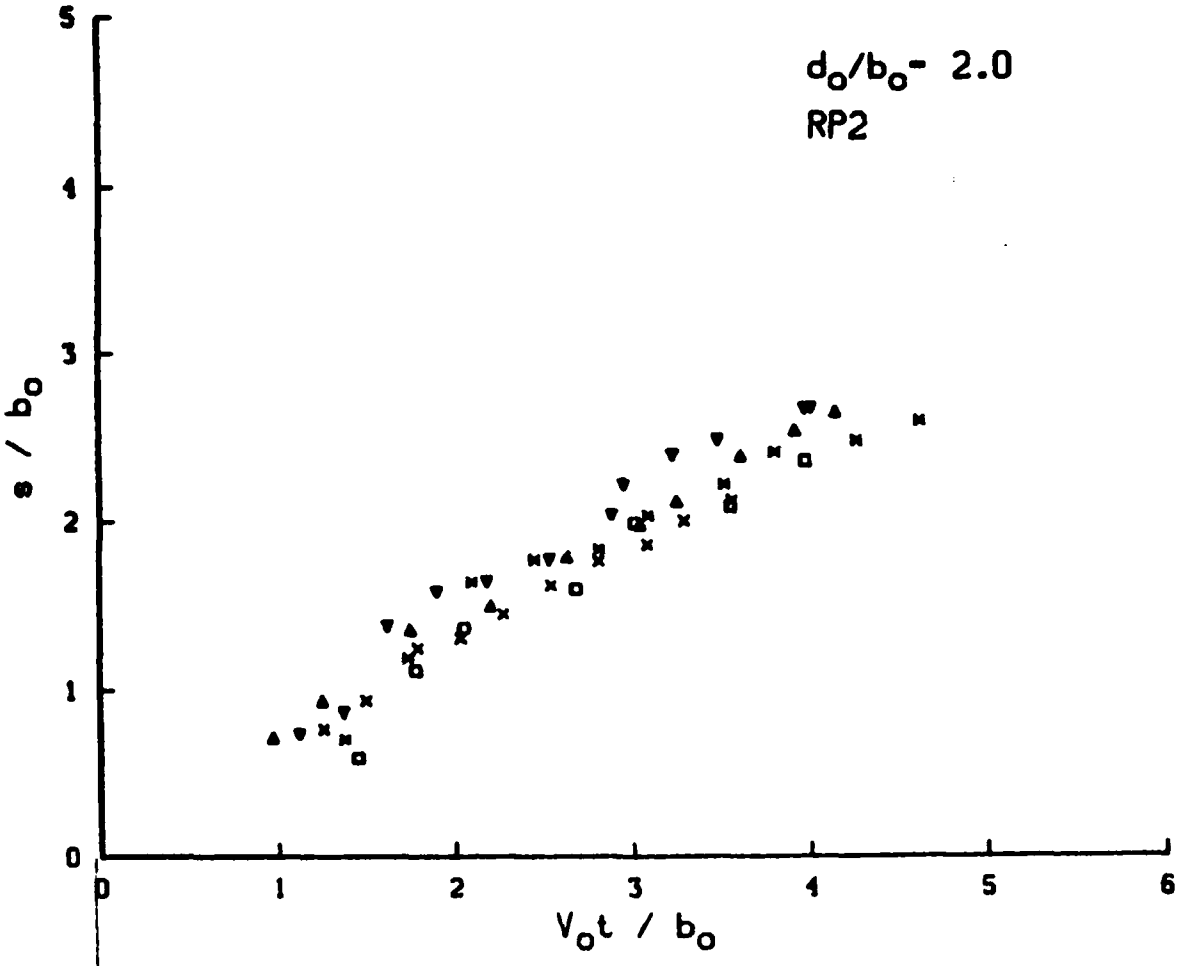

Figure 21. Surface Disturbance Position for RP2, d_0/b_0 = 2

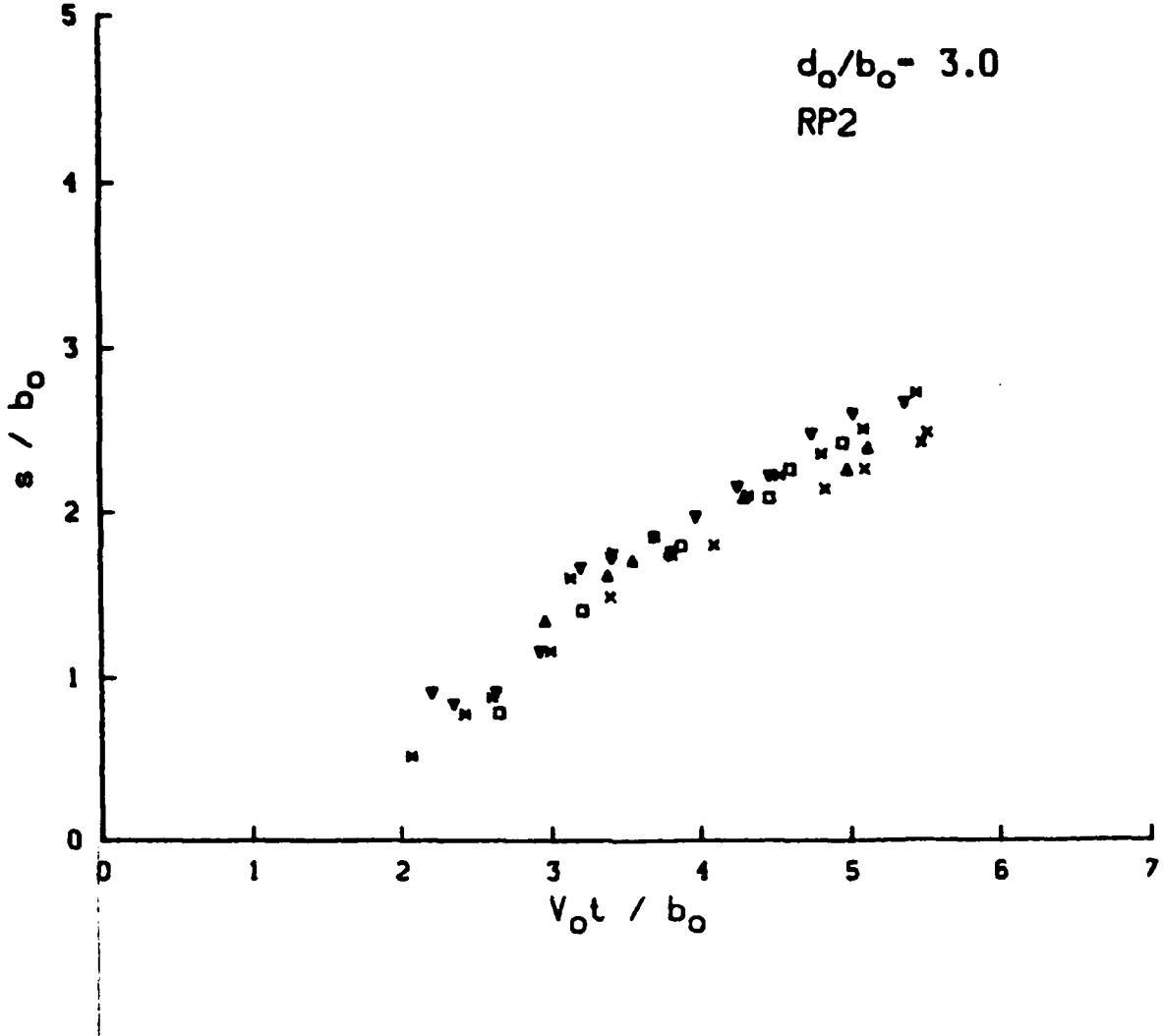

Figure 22. Surface Disturbance Position for RP2, d_o/b_o = 3

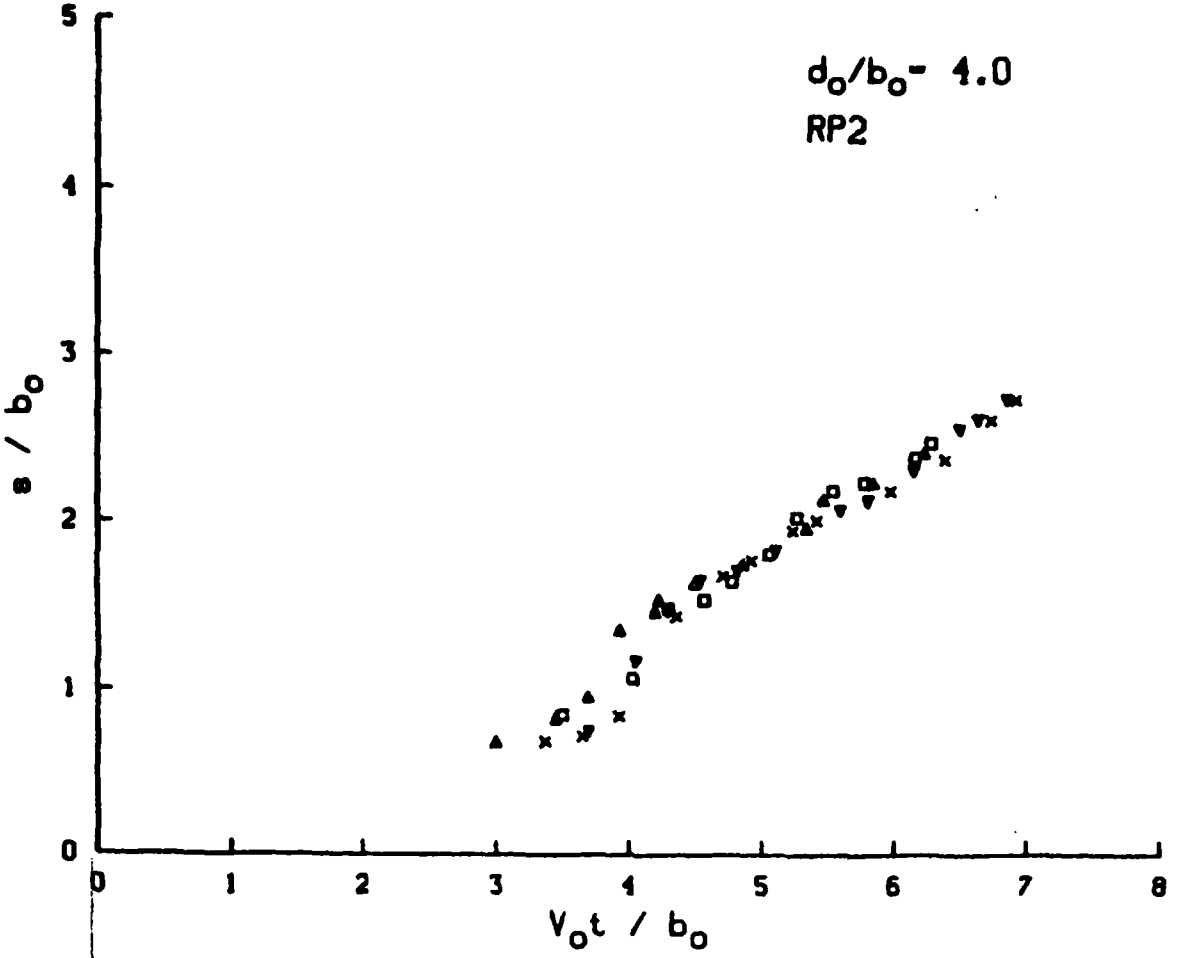

Figure 23. Surface Disturbance Position for RP2, d_o/b_o = 4

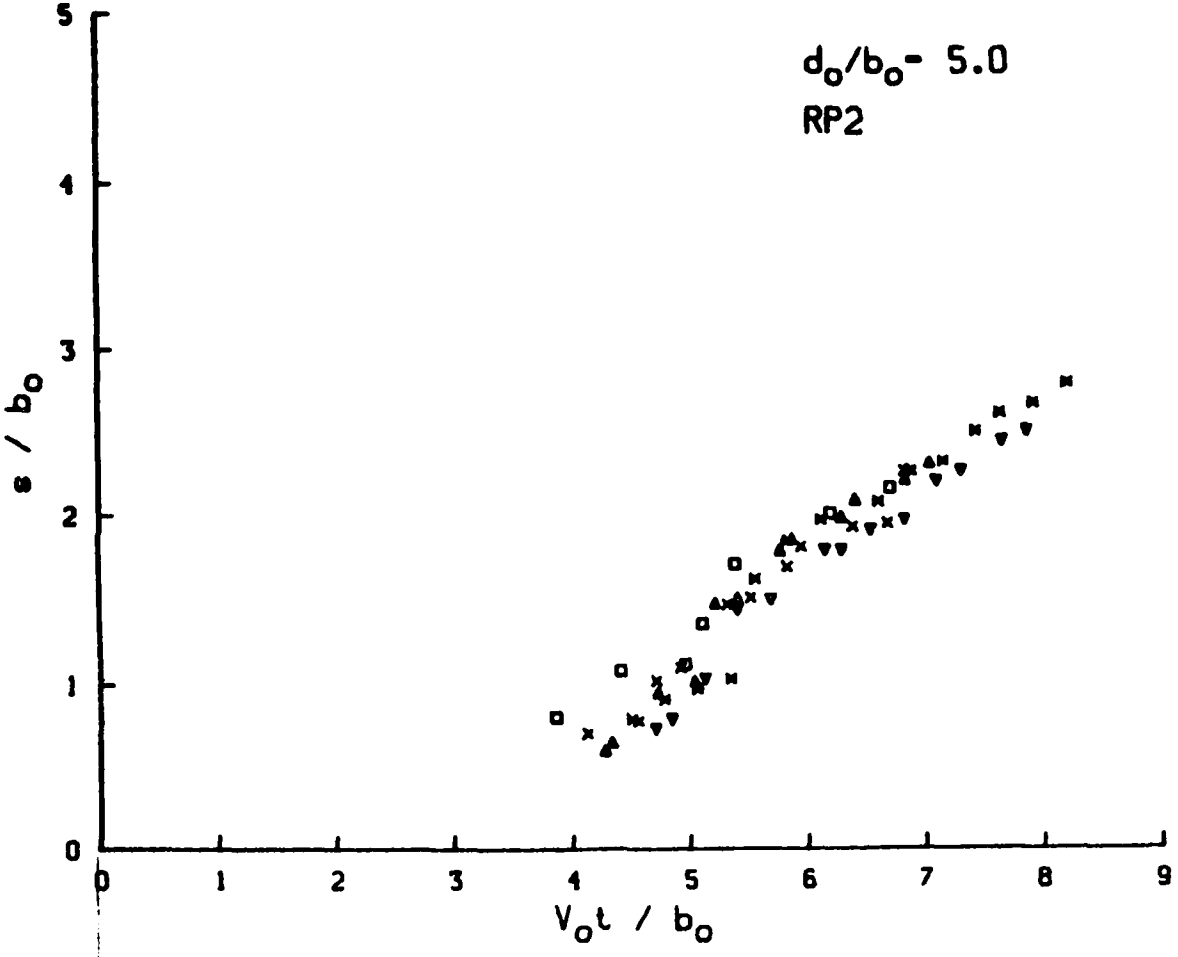

Figure 24. Surface Disturbance Position for RP2, d_o/b_o = 5

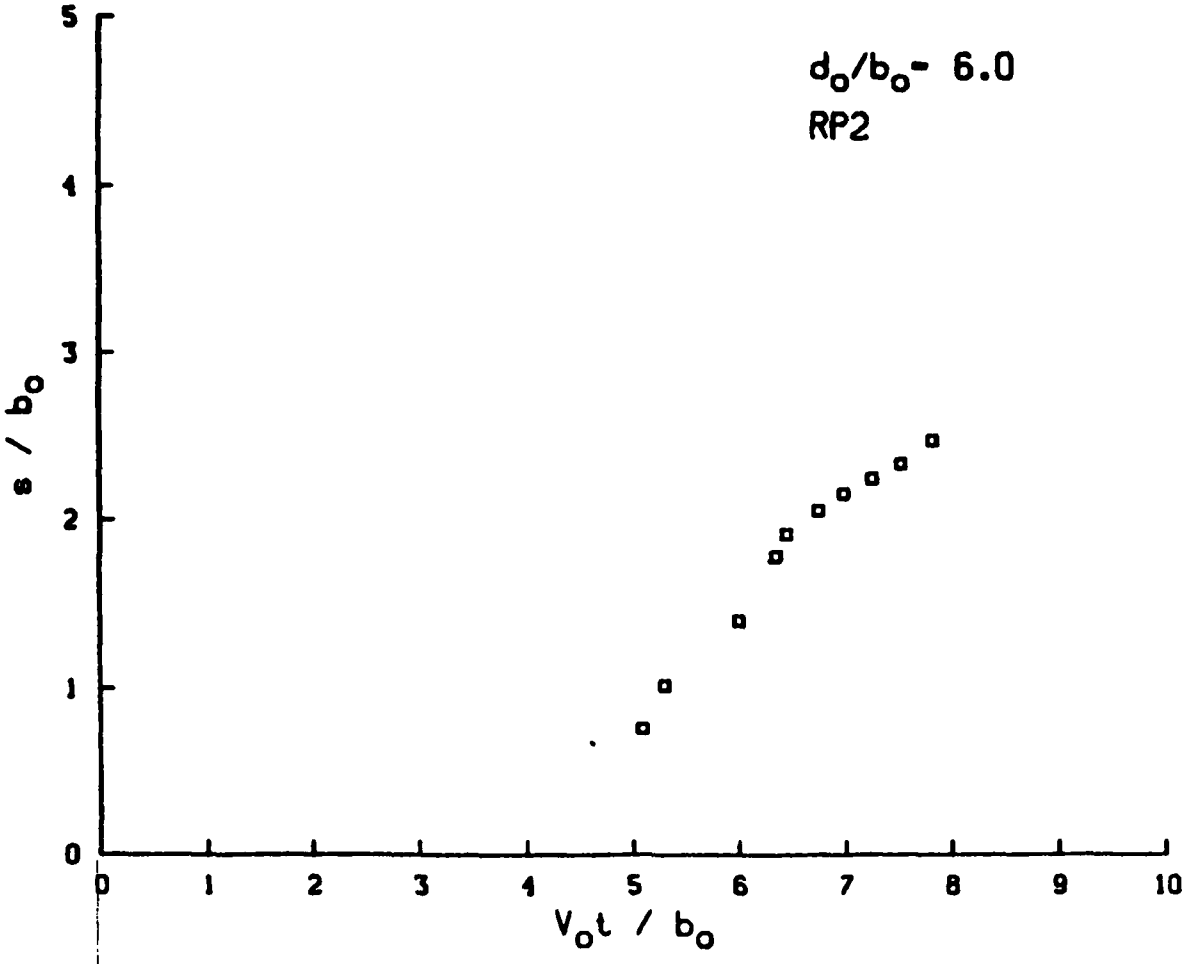

Figure 25. Surface Disturbance Position for RP2, d_o/b_o = 6

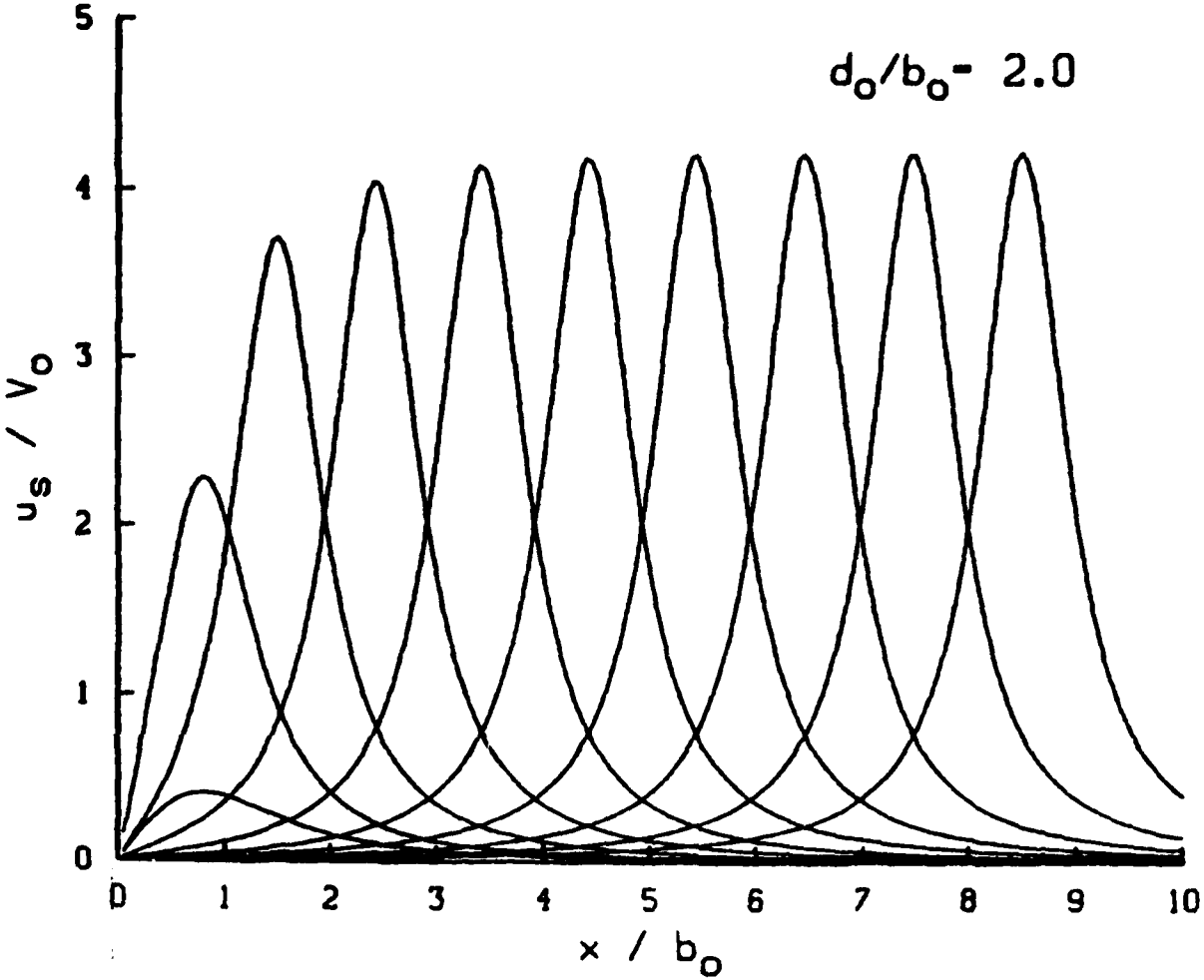

Figure 26. Surface Velocity Profile, d_o/b_o = 2, Inviscid Model

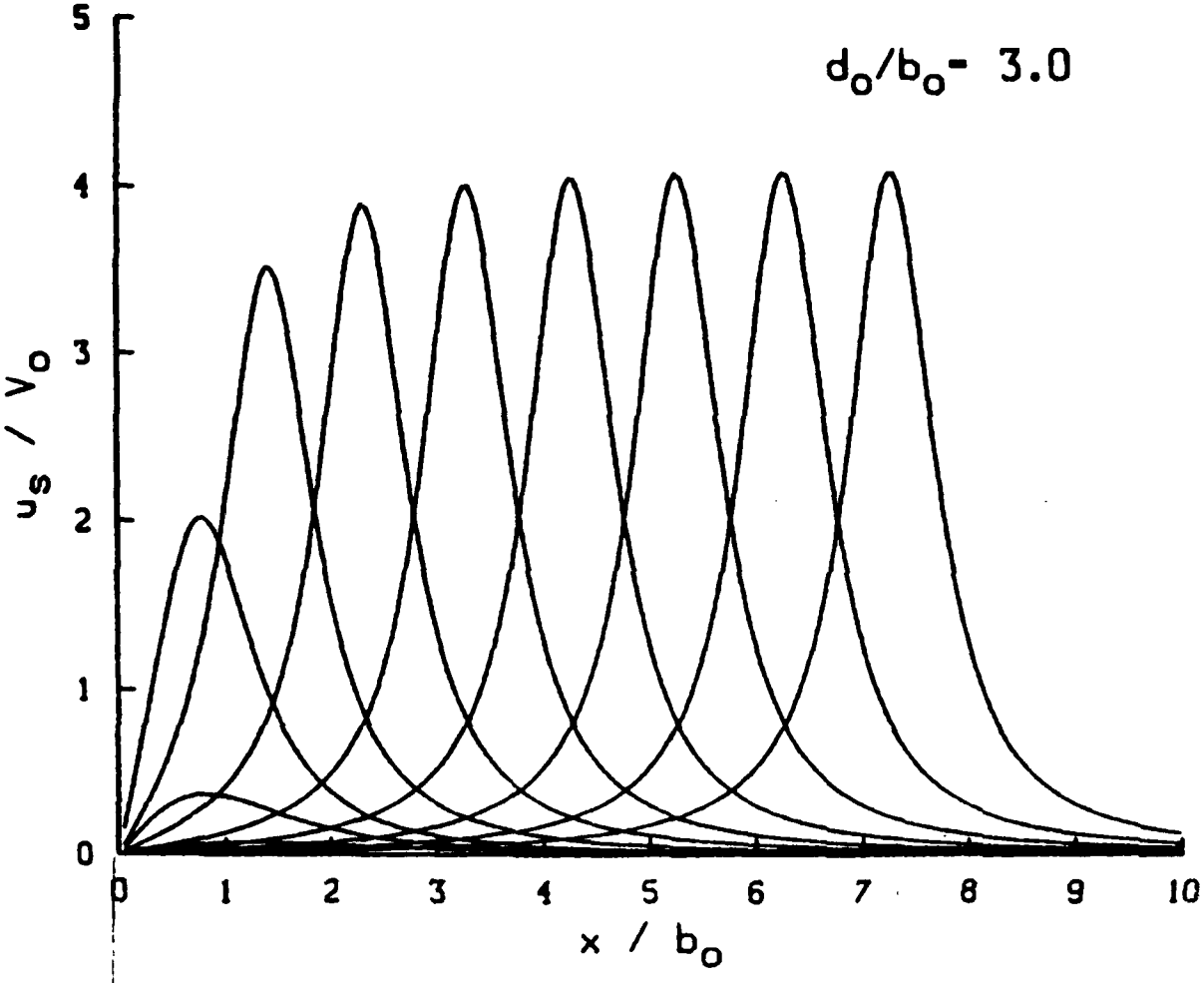

Figure 27. Surface Velocity Profile, d_o/b_o = 3, Inviscid Model

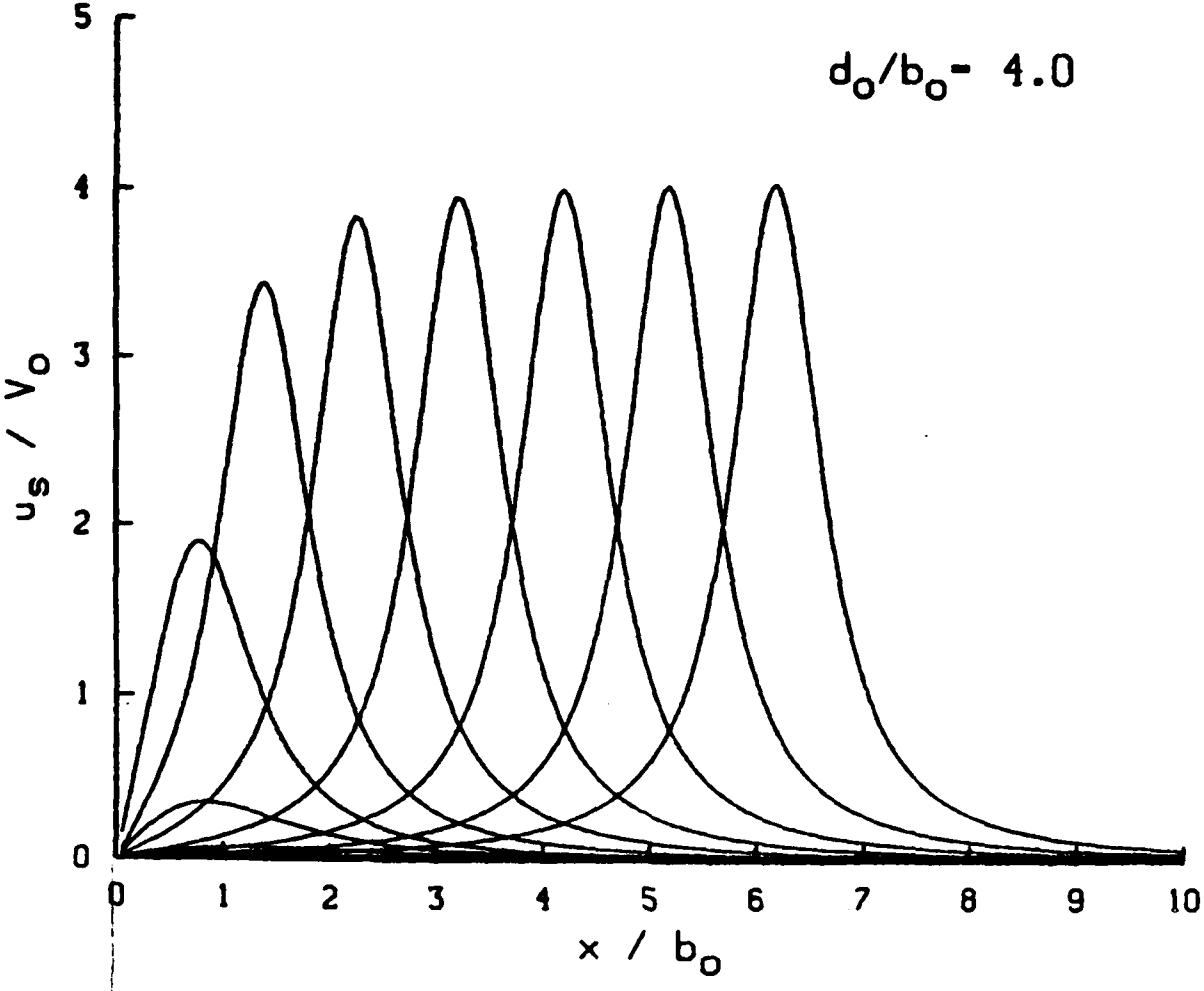

Figure 28. Surface Velocity Profile, d_o/b_o = 4, Inviscid Model

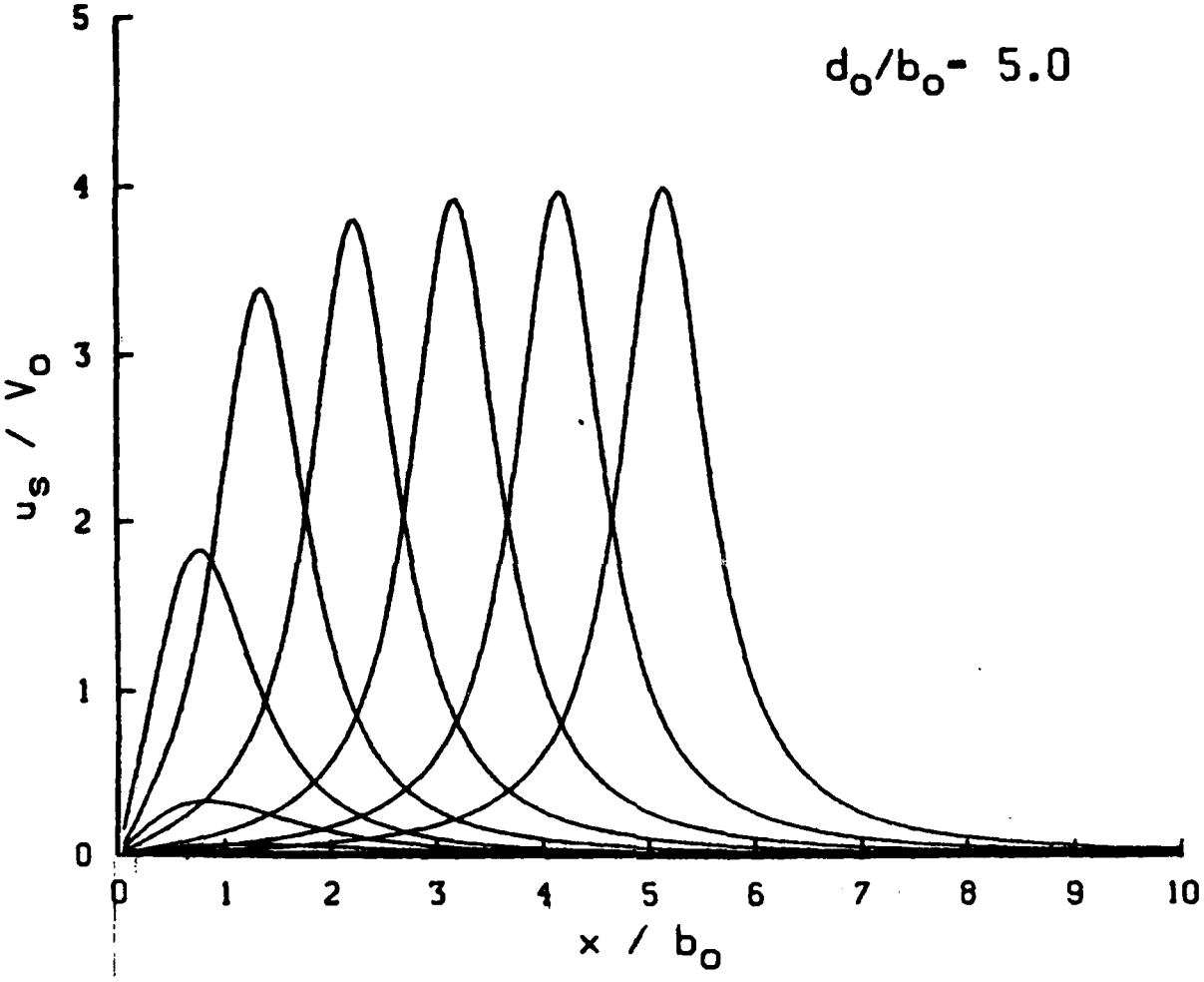

Figure 29. Surface Velocity Profile, d_o/b_o = 5, Inviscid Model

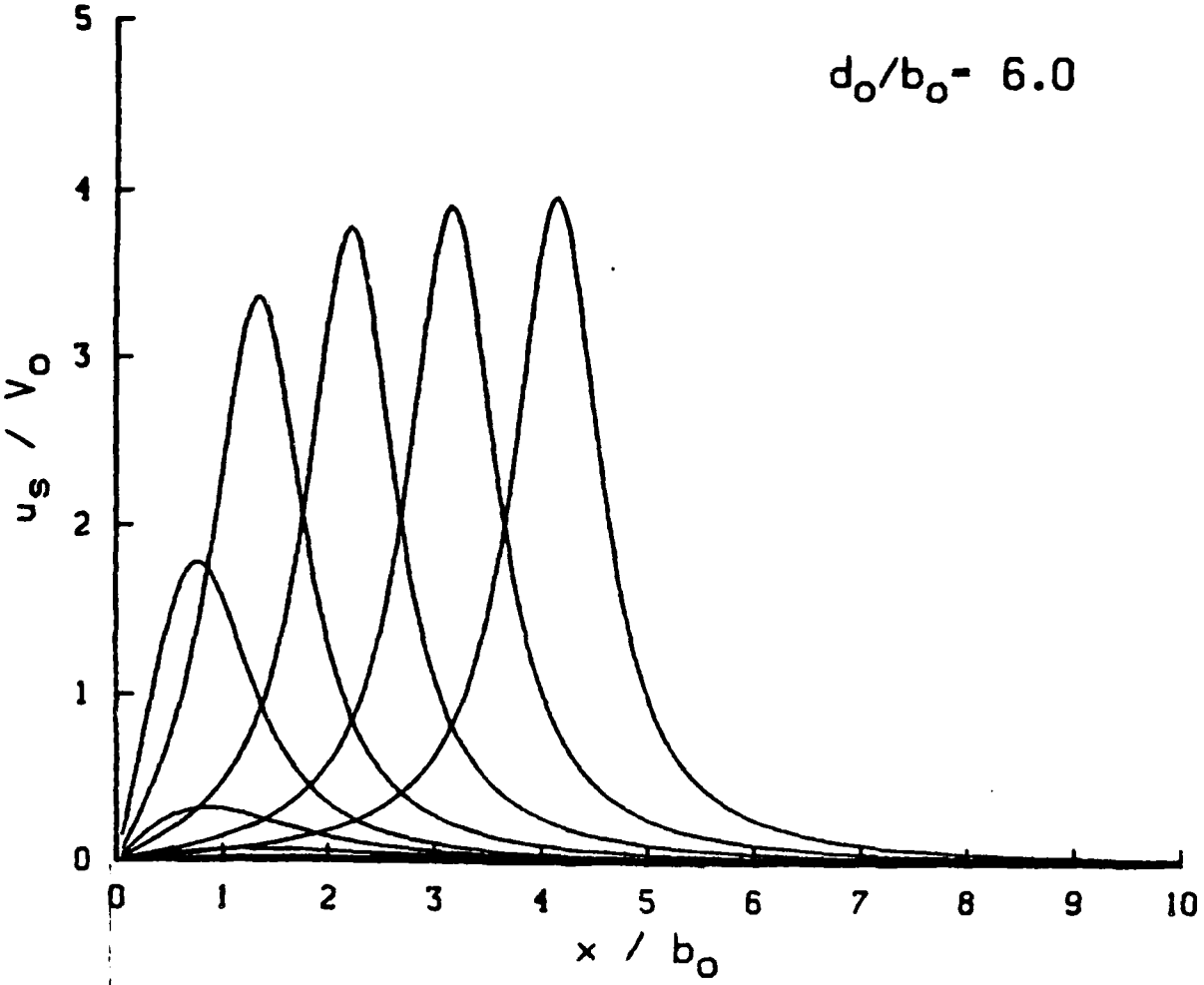

Figure 30. Surface Velocity Profile, d_o/b_o = 6, Inviscid Model

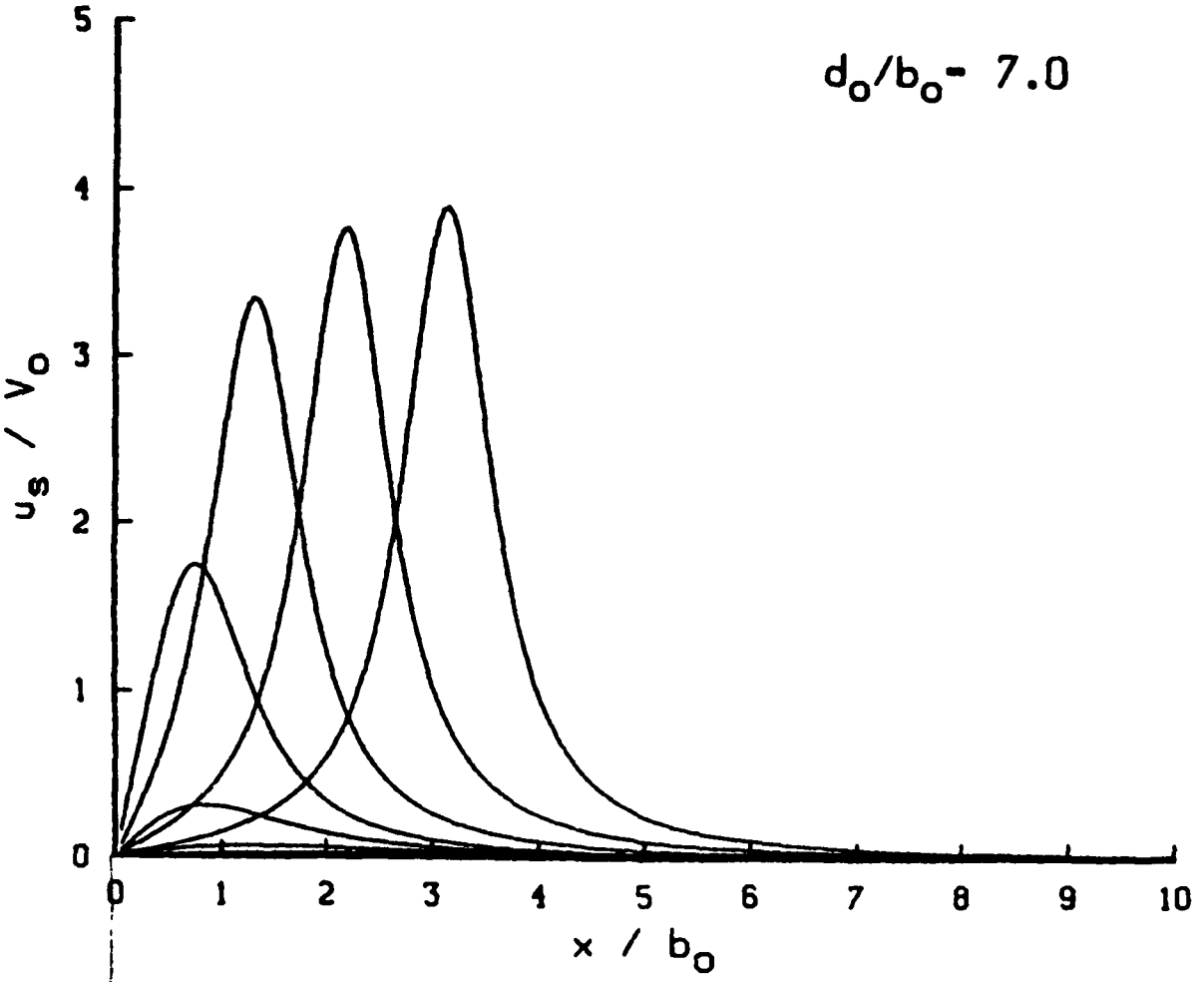

Figure 31. Surface Velocity Profile, d_o/b_o = 7, Inviscid Model

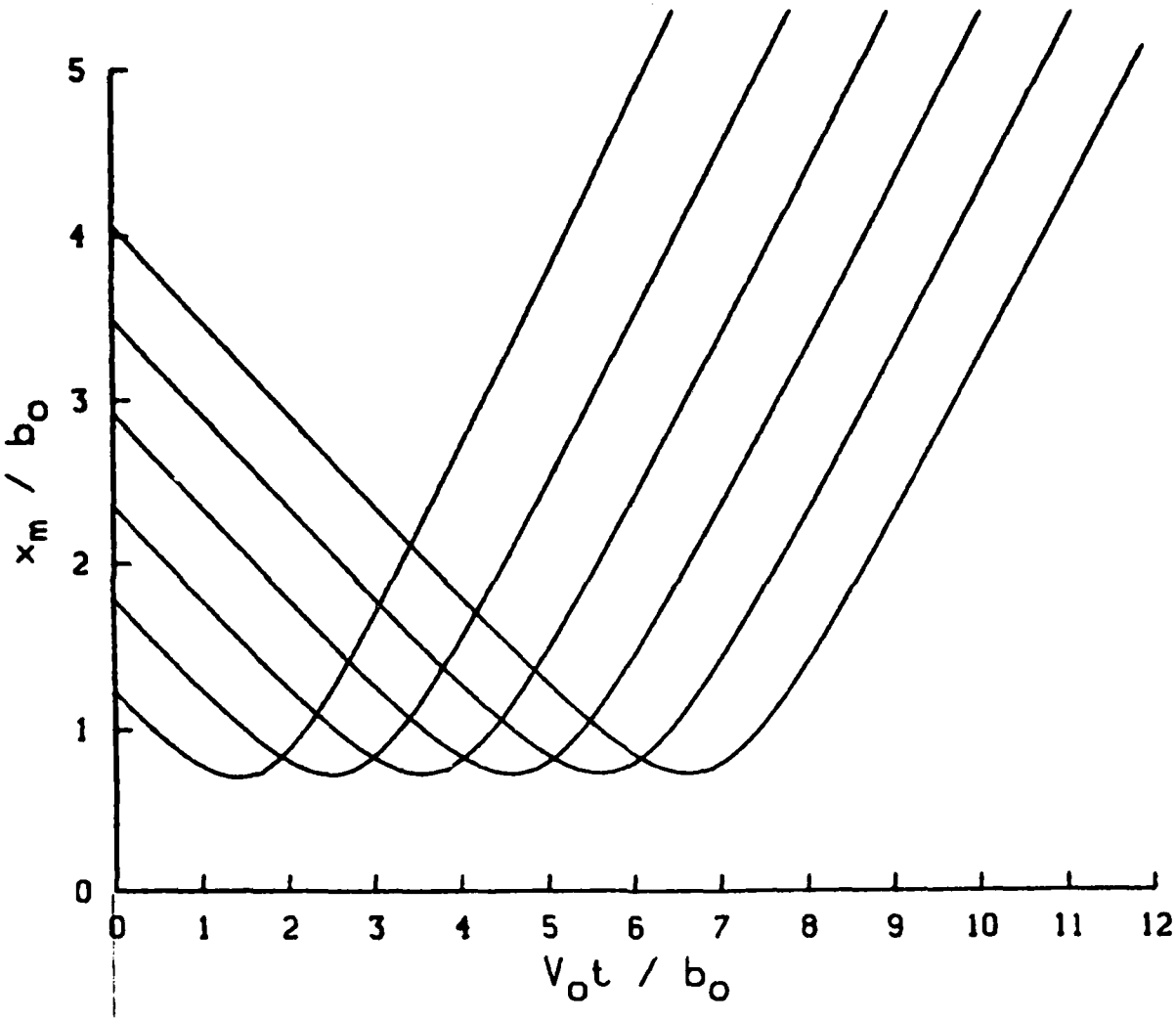

Figure 32. Position of Maximum Surface Velocity, Inviscid Model, d_o/b_o = 2 through 7

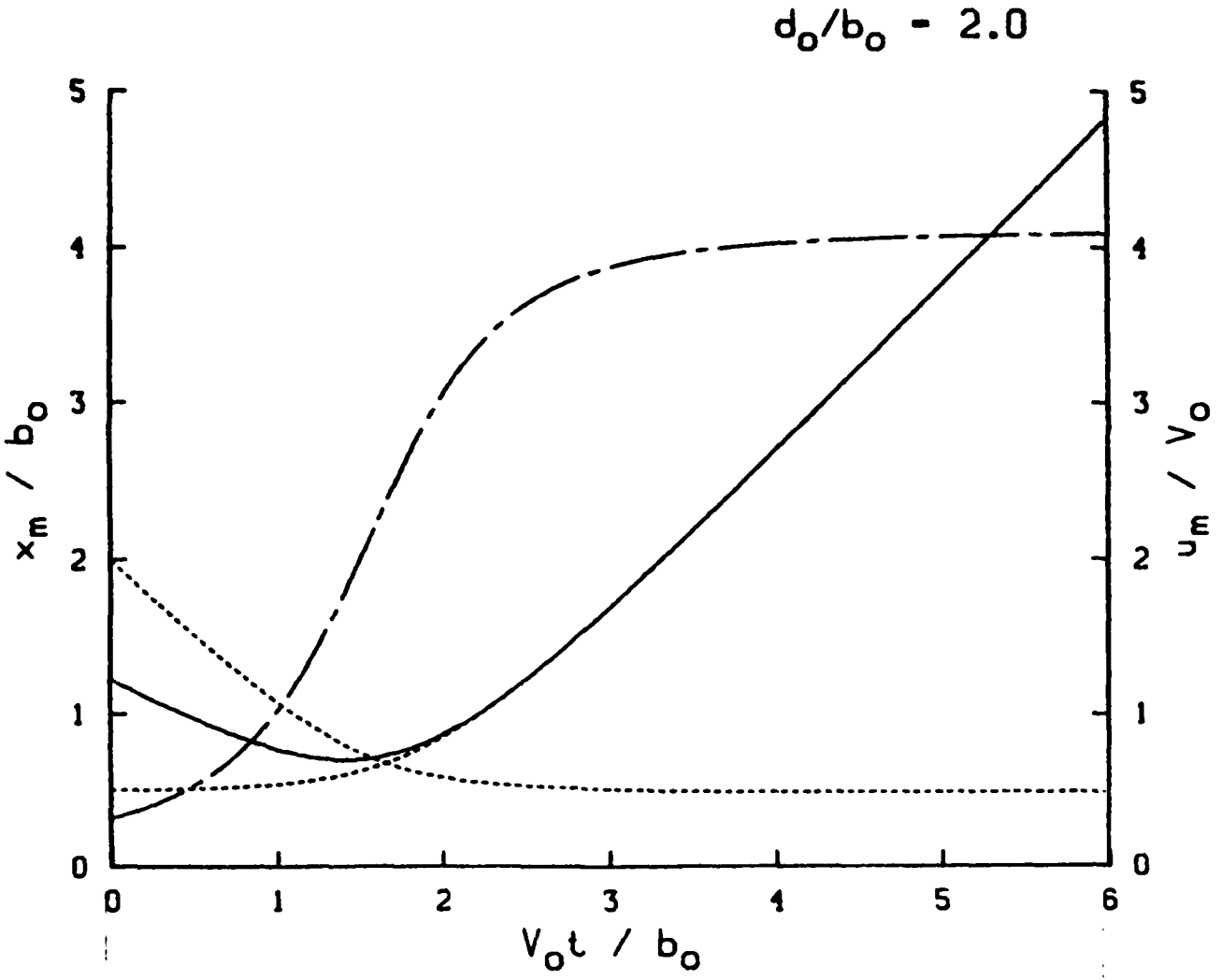

Figure 33. Position of Maximum Surface Velocity, Vortex Position, and Maximum Velocity, Inviscid Model, $d_o/b_o = 2$

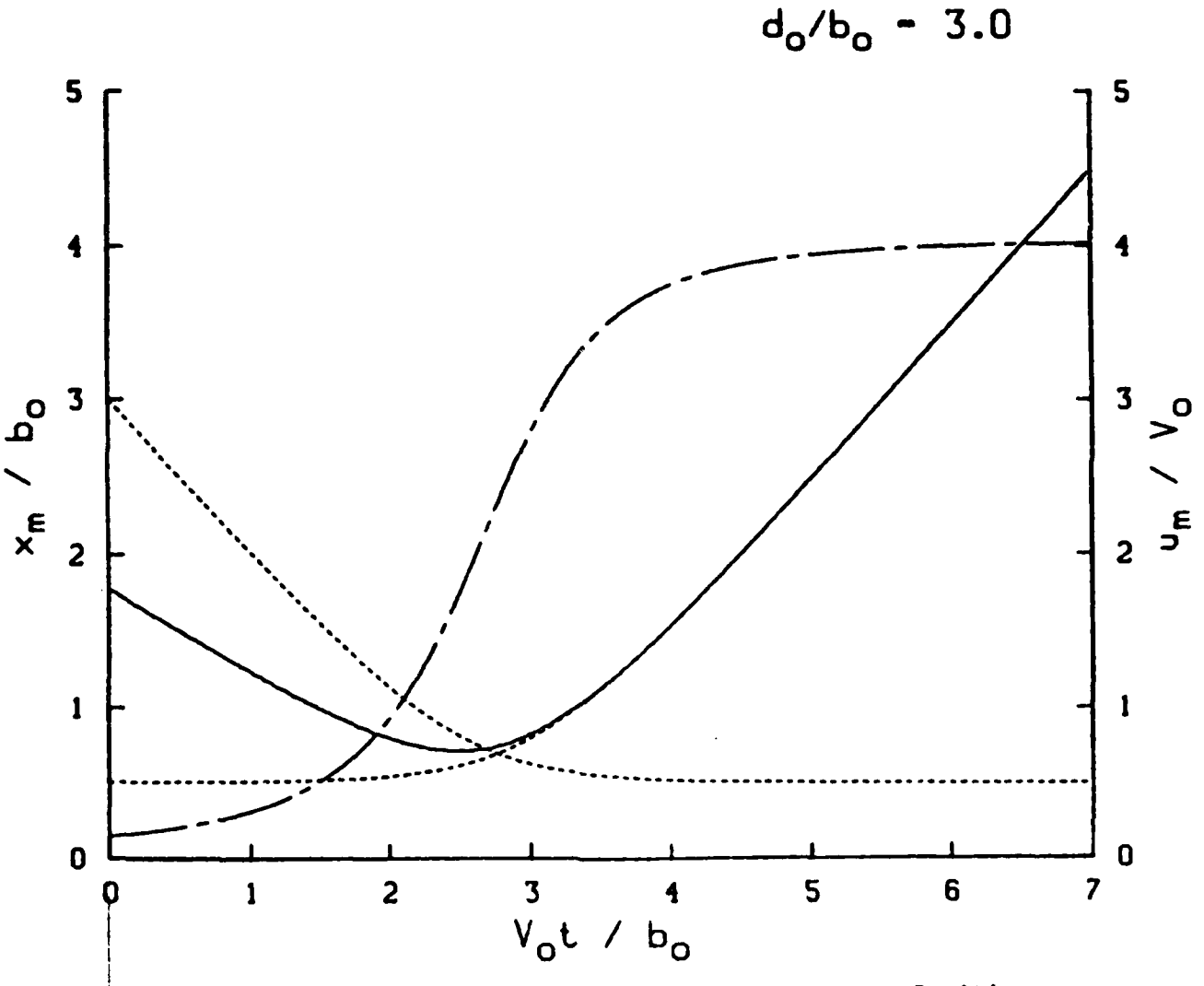

Figure 34. Position of Maximum Surface Velocity, Vortex Position, and Maximum Velocity, Inviscid Model, d_o/b_o = 3

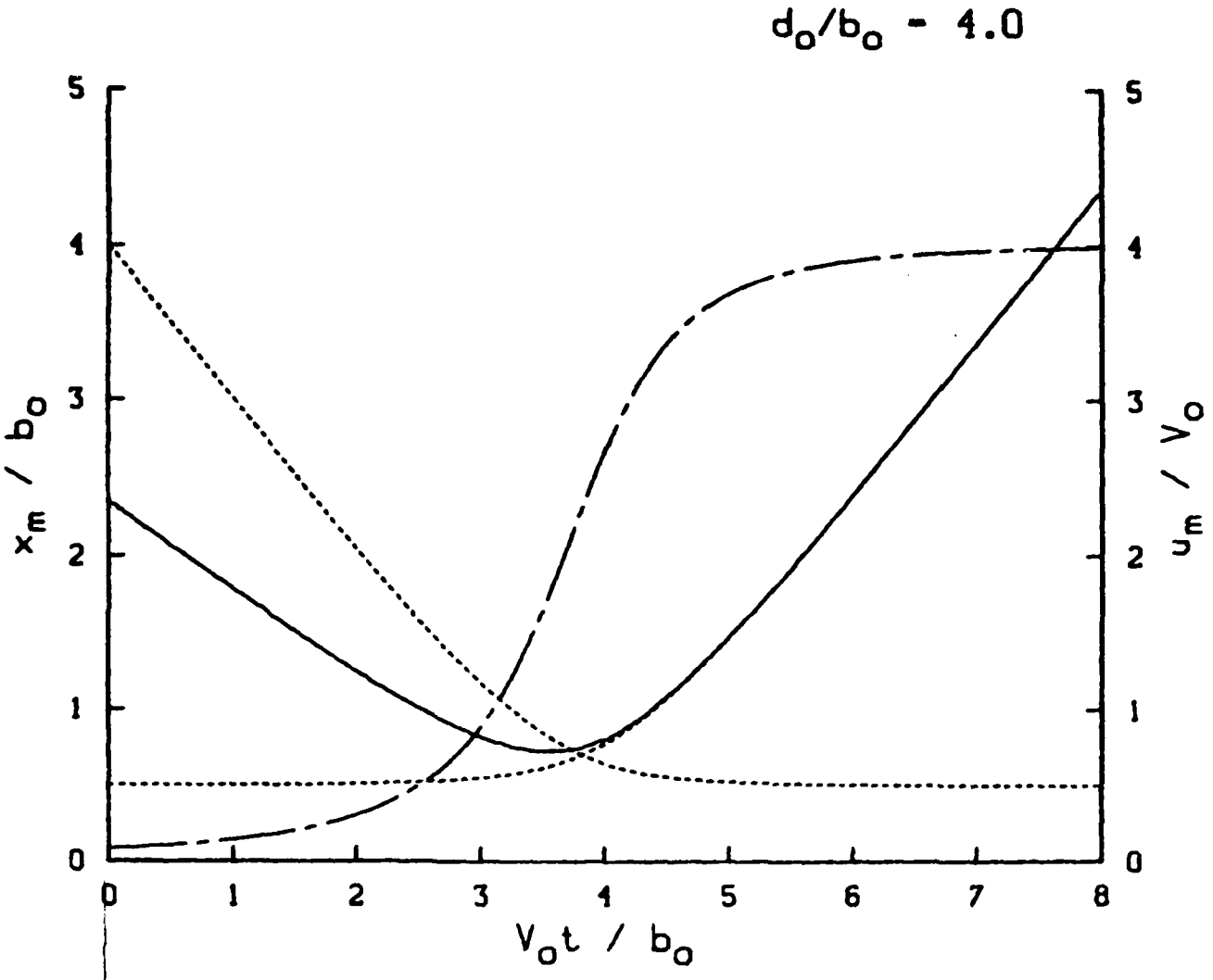

Figure 35. Position of Maximum Surface Velocity, Vortex Position, and Maximum Velocity, Inviscid Model, $d_o/b_o = 4$

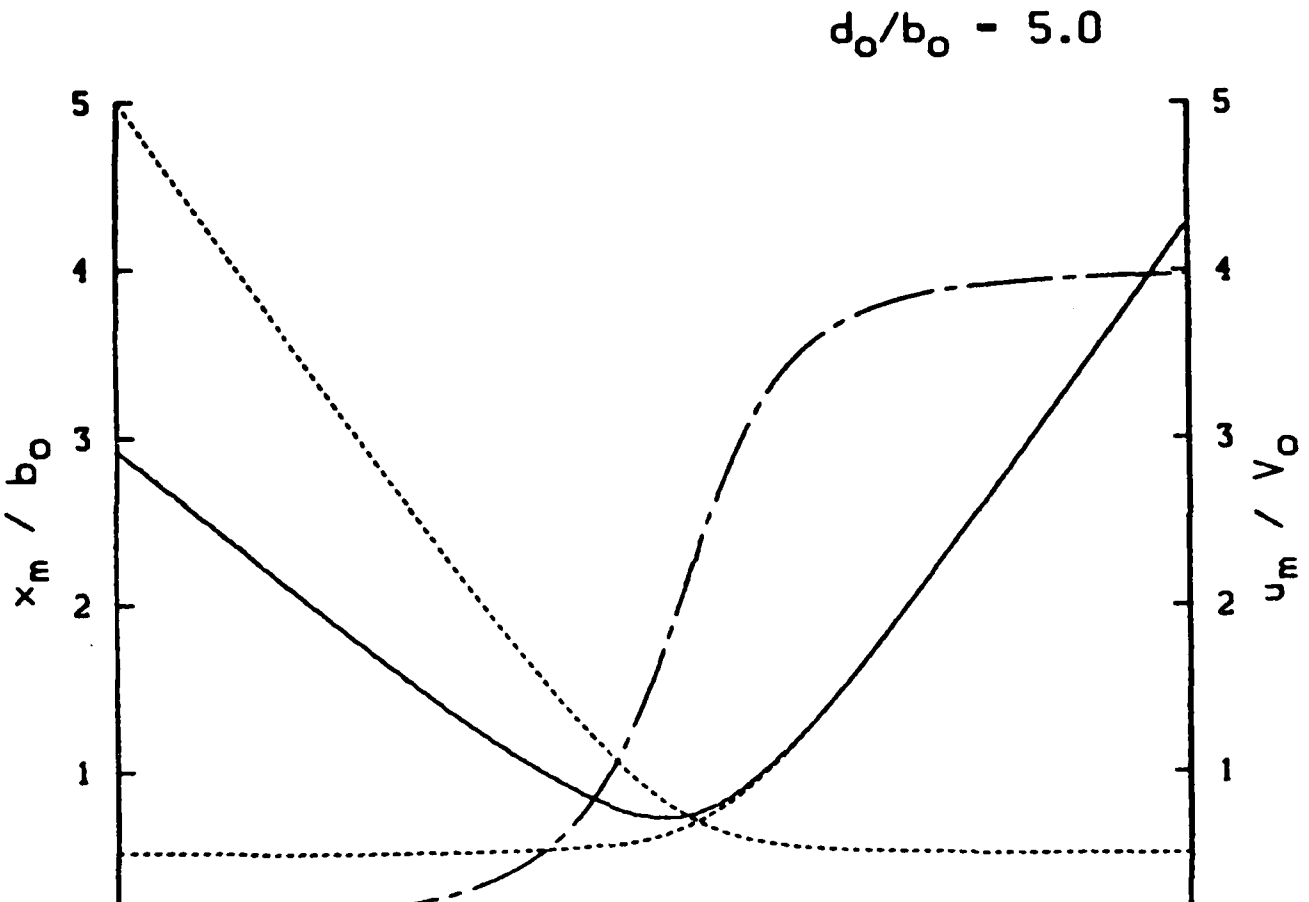

Figure 36. Position of Maximum Surface Velocity, Vortex Position, and Maximum Velocity, Inviscid Model, $d_o/b_o = 5$

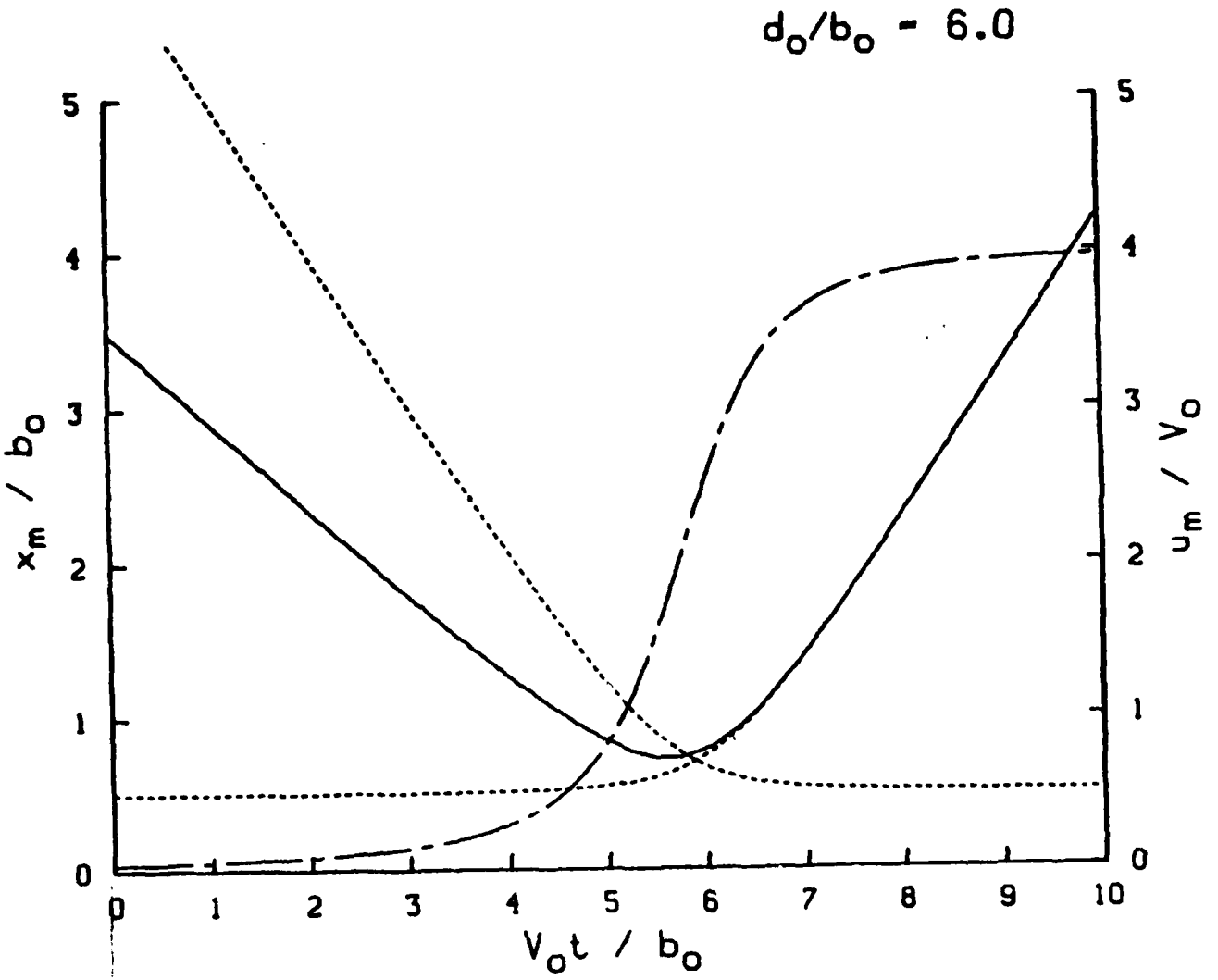

Figure 37. Position of Maximum Surface Velocity, Vortex Position, and Maximum Velocity, Inviscid Model, $d_o/b_o = 6$

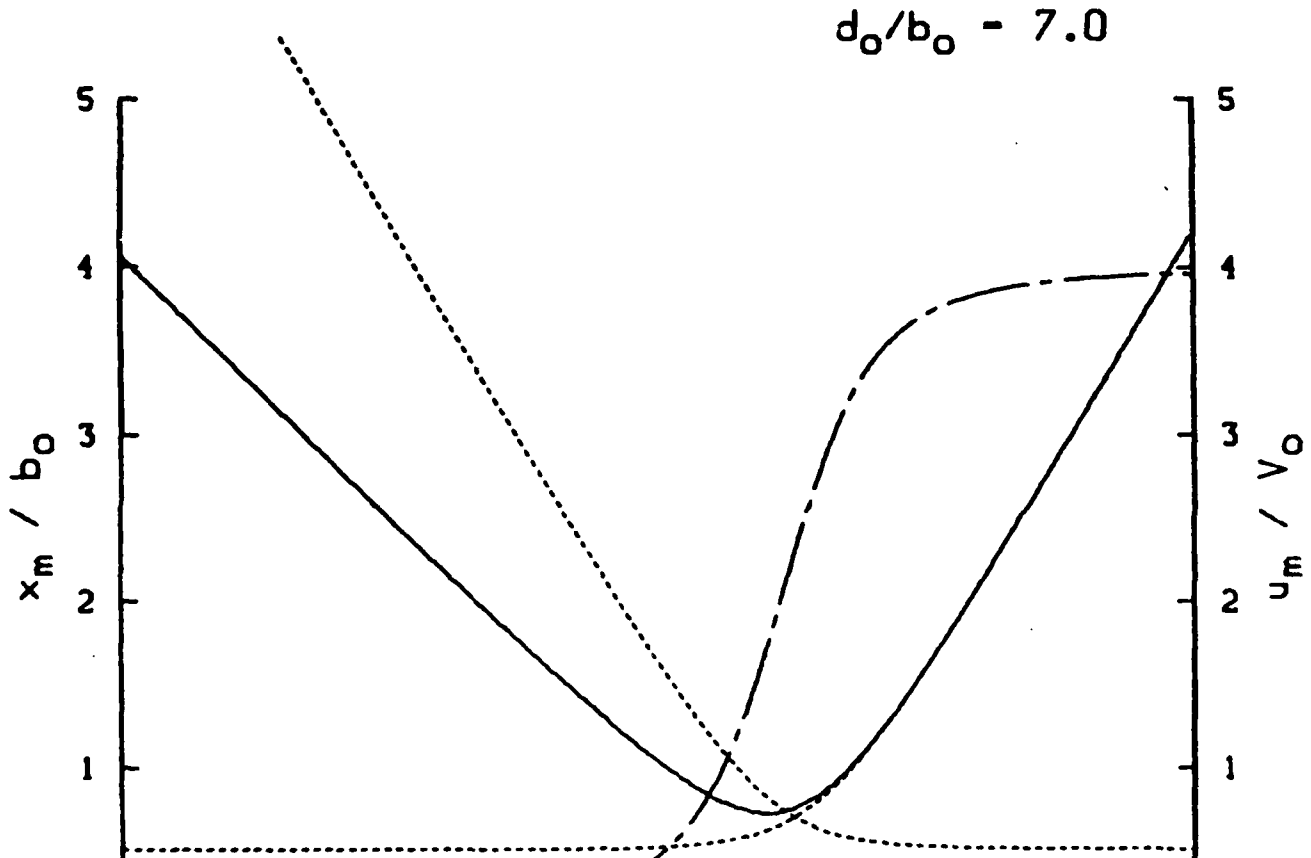

Figure 38. Position of Maximum Surface Velocity, Vortex Position, and Maximum Velocity, Inviscid Model, $d_o/b_o = 7$

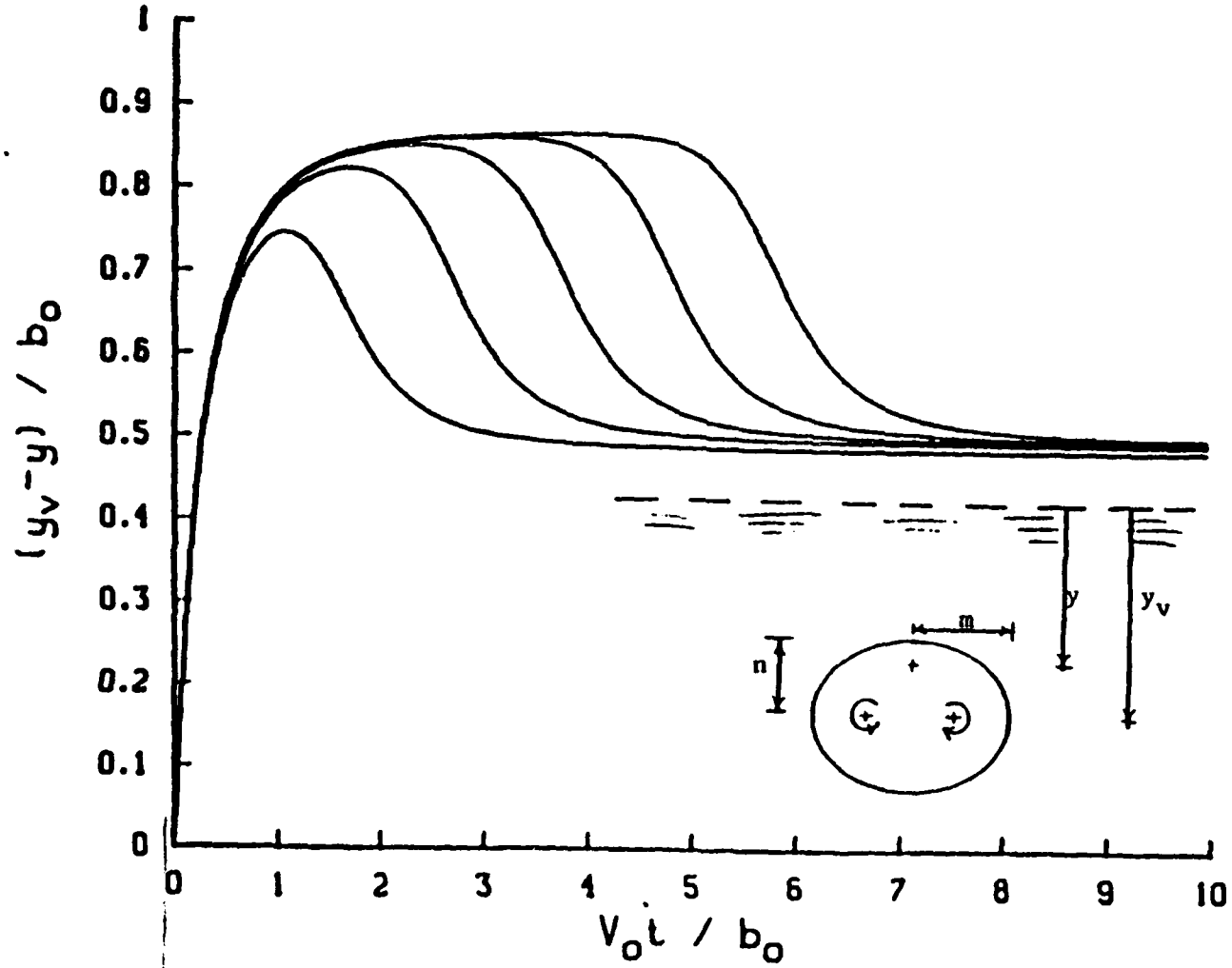

Figure 39. Position of Marker Particle Inside Recirculation Cell

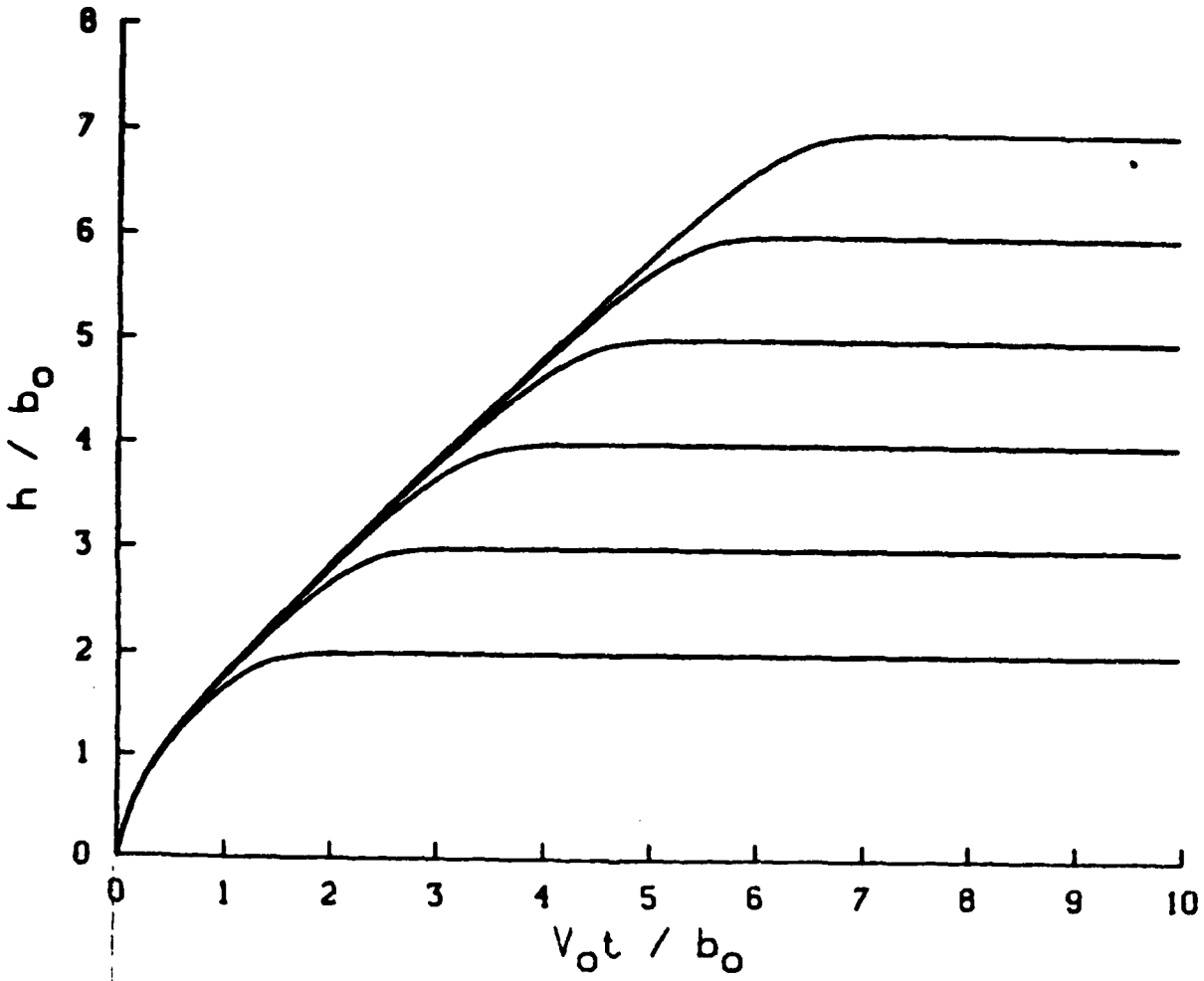

Figure 40. Position of Top of Recirculation Cell

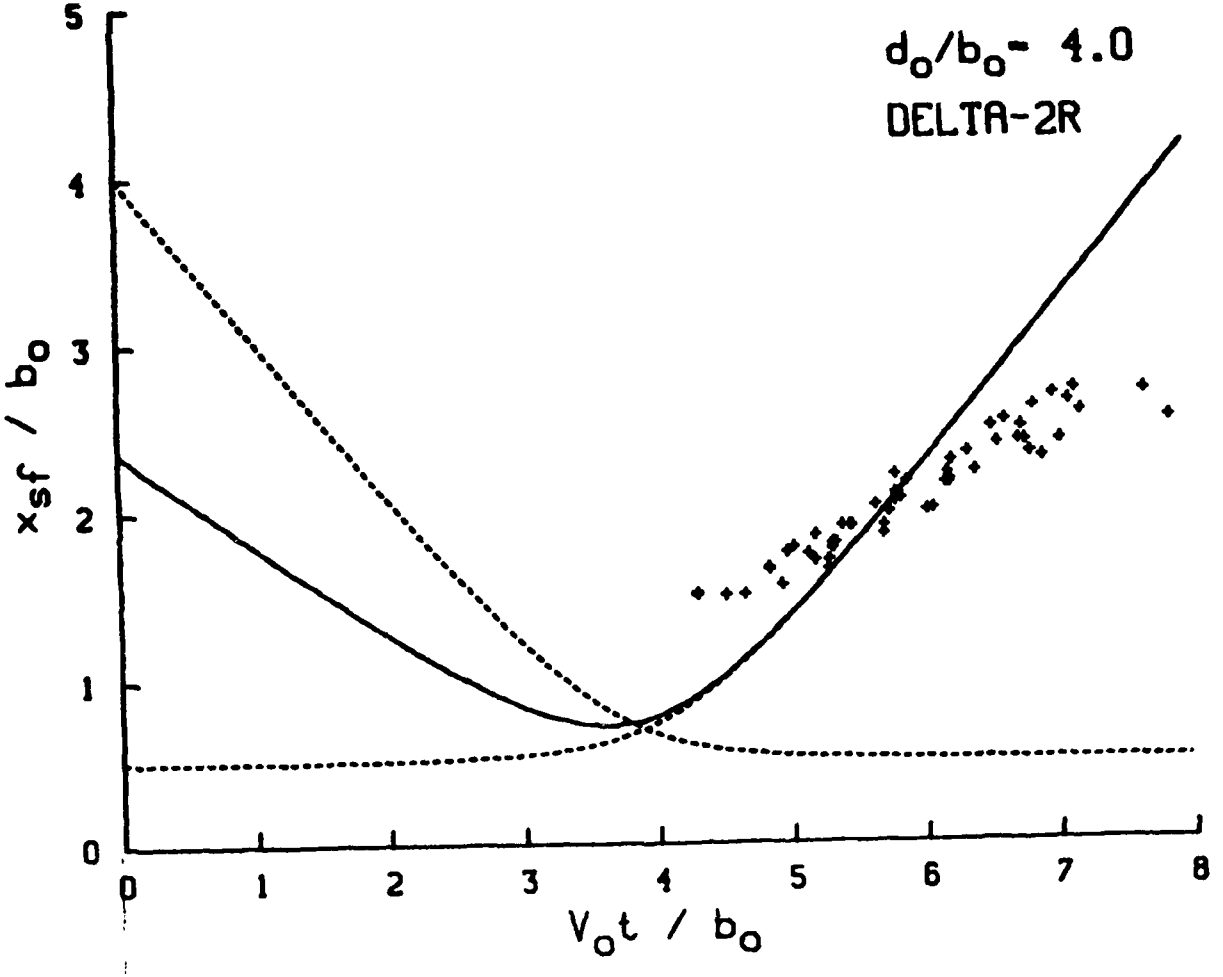

Figure 41. Comparison of Experimental Data and Inviscid Model, Delta-2R, d_o/b_o = 4

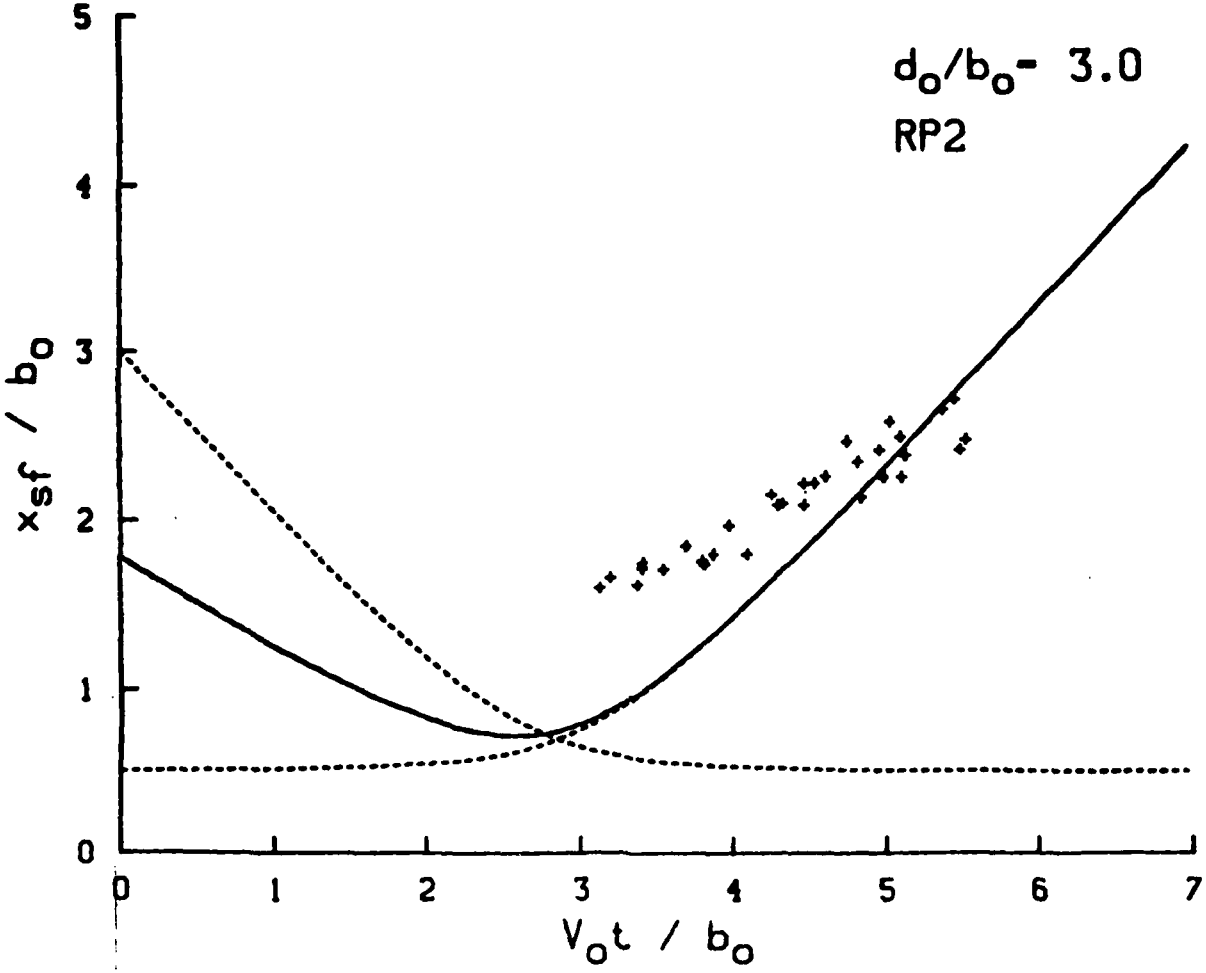

Figure 42. Comparison of Experimental Data and Inviscid Model, RP2, d_o/b_o = 3

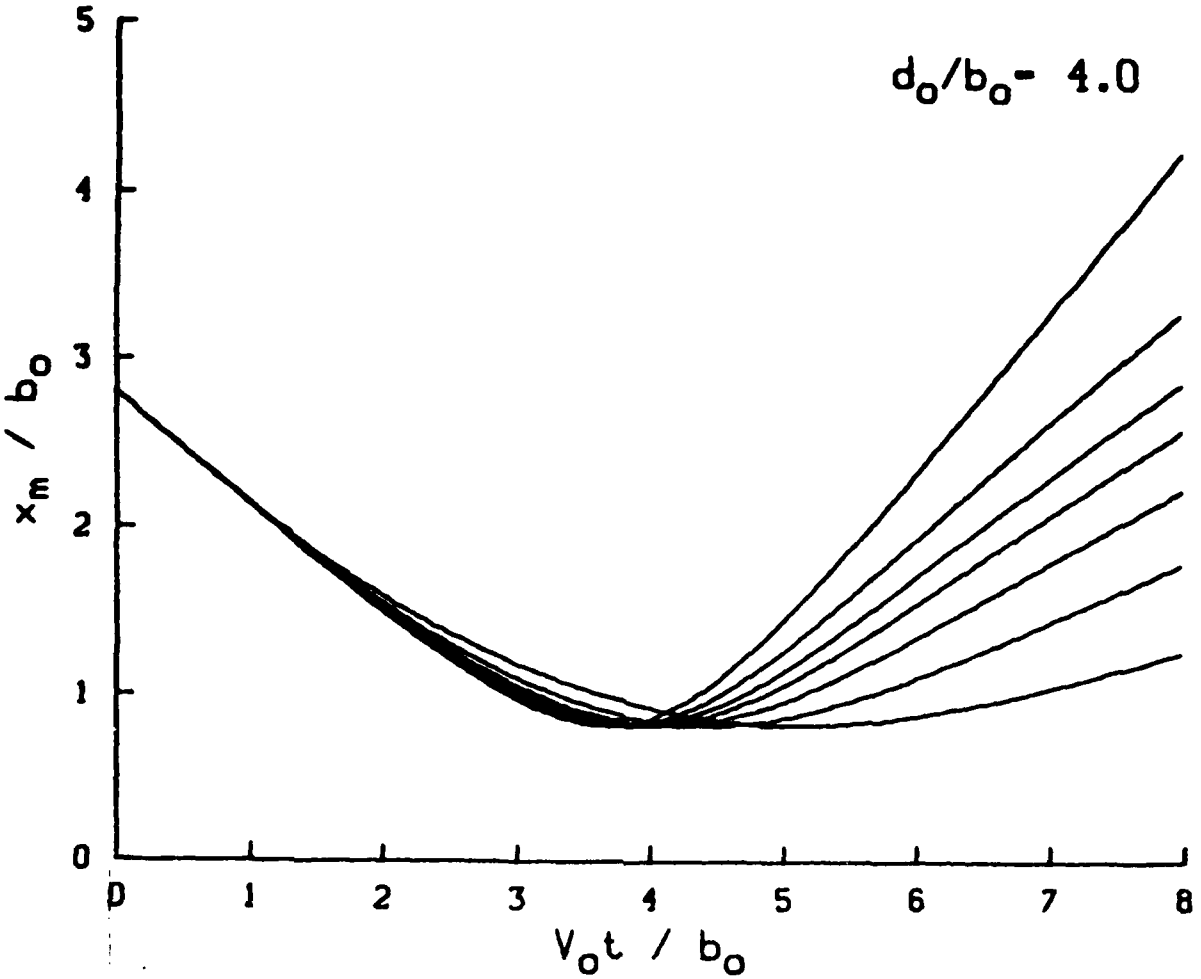

Figure 43. Position of Maximum Surface Velocity, Turbulence Model, A = 3, 4, 5, 6, 7, 9, ∞

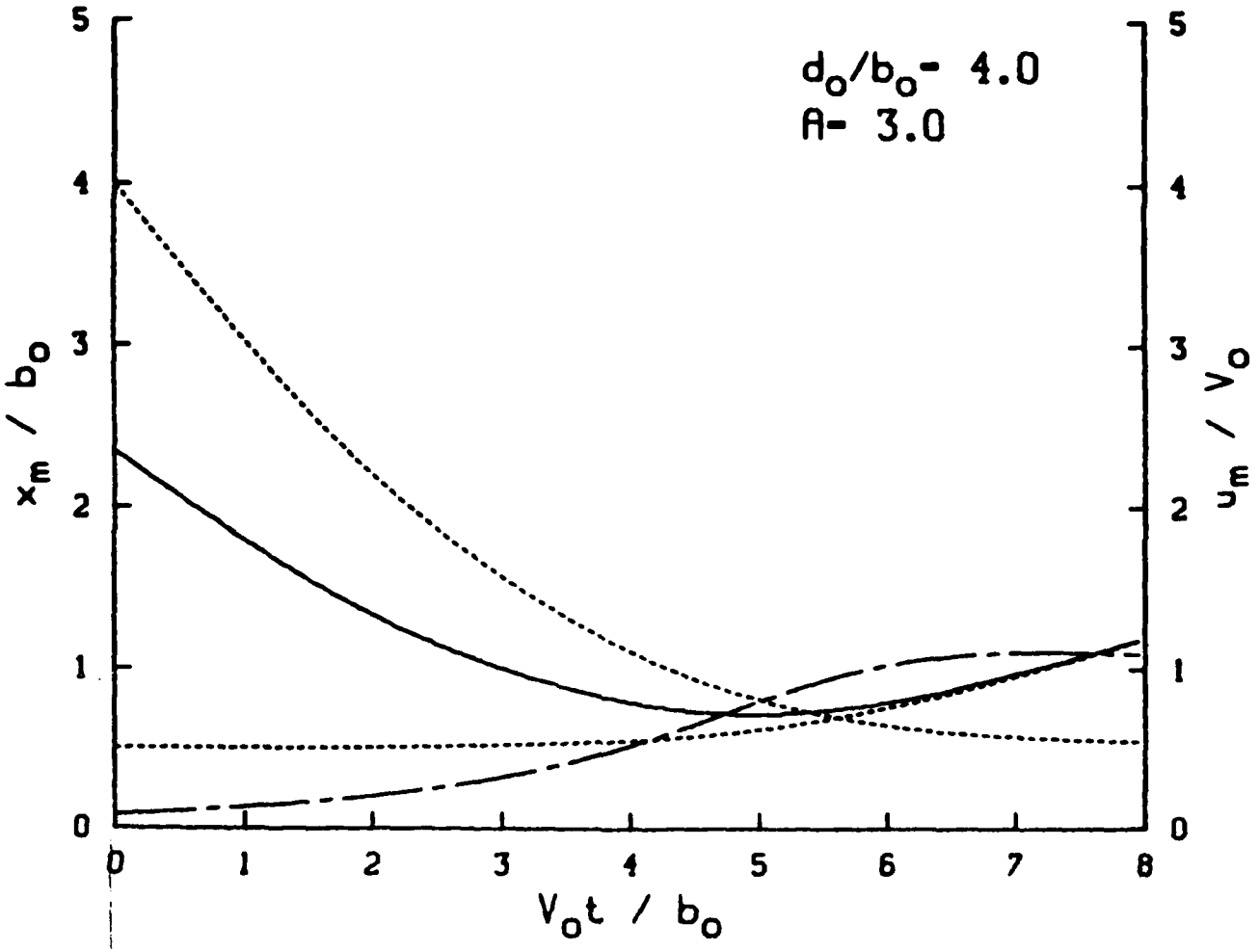

Figure 44. Position of Maximum Surface Velocity, Vortex Position, Maximum Velocity, Turbulence Model, d_o/b_o = 4, A = 3

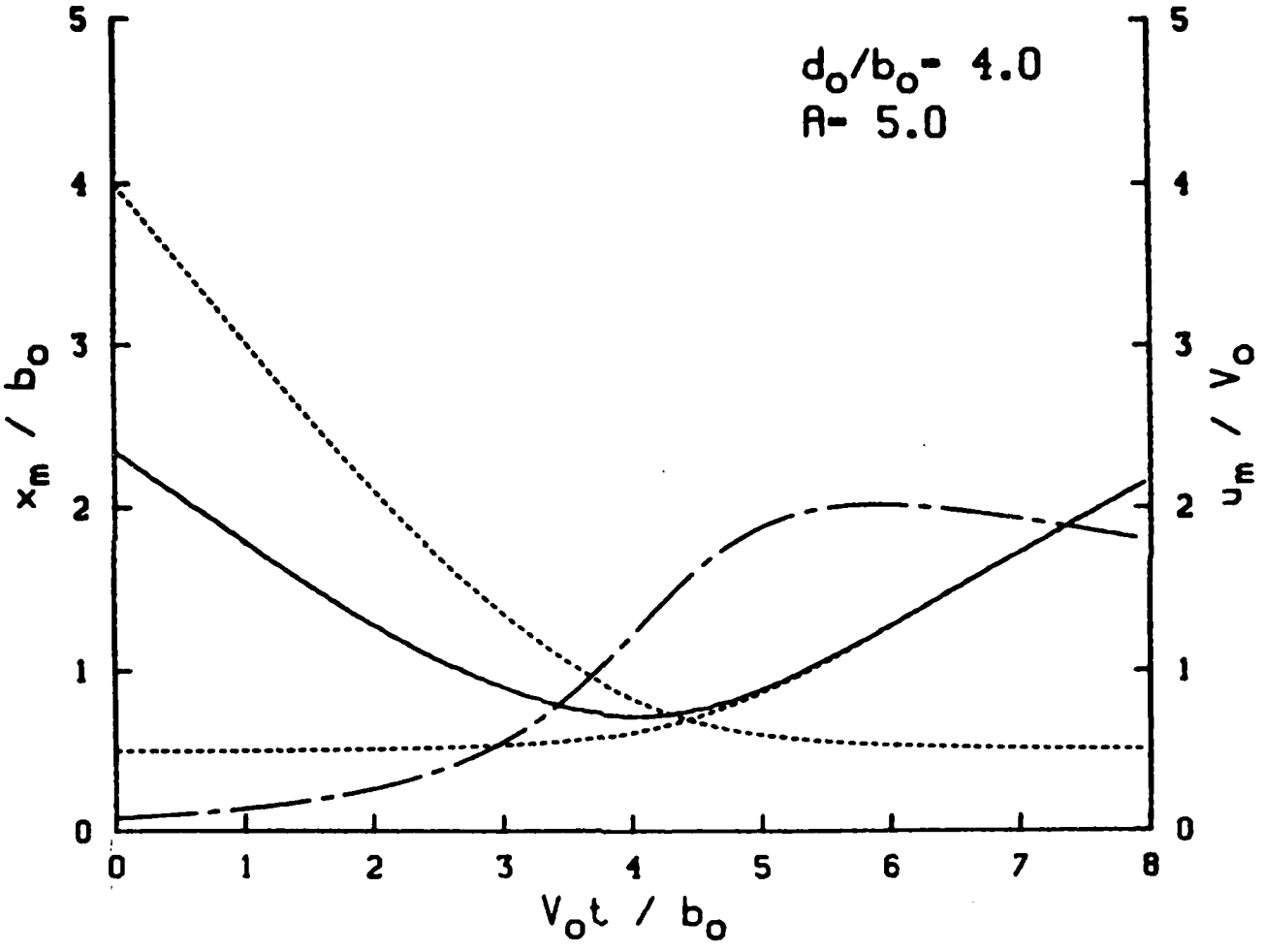

Figure 45. Position of Maximum Surface Velocity, Vortex Position, Maximum Velocity, Turbulence Model, d_o/b_o = 4, A = 5

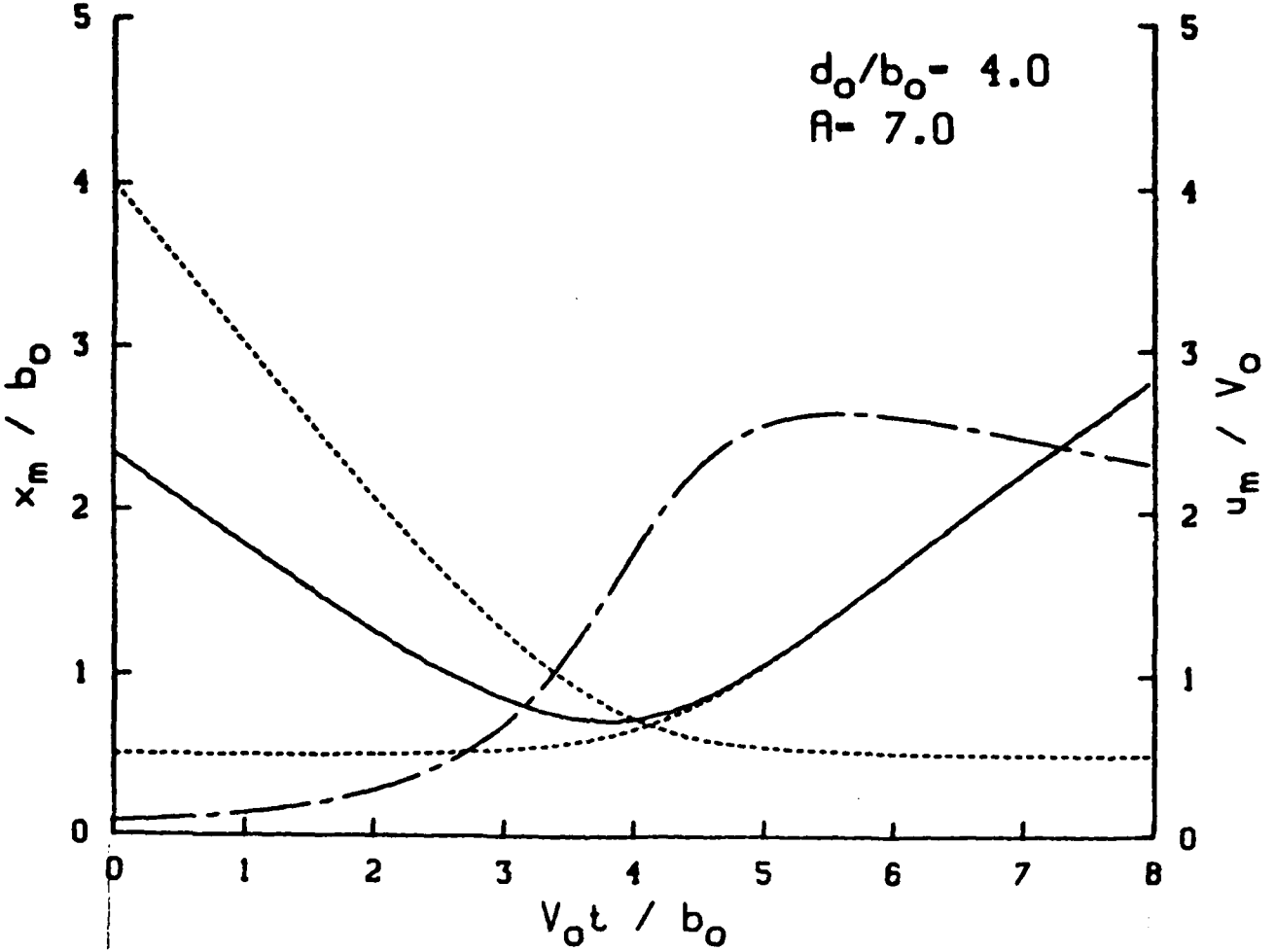

Figure 46. Position of Maximum Surface Velocity, Vortex Position, Maximum Velocity, Turbulence Model, d_o/b_o = 4, A = 7

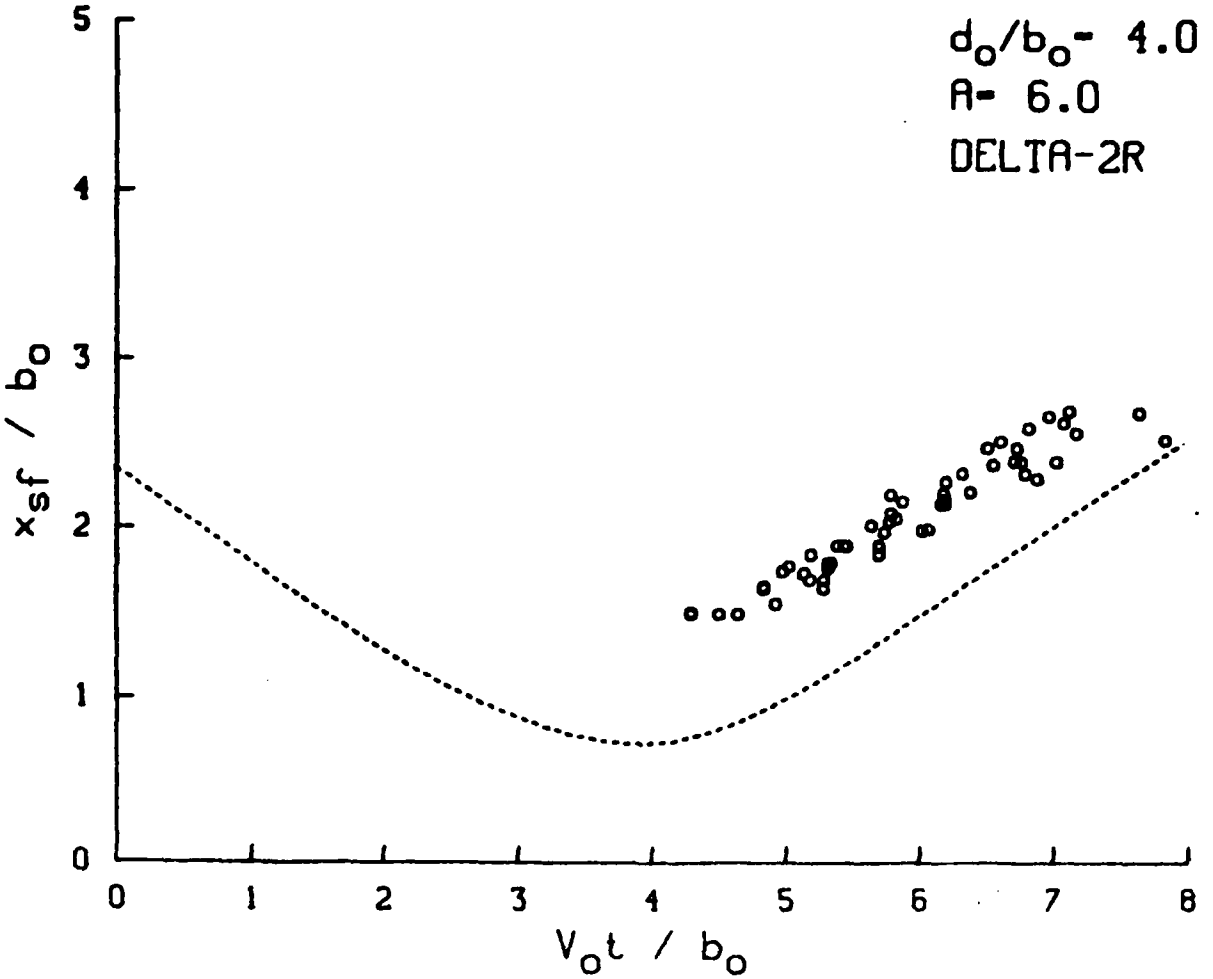

Figure 47. Comparison of Scar Front Position and Maximum Surface Velocity, Turbulence Model, Delta-2R, d_o/b_o = 4, A = 6

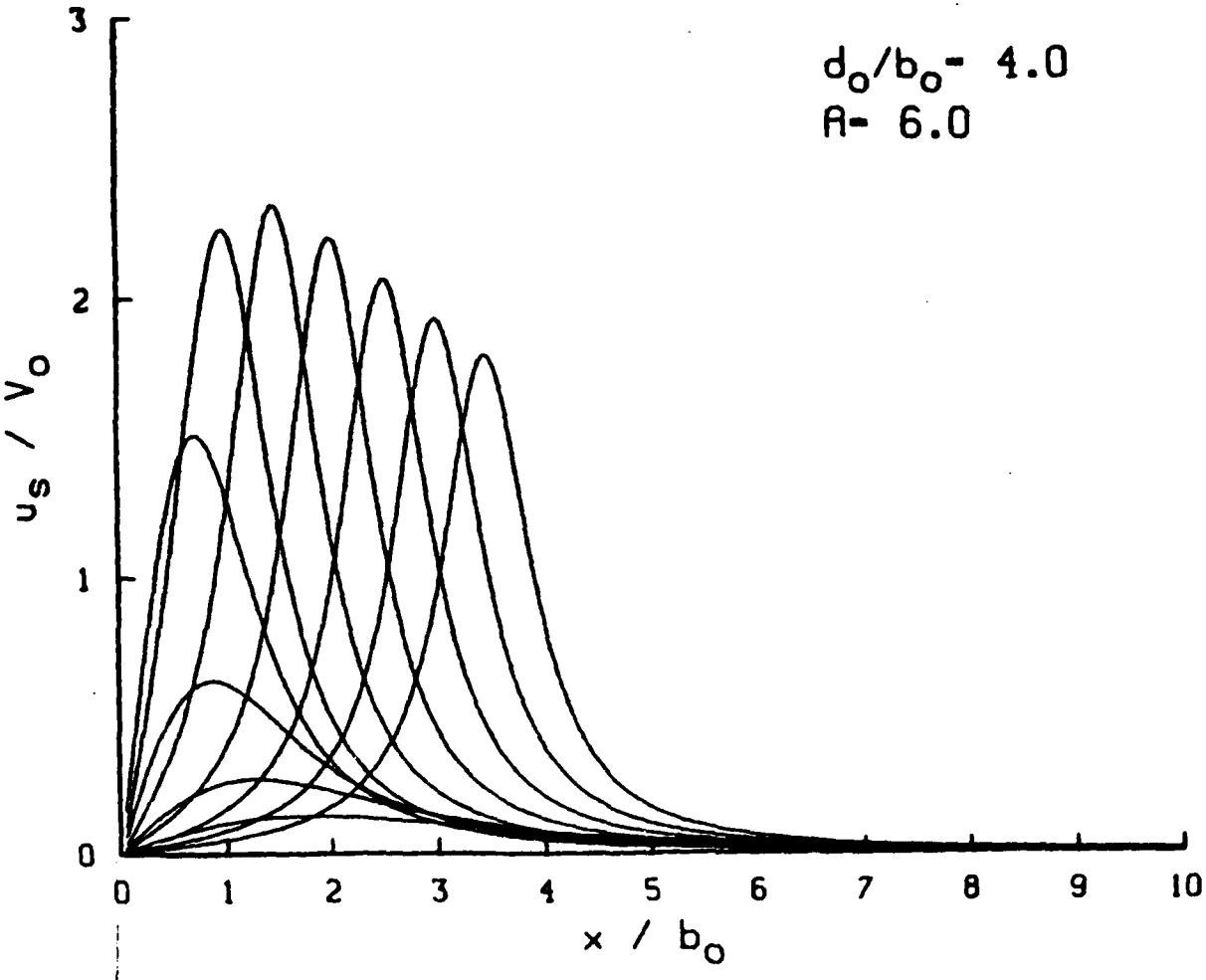

Figure 48. Surface Velocity Profiles, Turbulence Model d_o/b_o = 4, A = 6

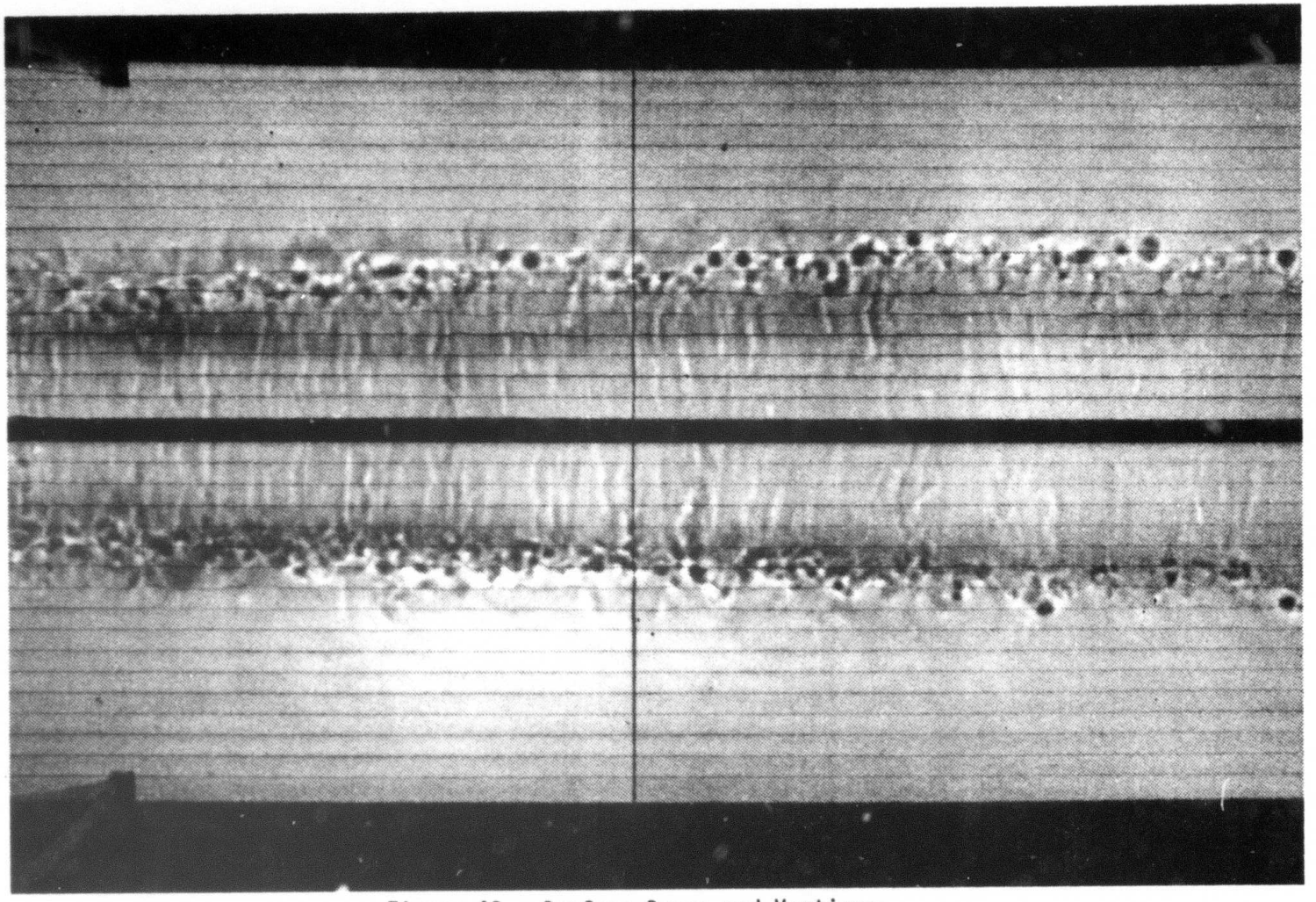

Figure 49. Surface Scars and Vortices

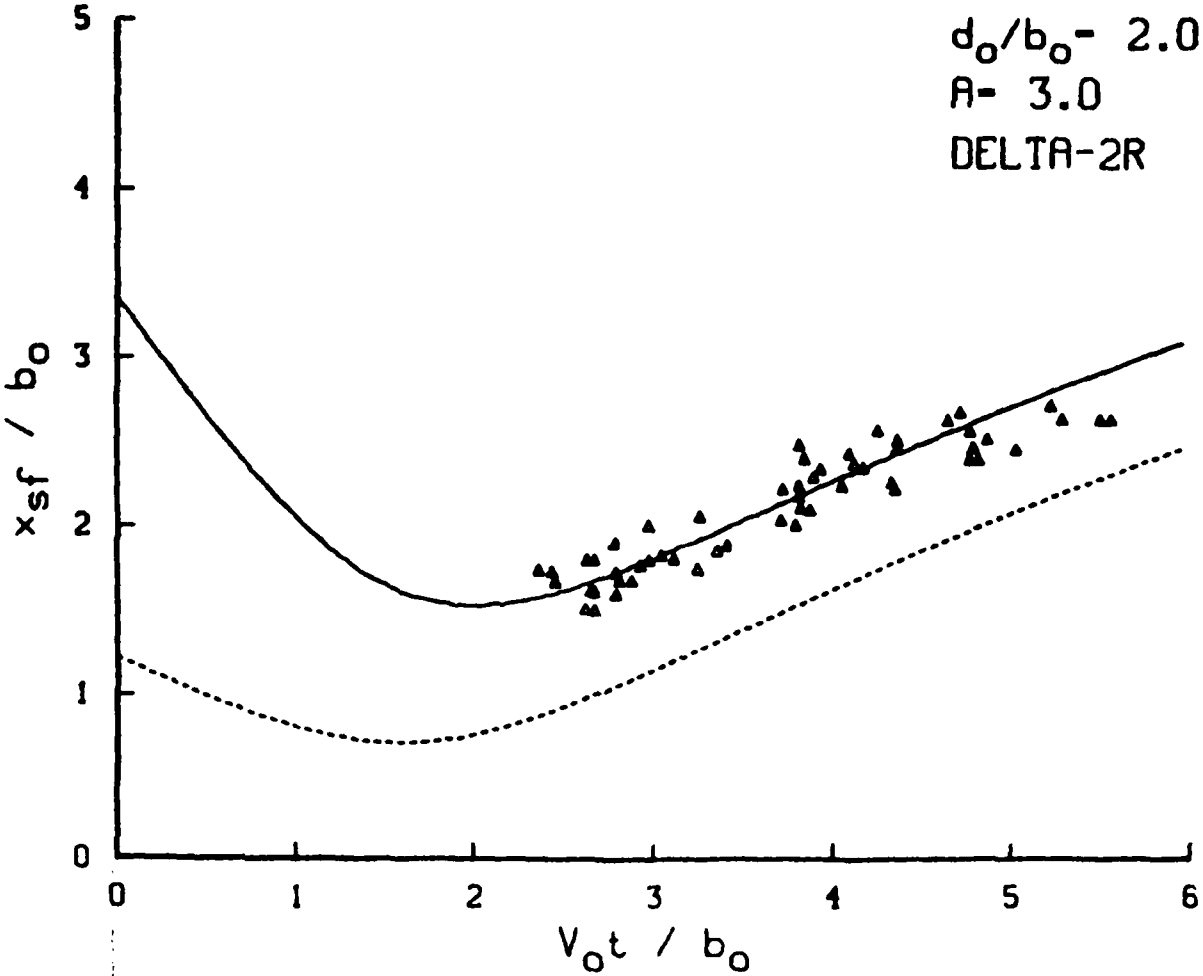

Figure 50. Scar Front Position, Delta-2R, d_o/b_o = 2, A = 3.0

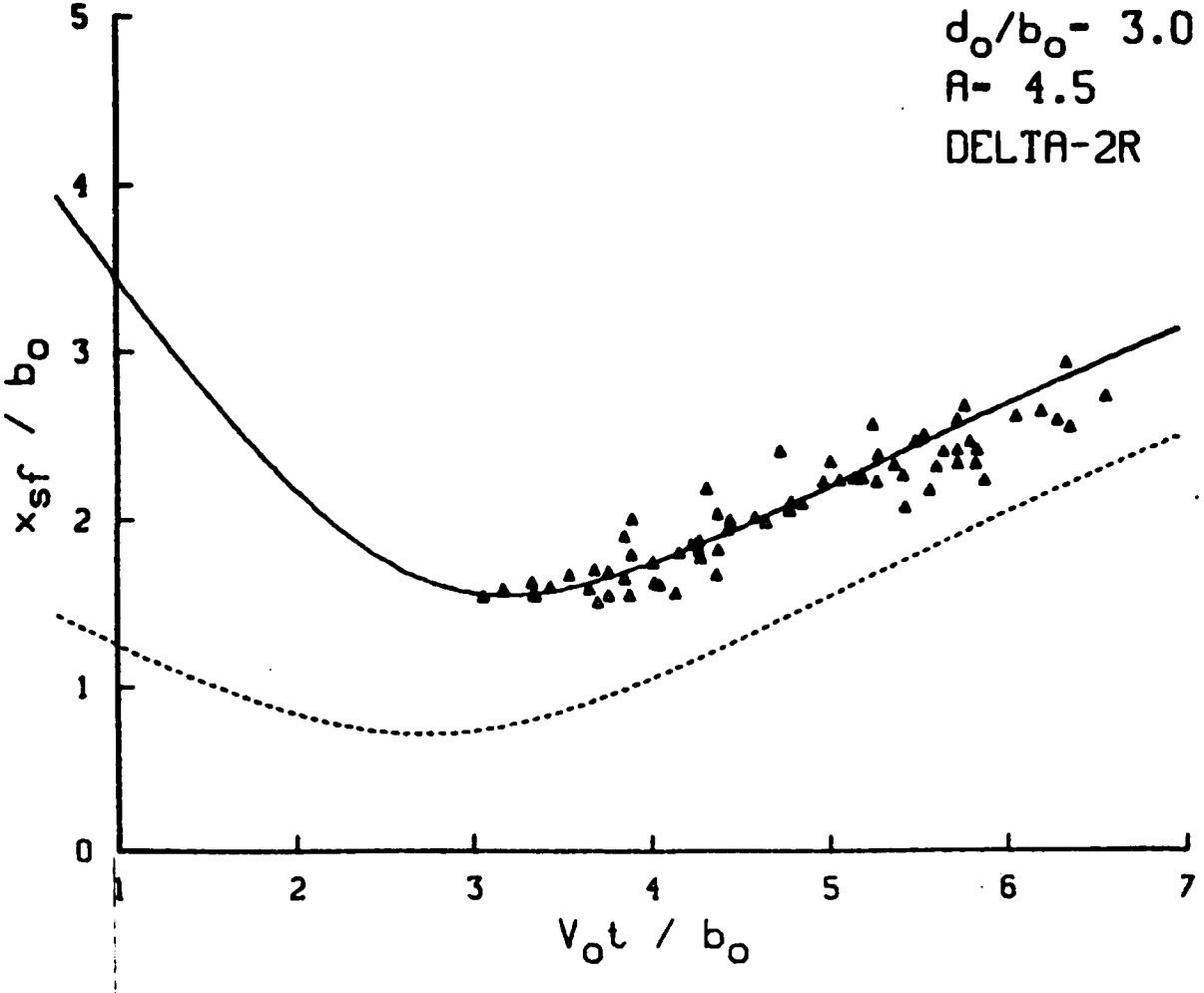

Figure 51. Scar Front Position, Delta-2R, d_o/b_o = 3, A = 4.5

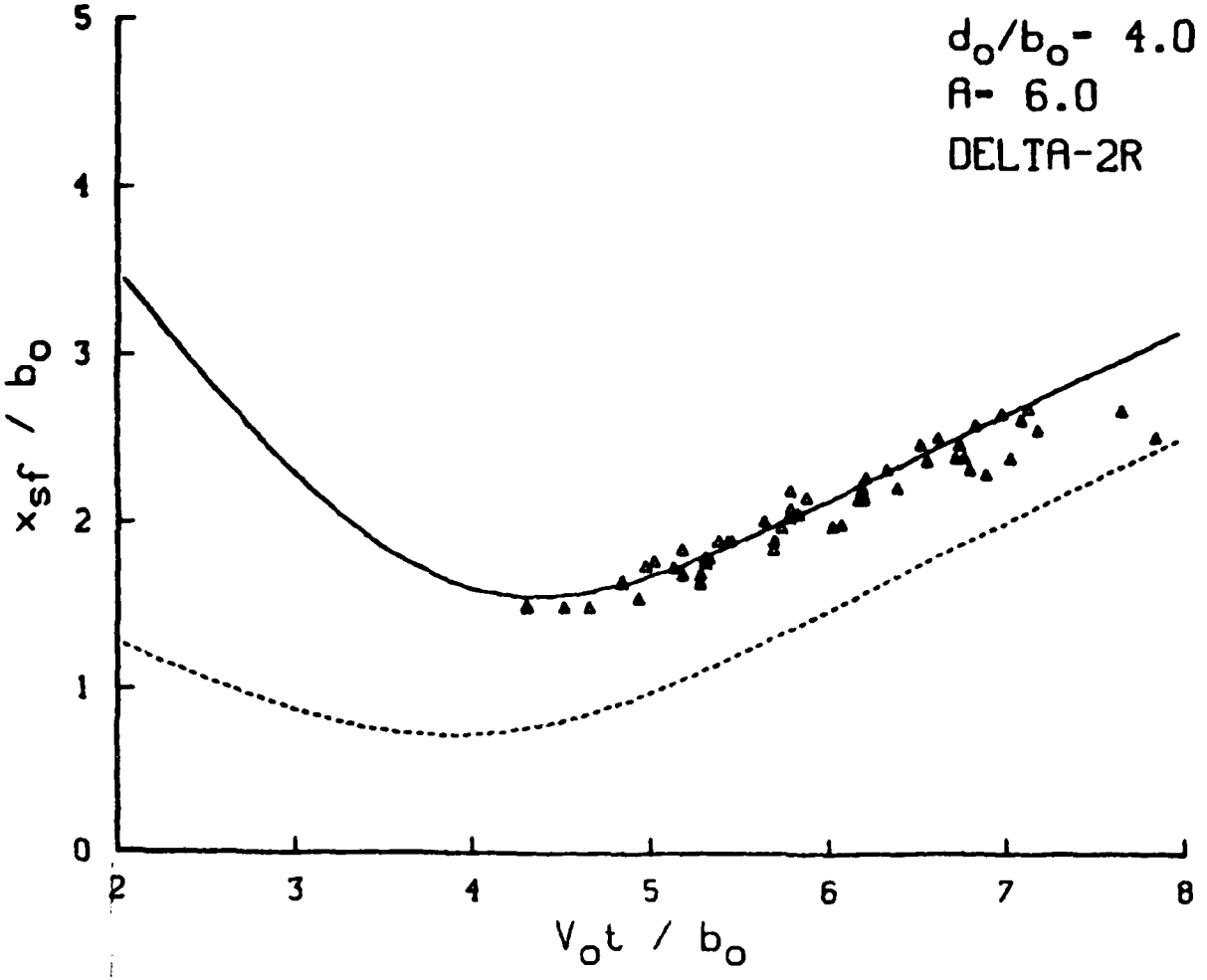

Figure 52. Scar Front Position, Delta-2R, d_o/b_o = 4, A = 6.0

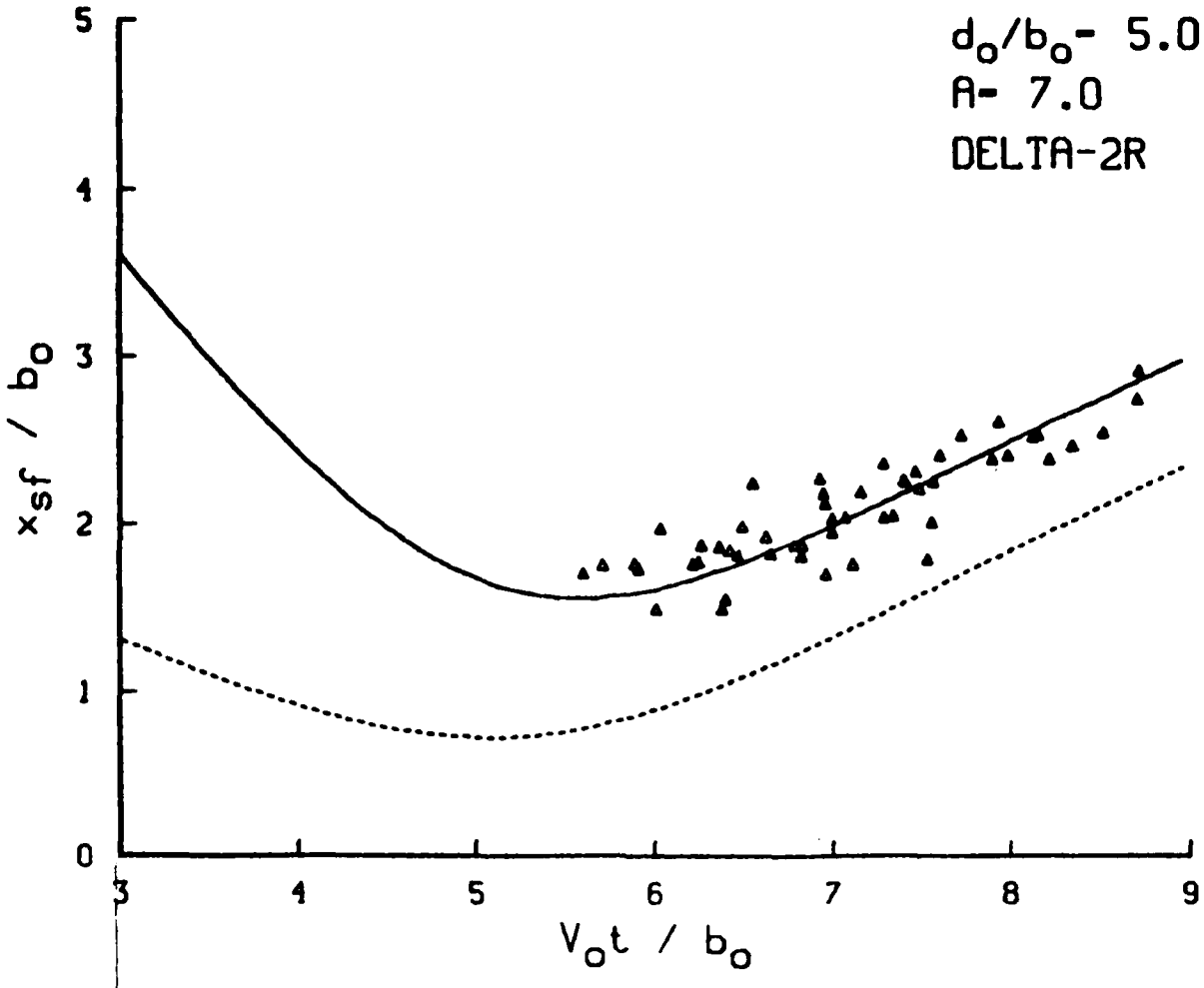

Figure 53. Scar Front Position, Delta-2R, d_o/b_o = 5, A = 7.0

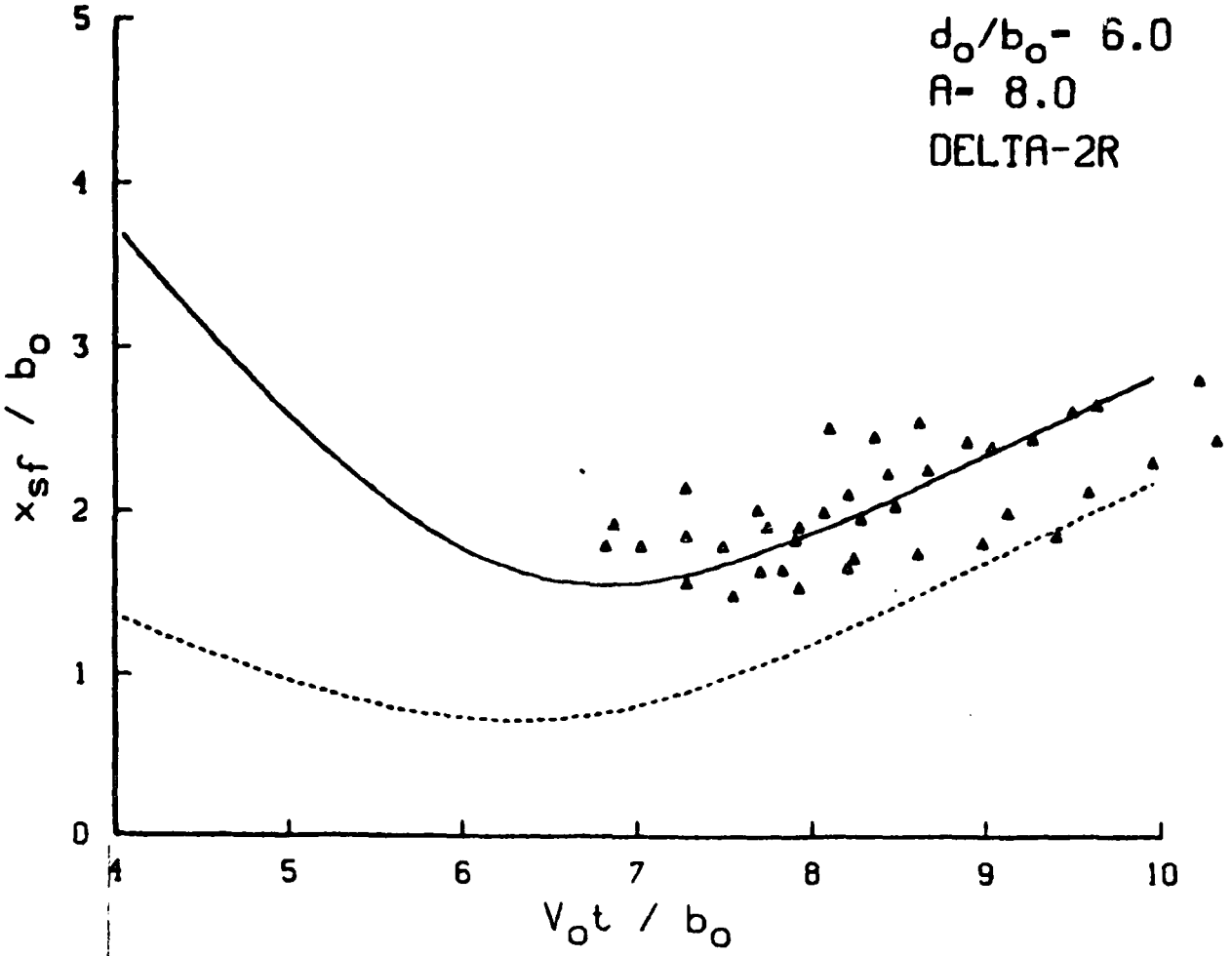

Figure 54. Scar Front Position, Delta-2R, d_o/b_o = 6, A = 8.0

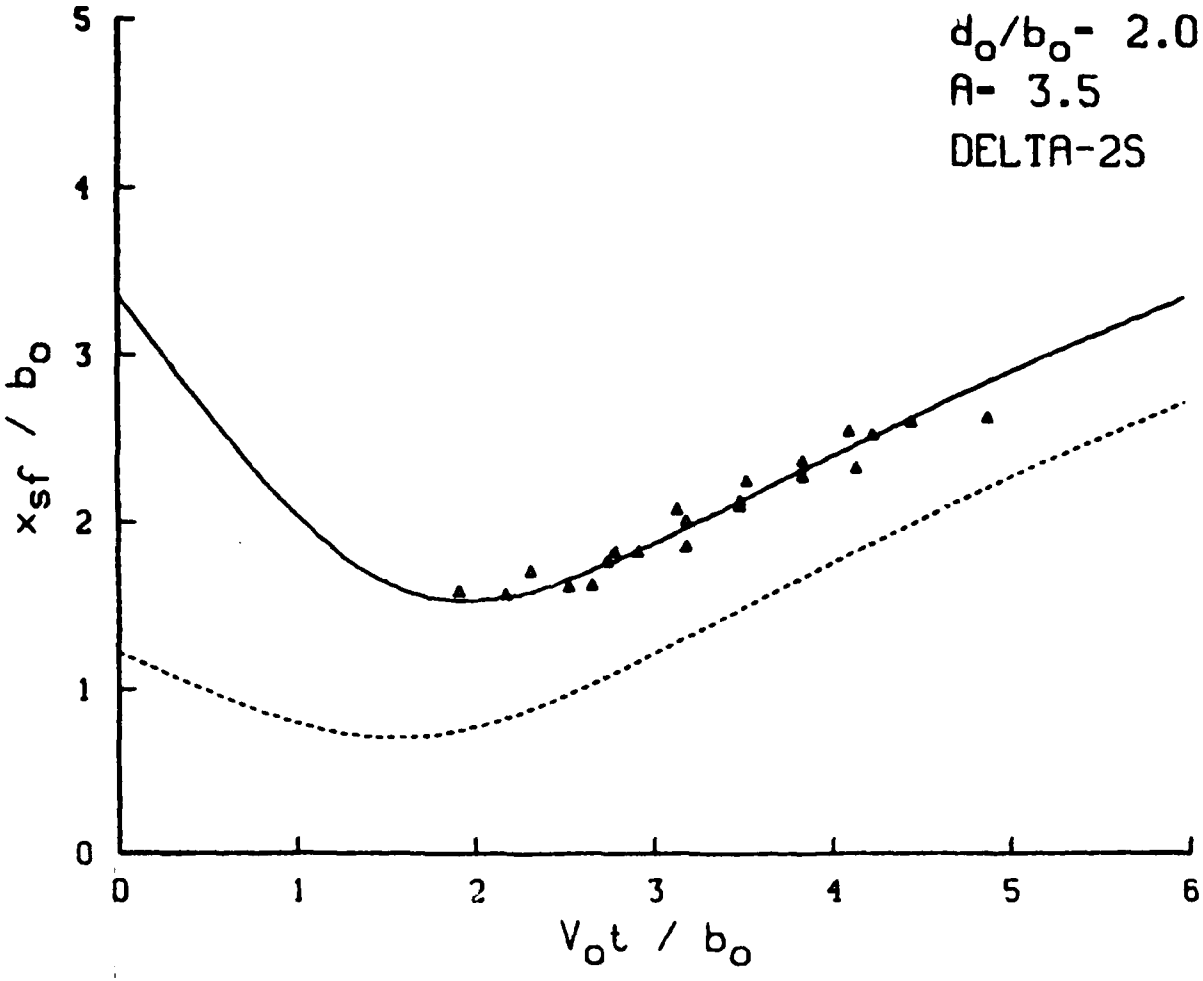

Figure 55. Scar Front Position, Delta-2S, d_o/b_o = 2, A = 3.5

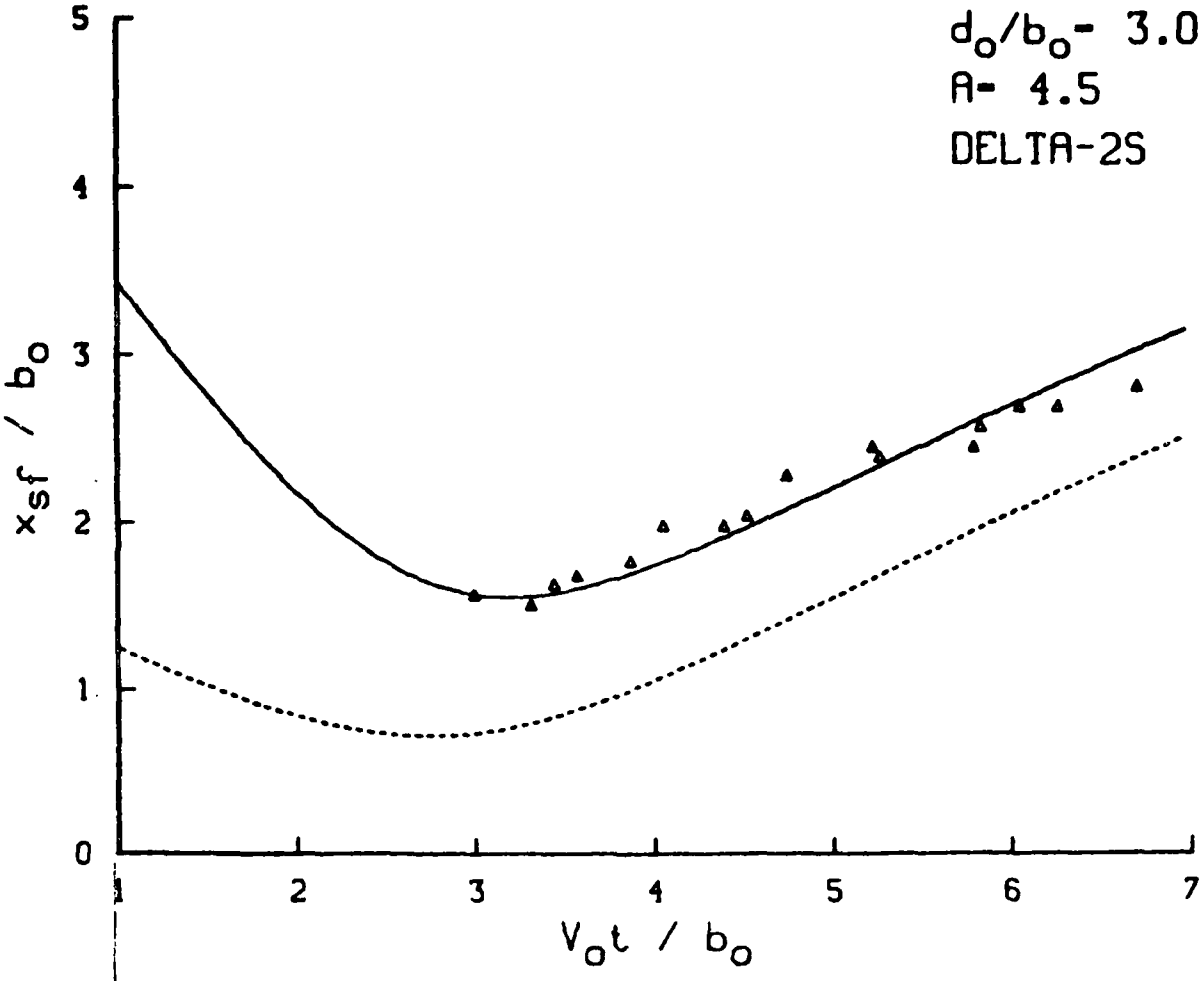

Figure 56. Scar Front Position, Delta-2S, d_o/b_o= 3, A = 4.5

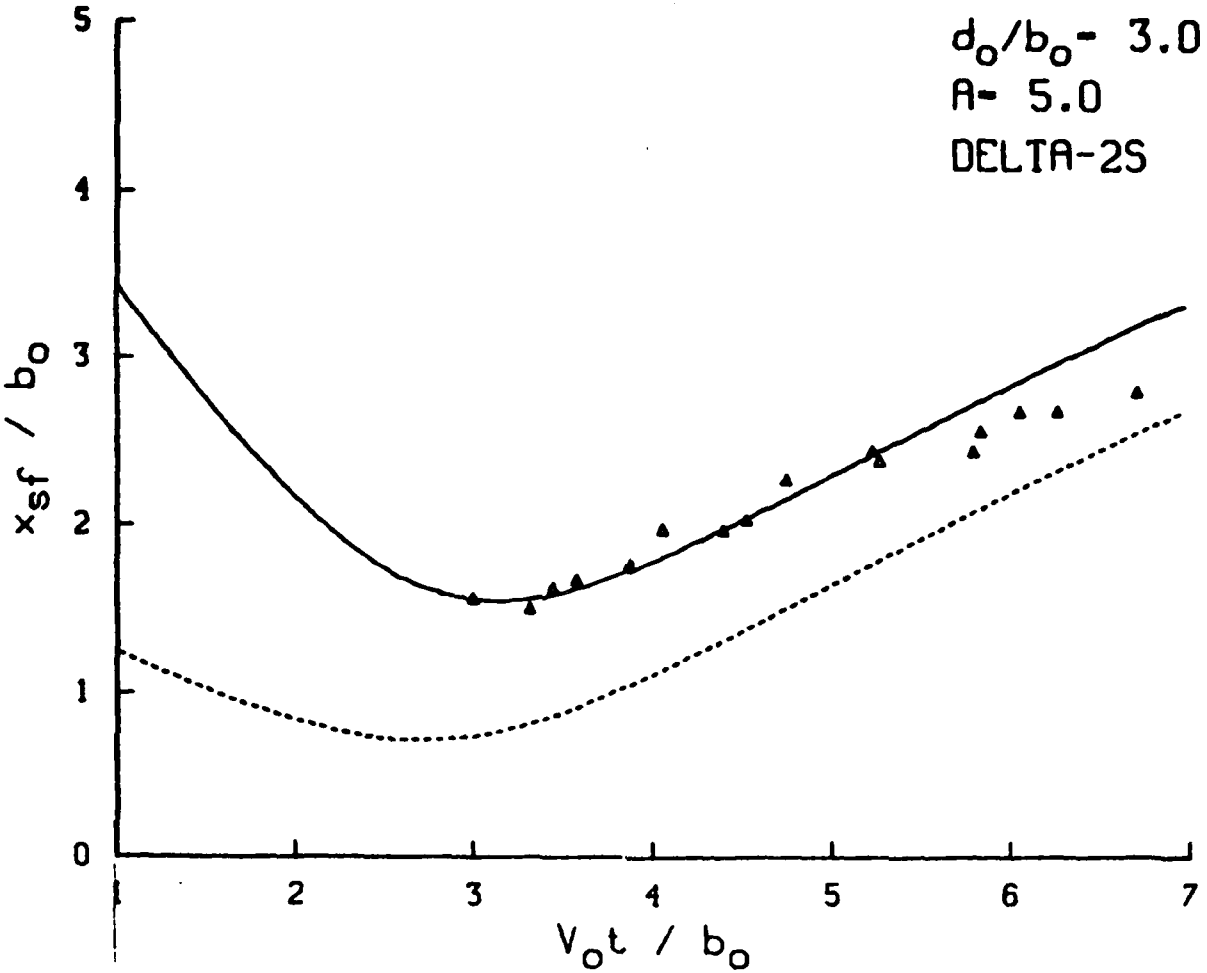

Figure 57. Scar Front Position, Delta-2S, d_o/b_o = 3, A = 5.0

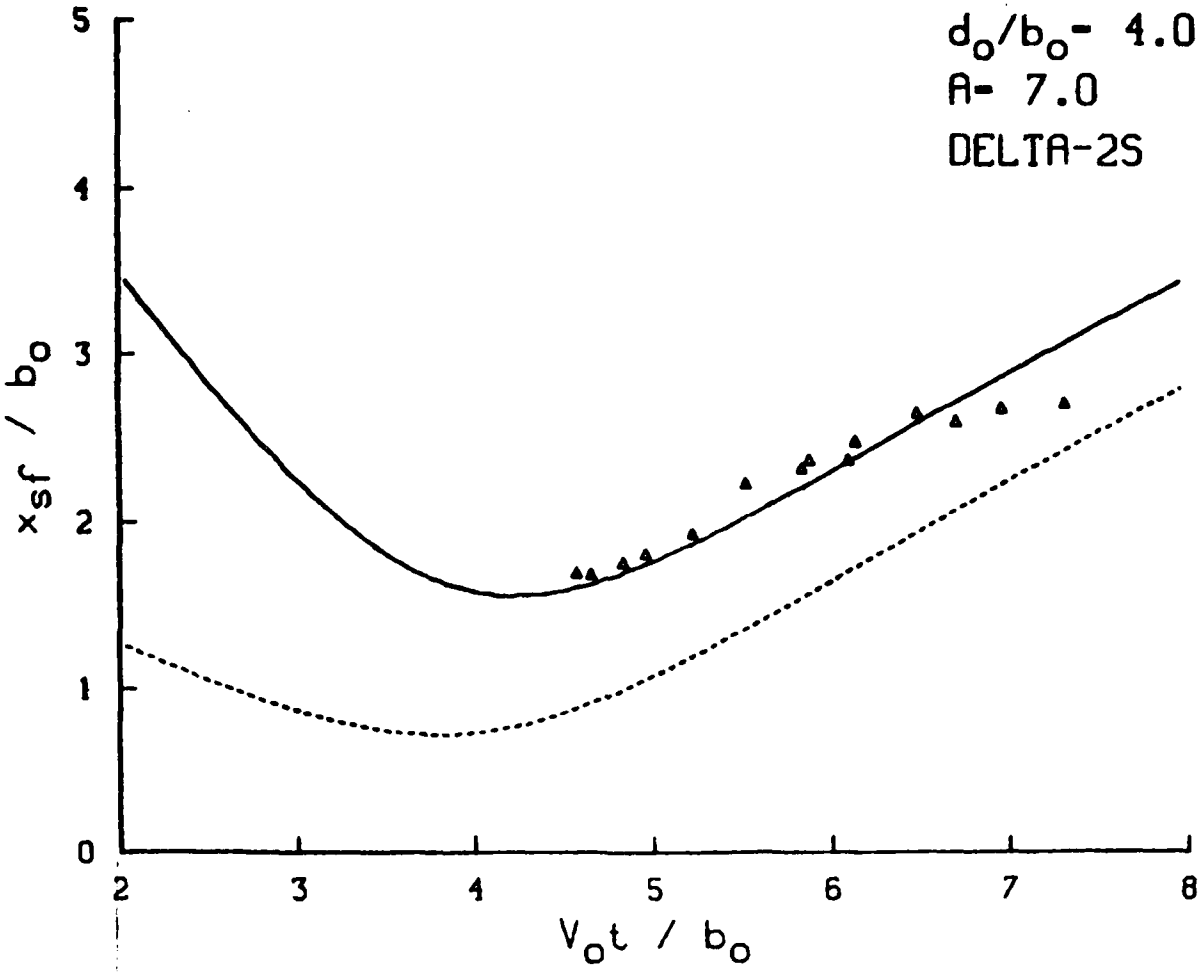

Figure 58. Scar Front Position, Delta-2S, d_o/b_o = 4, A = 7.0

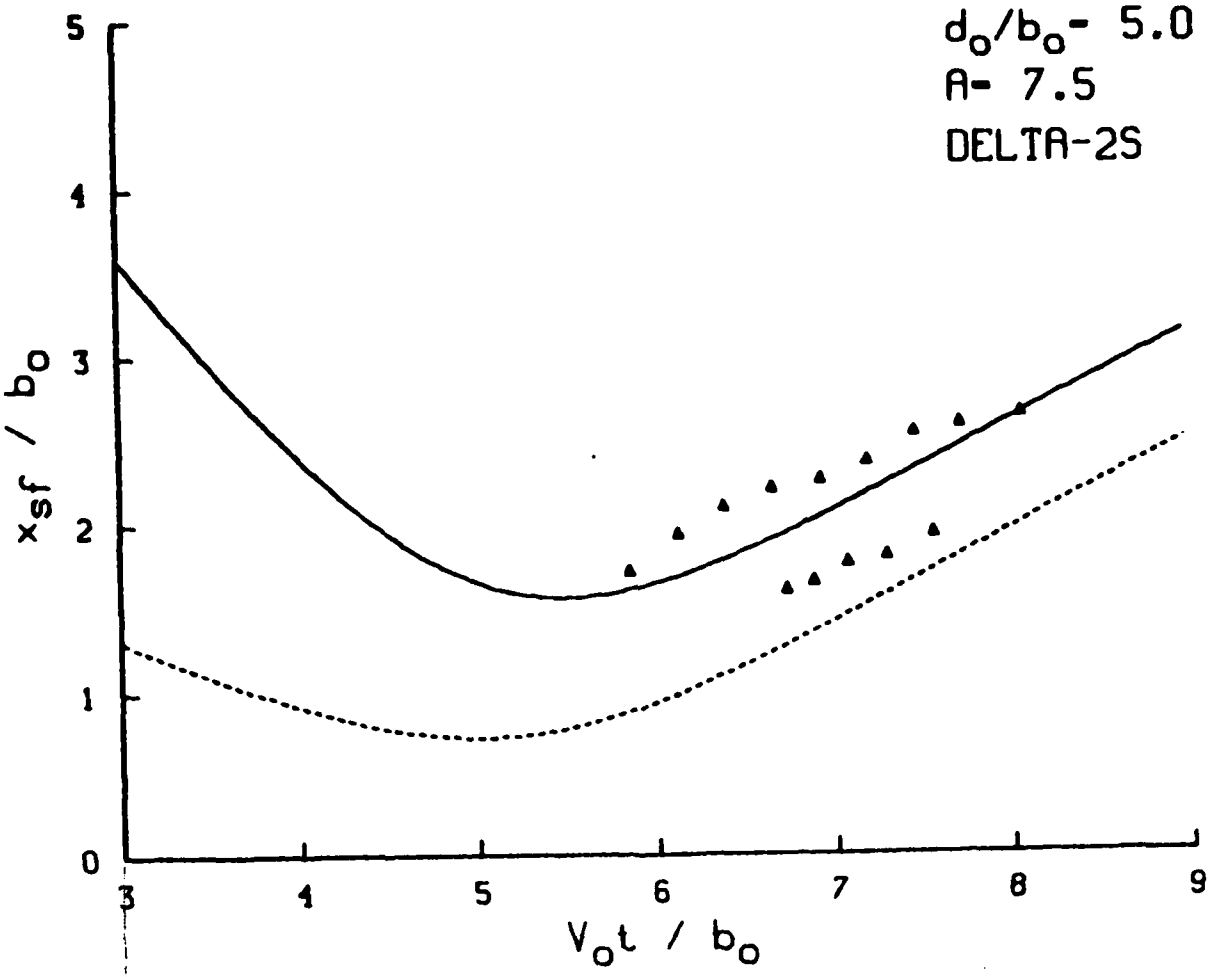

Figure 59. Scar Front Position, Delta-2S, d_o/b_o = 5, A = 7.5

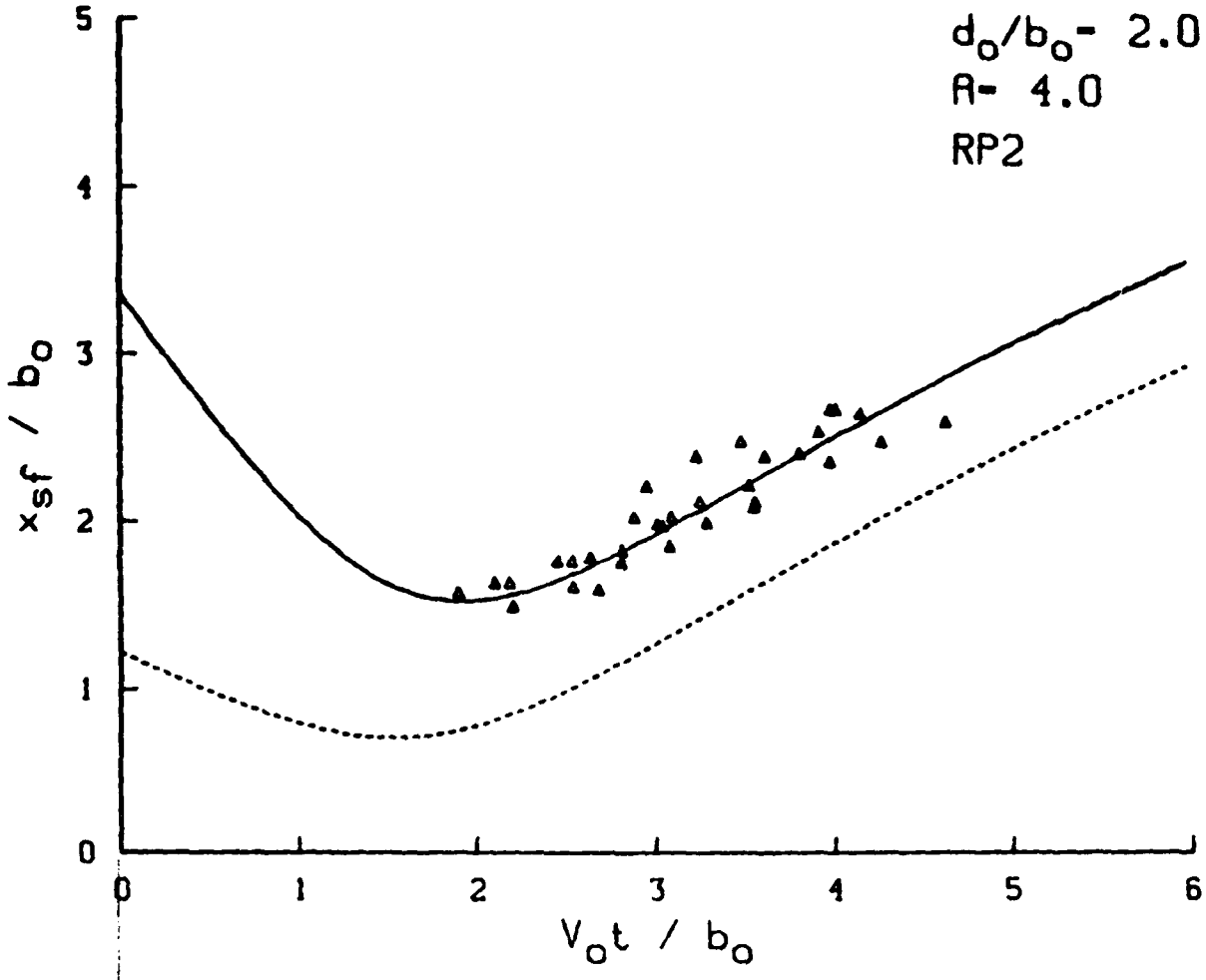

Figure 60. Scar Front Position, RP2, d_o/b_o = 2, A = 4.0

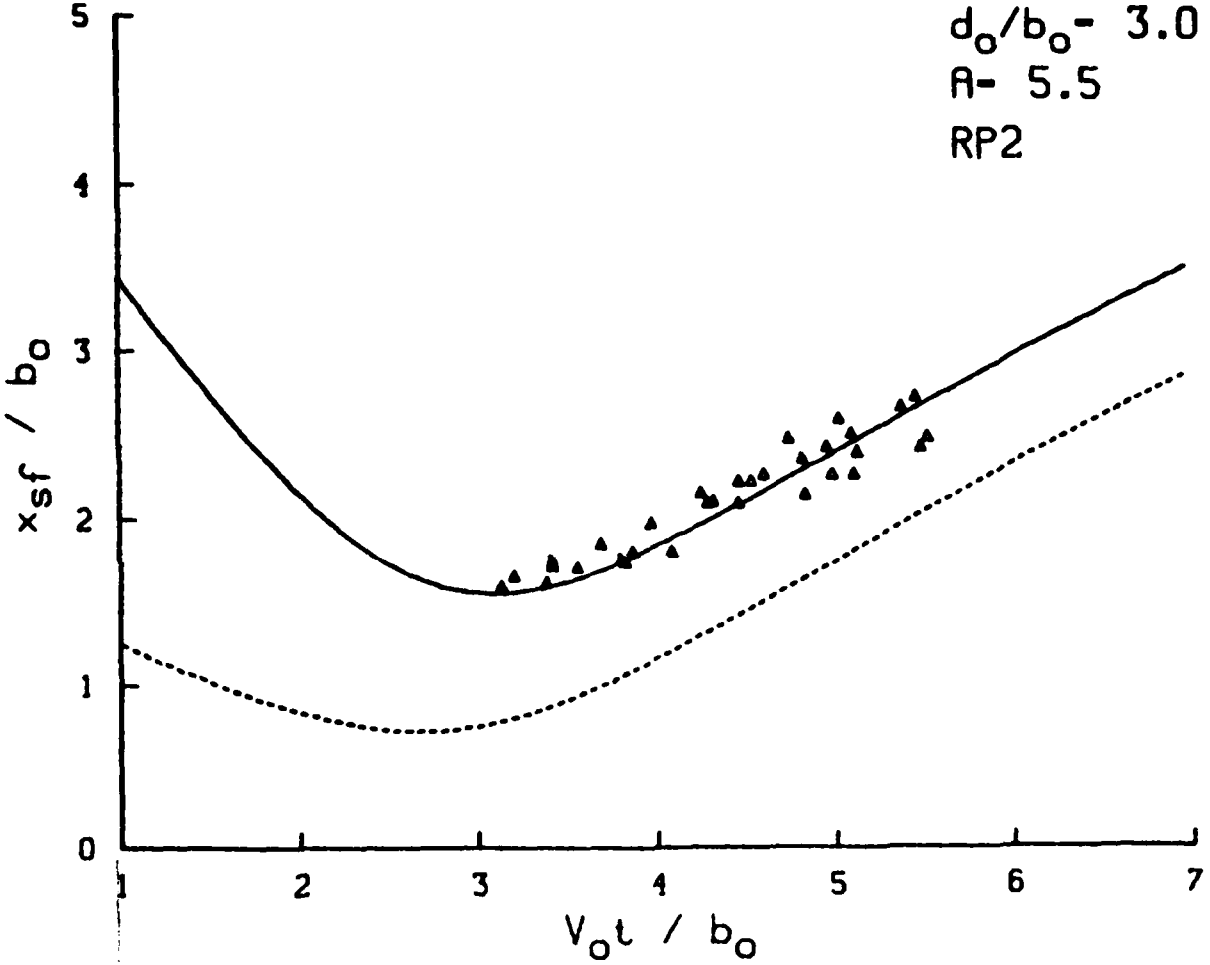

Figure 61. Scar Front Position, RP2, d_o/b_o = 3, A = 5.5

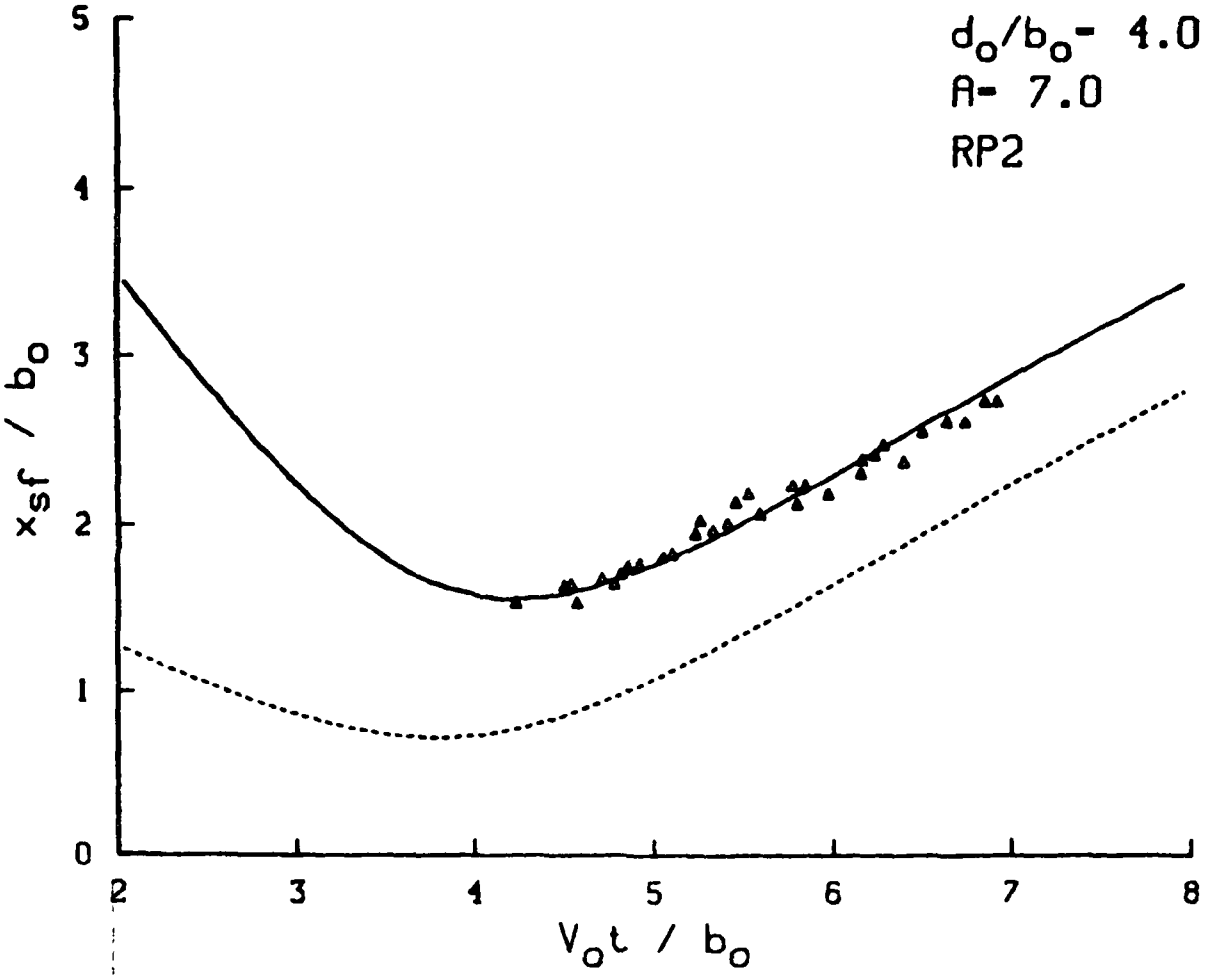

Figure 62. Scar Front Position, RP2, d_o/b_o = 4, A = 7.0

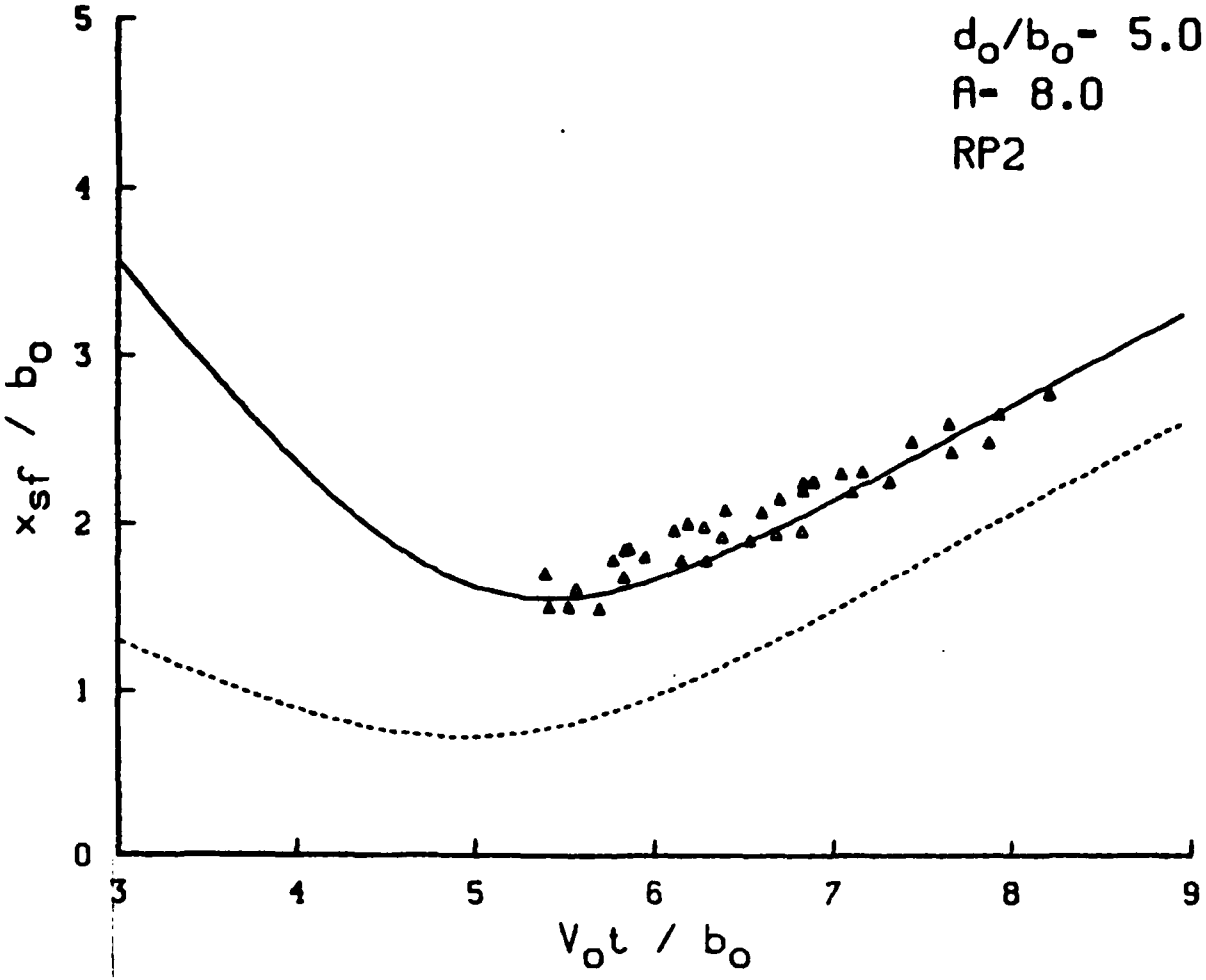

Figure 63. Scar Front Position, RP2, d_o/b_o = 5, A = 8.0

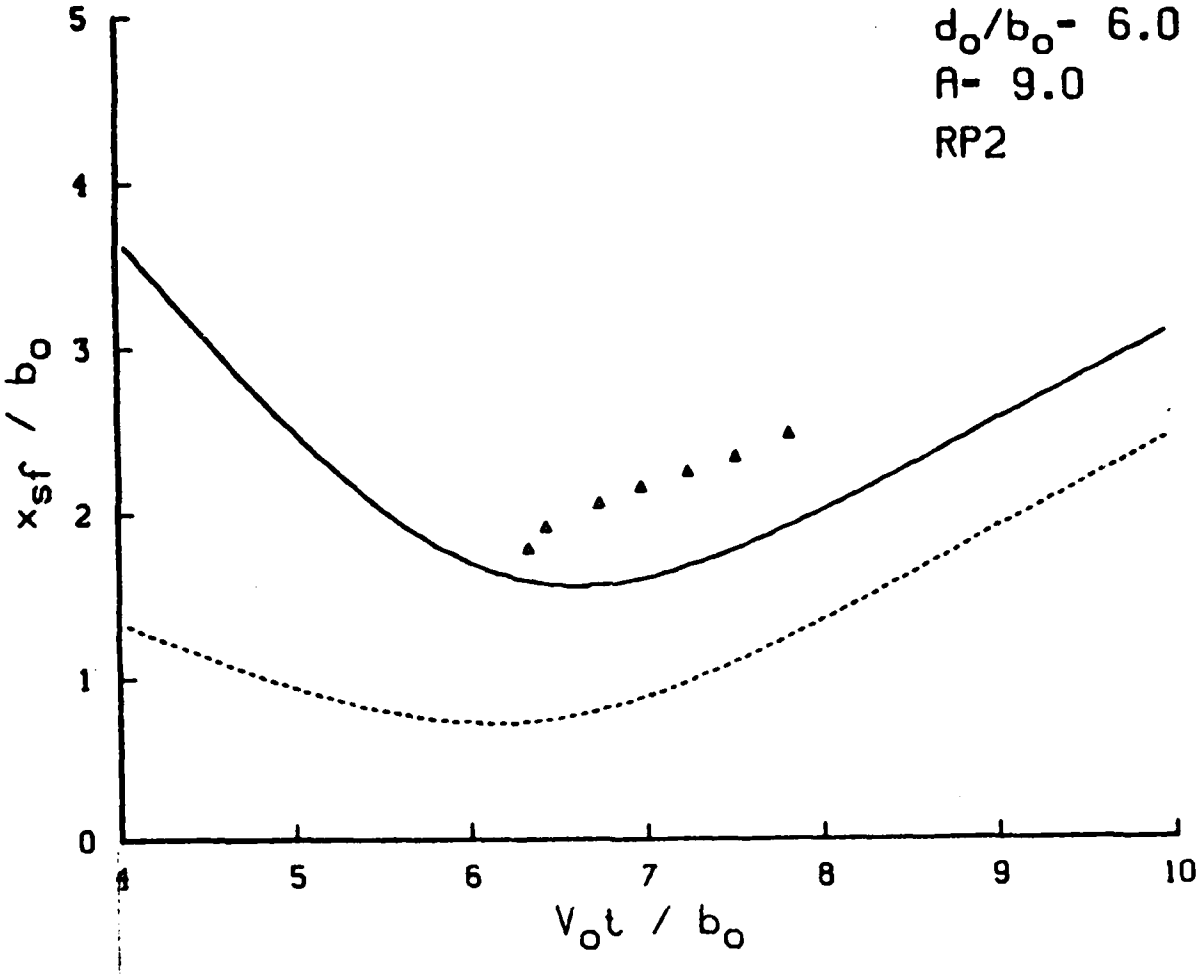

Figure 64. Scar Front Position, RP2, d_o/b_o = 6, A = 9.0

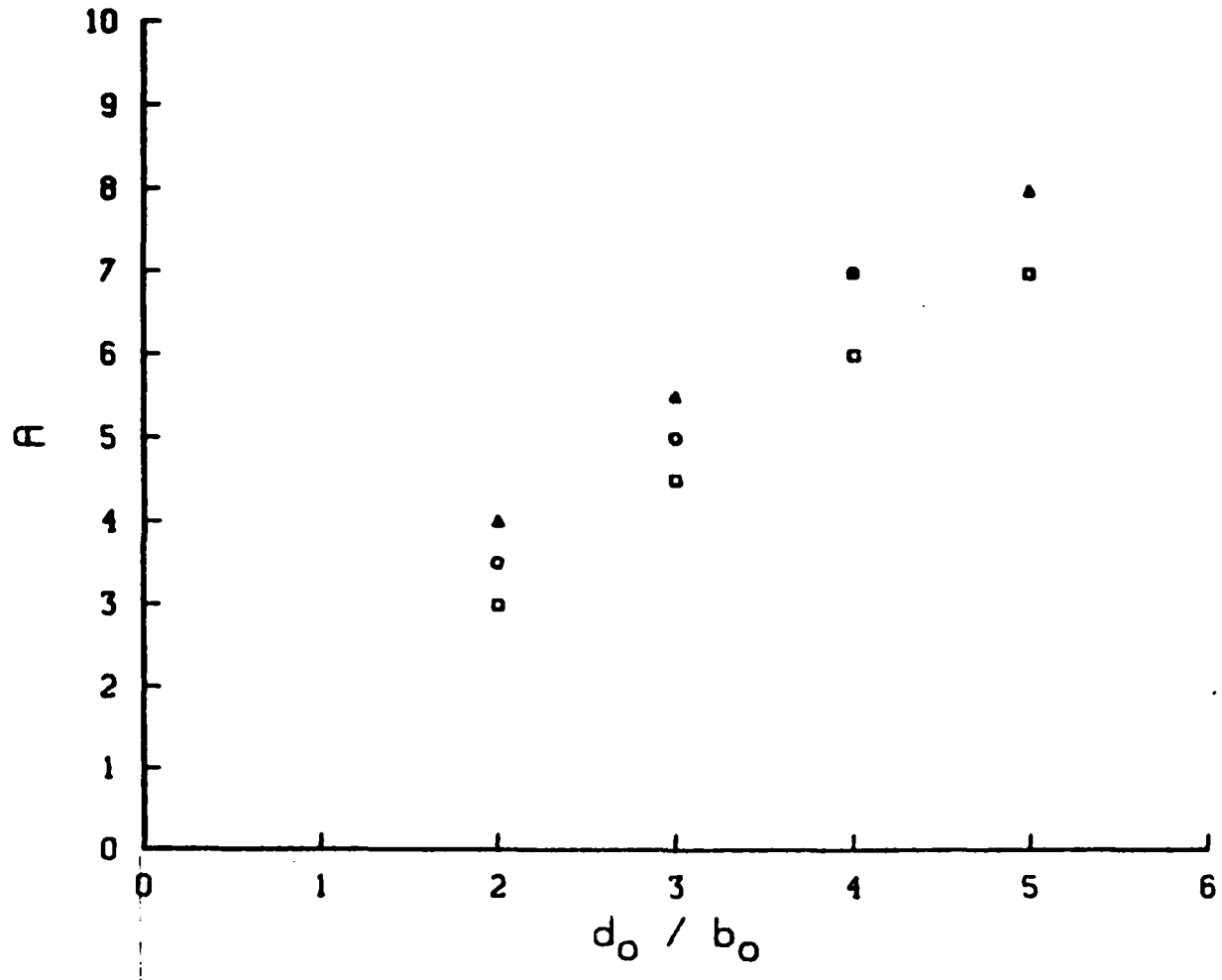

Figure 65. Dissipation Parameter A as Function of d_o/b_o

APPENDIX A: COMPUTER CODE FOR CALCULATING u_s/V_o

```
C*******************
C
C         PROGRAM TO PLOT THE SURFACE VELOCITY PROFILES
C                   EXPONENTIAL AND INVISCID CASES.
C
C*******************
      DIMENSION XC(1000),YO(1000),T(1000),XT(200),VT(200),XSC(2),YSC(2)
      DIMENSION SCL(2)
      DATA XSC/0.,0./,YSC/0.,3./,SCL/0.,10./
C     INITIAL PLOT DEVICE
      CALL COMERS
      CALL PAGE(14.,10.)
C     INPUT A VALUE
      WRITE(7,111)
      READ(7,*) AE
C     INITIALIZE: DO CAN BE CHANGED TO ANY VALUE
      DO=4.0
      TMAX=10.
      XMAX=10.
      DX=XMAX/200.
      NPT=1000
C     CALCULATE VORTEX POSITIONS
      CALL VCSIT(TMAX,XO,YO,DO,NPT,T,AE)
C     PLOT SETUP ROUTINES
      CALL NCURVE
      CALL AREA2D(9.,7.)
      CALL MX1ALF('L/CSTD','*')
      CALL MX2ALF('STANDARD','*')
      CALL MX3ALF('INSTRU','*')
      CALL HEIGHT(.24)
      CALL XFRVTK
      CALL YFRVTK
      CALL XINTAX
      CALL YINTAX
      CALL XAXANG(0.)
      CALL TRKCRV(.01)
      CALL YNAME('U!L.5*S!I.0*/V!I.5*O!L.0*$',100)
      CALL XNAME('X/E!L.5*C!L.0*$',100)
      CALL GRAF(0.0,1.,XMAX,0.,1.,3.)
      CALL MESSAG('D!L.5*O!I.0*/B!I.5*C!L.0*=$',100,6.,6.5)
```

```
      CALL BEAINC(DO,1,'ABUT','ABUT')
      XTH=FLOAT(I)/100.
      IF (AE.GE.1000.) GO TO 13
      CALL MESSAG('#A=*$',100,6.,6.0)
      CALL BEAINC(AE,1,'ABUT','ABUT')
      GO TO 14
13    CALL MESSAG('#INVISCID MODEL*$',100,6.,6.0)
      GO TO 14
C  CALCULATE VELOCITIES
14    DO 10 I=100,NPT,100
      IF ((T(I)/AE).LT.0.00625) GO TO 7
      GT=(1.-EXP(-AE/T(I)))*2.0*YO(I)
      GO TO 8
7     GT=1.
8     YY=YO(I)**2
      DO 20 J=1,200
      XT(J)=DX*FLOAT(J)
      VT(J)=GT*(1./((XT(J)-XO(I))**2+YY)-1./((XT(J)+XO(I))**2+YY))
20    CONTINUE
C  PLOT DATA
      CALL CURVE(XT,VT,200,0)
      CALL CURVE(XCL,YSC,2,0)
      CALL CURVE(XSC,YSC,2,0)
10    CONTINUE
      CALL ENDPL(0)
5     CONTINUE
      CALL DONEPL
      STOP
111   FORMAT('  ENTER THE DESIRED A VALUE ',/,' IF A > 1000, INVISCID
     *CASE ASSUMED')
      END
CCCCC
C          SUBROUTINE POSIT
C
CCCCC
      SUBROUTINE POSIT(TMAX,XO,YO,DOEO,NPTS,T,AA)
      DIMENSION T(NPTS),XO(NPTS),YO(NPTS)
      DT=TMAX/FLOAT(NPTS)
      XO(1)=.5
      YO(1)=DOEO
      T(1)=0.0
      C=1./DOEO/DOEO+4.0
      DO 10 I=2,NPTS
      IF ((T(I-1)/AA).LT.0.00625)  GO TO 5
      TEX=1.-EXP(-AA/T(I-1))
      GO TO 6
5     TEX=1.0
6      XO(I)=XO(I-1)+TEX*(((C*(XO(I-1)**2)-1.)**1.5)/
```

```
     X    (2.*C*XO(I-1)**3))*DT
      YO(I)=YO(I-1)-TEX*((JC*(YO(I-1)**2)-1.)**1.5)/
     X    (2.*C*YO(I-1)**3))*DT
      T(I)=T(I-1)+DT
10    CONTINUE
      RETURN
      END
```

APPENDIX B: COMPUTER CODE FOR CALCULATING x_m/b_o

```
CCCCCCCCCCCCCCCCCCCCCCCCCCCCCCCCCCCCCCCCCCCCCCCCCCCCCCCCCCCCCCCCCCCCCCCCCCCC
C                                                                            C
CPROGRAM TO COMPUTE THE POSITION OF THE MAXIMUM SURFACE VELOCITY             C
C      FO VALUES OF DO/BO OF 2-7 AND PLOT                                    C
C      ON THE SAME GRAPH                                                     C
C                                                                            C
CCCCCCCCCCCCCCCCCCCCCCCCCCCCCCCCCCCCCCCCCCCCCCCCCCCCCCCCCCCCCCCCCCCCCCCCCCCC
      DIMENSION XBO(300),YBO(300),T(300),X1(300),X2(300)
      DIMENSION XSC(2),YSC(2),SC(2)
      DATA XSC/0.,0./,YSC/0.,5./,SC/0.,12./
C  PLOT INITIALIZE
      CALL COMPRS
      CALL PAGE (14.,10.)
      CALL NCPLOT
C INITIALIZE VALUES
      TMAX=12.
      BO=3.7
      NPT=200
C  GRAPHING ROUTINES
      CALL AREA2D (9.,7.)
      CALL MX1ALP('L/CSTD','(')
      CALL MX2ALP('STANDARD','(')
      CALL MX3ALP('INSTRU','(')
      CALL HEIGHT(.24)
      CALL XGRVTK
      CALL YGRVTK
      CALL THKCRV(.01)
      CALL XINTAX
      CALL YINTAX
      CALL YAXANG(0.)
      CALL YNAME ('X/L.5)M/L.0) / B/L.5)O/L.0)$',100)
      CALL XNAME ('(V/L.5)C/L.0)T / E/L.5)O/L.0)$',100)
      CALL GRAF (0.0,1.,TMAX,0.,1.,5.0)
C  CALCULATE VELOCITIES
      DO 20 J=2,7
      DOBO=FLOAT(J)
      XK=4.+1./DOBO/DOBO
      CALL XYTIM(TMAX,NPT,XBO,YBO,DOBO,BO,T)
      DO 10 I=1,NPT
      A=(4.*XK*XBO(I)**2-4.0)*XK*XBO(I)**2+4.0
```

```
      B=XBO(I)**2/3./(XK*XBO(I)**2-1.)
      C=(XK*XBO(I)**2-2.)*XEO(I)**2/3./(XK*XBO(I)**2-1.)
      IF (A.LT.0.0) GO TO 98
      XX1=C+B*SQRT(A)
      XX2=C-B*SQRT(A)
      X1(I)=SQRT(XX1)
      IF(XX2.LT.0.0) XX2=0.0
      X2(I)=SQRT(XX2)
      GO TO 88
98    CONTINUE
      X1(I)=-9999.
      X2(I)=-9999.
88    CONTINUE
10    CONTINUE
C  PLOT DATA
      CALL CURVE (T,X1,NPT,0)
      CALL CURVE(SC,XSC,2,0)
      CALL CURVE(XSC,YSC,2,0)
20    CONTINUE
      CALL ENDEL(0)
      CALL DONEPL
      STOP
      END
CCCCCCCCCCCCCCCCCCCCCCCCCCCCCCCCCCCCCCCCCCCCCCCCCCCCCCCCCCCCCCCCCCCCCCCCCCCC
C SUBROUTINE TO COMPUTE XO/EO AND YO/BO AS A FUNCTION OF NON-DIM
C     TIME, VOT/EO
C
C     INPUT PARAMETERS:
C           TMAX              MAX TIME DESIRED
C           NPOINT            TOTAL # OF POINTS OF INTEREST (MAX=1000)
C           DOBO              DO/BO
C           EO                BO
C
C     OUTPUT PARAMETERS:
C           XBO                ARRAY OF XO/BO
C           YBO                ARRAY OF YO/BO
C           T                 ARRAY OF NON-DIM TIME VOT/BO
C
C
CCCCCCCCCCCCCCCCCCCCCCCCCCCCCCCCCCCCCCCCCCCCCCCCCCCCCCCCCCCCCCCCCCCCCCCCCCCC
      SUBROUTINE XYTIM(TMAX,NPOINT,XEO,YBO,DOBO,BO,T)
      DIMENSION T(1000),YBO(1000),XBO(1000)
      T(1)=0.
      XM=2.*DOEO
      XA=XM**2/(1.+XM**2)
      XB=(XM**2-1.)/XM
      XC=1.+XM**2
      A=2.+(T(1)*2./XA**2-XE)**2
```

```
      Y1=SQRT(1./XC+(A+SQRT(A**2-4.))/2./XC)
      Y2=SQRT(1./XC+(A-SQRT(A**2-4.))/2./XC)
      IF (ABS(Y1*DOBO-DOBO).LT.0.01) GO TO 5
      YBO(1)=Y2*DOBO
      IXL=0
      GO TO 6
    5 IXL=1
      YBO(1)=Y1*DOBO
    6 CONTINUE
      IL=0
      IF((Y1-Y2)/DOBO.GE.0.02) IL=1
      XX1=Y1-Y2
      NTRANS=NPOINT
      IL2=IL
      XBO(1)=.5
      DO 10 I=2,NPOINT
      T(I)=TMAX/FLOAT(NPOINT)*FLOAT(I-1)
      A=2.+(T(I)*2./XA**2-XE)**2
      Y1=SQRT(1./XC+(A+SQRT(A**2-4.))/2./XC)
      Y2=SQRT(1./XC+(A-SQRT(A**2-4.))/2./XC)
      XX2=Y1-Y2
      IF((XX2.GE.XX1).AND.(I.LT.NTRANS)) GO TO 18
      GO TO 19
   18 IL2=IABS(IL2-1)
      NTRANS=I
   19 CONTINUE
      IF(IL.EQ.IL2) GO TO 15
      IXL=IABS(IXL-1)
      IL=IABS(IL-1)
   15 CONTINUE
      YBO(I)=Y1*DOBO
      IF (IXL.EQ.0) YBO(I)=Y2*DOBO
      XX1=XX2
      XBO(I)=YBO(I)/SQRT((4.+1./DOBO**2)*YBO(I)**2-1.)
   10 CONTINUE
      RETURN
      END
```

APPENDIX C: COMPUTER CODE FOR CALCULATING x_m/b_o, x_v/b_o, y_v/b_o, u_m/b_o

```
CCCCCCCCCCCCCCCCCCCCCCCCCCCCCCCCCCCCCCCCCCCCCCCCCCCCCCCCCCCCCCCCCCCCCCCCCCC
C                                                                      C
C   PROGRAM TO CALCULATE MAX SURFACE VELOCITY (US), MAX VELOCITY       C
C         POSITION (XM) AND VORTEX POSITION (XV,YV) AS FXNS OF         C
C         VOT/BO                                                       C
C         AND PLOT ON THE SAME GRAPH                                   C
C                                                                      C
CCCCCCCCCCCCCCCCCCCCCCCCCCCCCCCCCCCCCCCCCCCCCCCCCCCCCCCCCCCCCCCCCCCCCCCCCCC
C
CC  INITIALIZE
C
      DIMENSION XMX(300),UVE(300),T(300),XBO(300),YBO(300)
      DIMENSION S0(2),SX(2),S5(2),SY(5)
      DATA S0/0.,0./,SY/0.,5./
      SX(1)=0.
C
CCC SET UP PLOTTING ROUTINES
C
      CALL CCMERS
      CALL PAGE(14.,10.)
C   START LOOP
      DO 50 IL=2,7
      DOBO=FLOAT(IL)
      TMAX=DOBO+4.
      SX(2)=TMAX
      S5(1)=TMAX
      S5(2)=TMAX
C
CC  ADDITIONAL PLOTTING ROUTINES
C
      CALL NCPSDR
      CALL AREA2D(9.,7.)
      CALL MX1ALF('L/CSTD','*')
      CALL MX2ALF('STANDARD','*')
      CALL MX3ALF('INSTRU','*')
      CALL FRIGHT(.24)
      CALL XPRVTK
      CALL YPRVTK
      CALL XINTAX
      CALL YINTAX
```

```
      CALL MAXANG(0.)
      CALL THKCHV(.01)
      CALL XNAME('XIL.5*MIL.0* / BIL.5*OIL.0*$',100)
      CALL XNAME('$VIL.5*OIL.0*T / BIL.5*OIL.0*$',100)
      CALL GBAF(0.0,1.,TMAX,0.,1.,5.)
      CALL MESSAG('DIL.5*OIL.0*/BIL.5*OIL.0* =$',100,6.,7.5)
      CALL BEAINC(DOBO,1,'AEUT','ABUT')
      EO=3.7
      NPT=300
C  CALL TO SUBROUTINE XYTIM CALCULATES XV,YV FOR VOT/BO
      CALL XYTIM(TMAX,NPT,XEO,YBO,DOEO,BO,T)
C
      DO 20 I=1,NPT
      XMX(I)=0.
      UVM(I)=0.
      XO=XBO(I)*BO
      YO=YEO(I)*EO
C  CALCULATE MAXIMUM VELOCITY, POSITION
      DO 30 J=1,1000
      Y=0.0
      X=BO*TMAX/1000.*FLOAT(J-1)
      UV=BO*YO*(-1./((X+XO)**2+YO**2)+1./((X-XO)**2+YO**2)
     X -1./((X+XO)**2+YO**2)+1./((X-XO)**2+YO**2))
      IF(UV.GT.UVM(I)) XMX(I)=X/BO
      IF(XMX(I).GE.4.9) XMX(I)=XBO(I)
      IF(UV.GT.UVM(I)) UVM(I)=UV
      X=X/EO
30    CONTINUE
20    CONTINUE
C  PLOT DATA
      CALL CURVE(T,XMX,NPT,0)
      CALL BASE
      CALL CURVE(T,XBO,NPT,0)
      CALL CURVE(T,YBO,NPT,0)
      CALL CENDSH
      CALL YGRAXS(0.0,1.0,5.0,7.,'UIL.5*MIL.0# / VIL.5*OIL.0*$',
     X-100,9.0,0.)
      CALL CURVE (T,UVM,NPT,0)
      CALL RESET('CHNDSH')
      CALL CURVE (SX,S0,2,0)
      CALL CURVE (S0,SY,2,0)
      CALL CURVE (S5,SY,2,0)
      CALL ENDPL(0)
50    CONTINUE
      CALL DONEPL
      STOP
      END
```

```
      SUBRCUTINE XYTIM(TMAX,NPOINT,XBO,YBO,DOBO,BO,T)
      DIMENSICN T(1000),YBC(1000),XBO(1000)
      T(1)=0.
      XM=2.*DOBO
      XA=XM**2/(1.+XM**2)
      XB=(XM**2-1.)/XM
      XC=1.+XM**2
      A=2.+(T(1)*2./XA**2-XB)**2
      Y1=SQRT(1./XC+(A+SQRT(A**2-4.))/2./XC)
      Y2=SQRT(1./XC+(A-SQRT(A**2-4.))/2./XC)
      IF (ABS(Y1*DOBO-DOBO).LT.001) GO TO 5
      YBO(1)=Y2*DOBO
      IXL=0
      GO TC 6
    5 IXL=1
      YBO(1)=Y1*DOBO
    6 CONTINUE
      IL=0
      IF((Y1-Y2)/DOBO.GE.0.02) IL=1
      XX1=Y1-Y2
      NTRANS=NPOINT
      IL2=IL
      XBO(1)=.5
      DO 10 I=2,NPOINT
      T(I)=TMAX/FLOAT(NPOINT)*FLOAT(I-1)
      A=2.+(T(I)*2./XA**2-XB)**2
      Y1=SQRT(1./XC+(A+SQRT(A**2-4.))/2./XC)
      Y2=SQRT(1./XC+(A-SQRT(A**2-4.))/2./XC)
      XX2=Y1-Y2
      IF((XX2.GE.XX1).AND.(I.LT.NTRANS)) GO TO 18
      GO TC 19
   18 IL2=IABS(IL2-1)
      NTRANS=I
   19 CONTINUE
      IF(IL.EQ.IL2) GO TO 15
      IXL=IABS(IXL-1)
      IL=IABS(IL-1)
   15 CONTINUE
      YBO(I)=Y1*DOBO
      IF (IXL.EQ.0) YBO(I)=Y2*DOBO
      XX1=XX2
      XBO(I)=YBO(I)/SQRT((4.+1./DOBO**2)*YBO(I)**2-1.)
   10 CONTINUE
      RETURN
      END
```

APPENDIX D: COMPUTER CODE FOR CALCULATING POSITION OF MARKER PARTICLE

```
CCCCCCCCCCCCCCCCCCCCCCCCCCCCCCCCCCCCCCCCCCCCCCCCCCCCCCCCCCCCCCCCCCCCCCCCCCCC
C                                                                             C
C     PROGRAM TO CALCULATE POSITION OF FLUID PARTICLE ON Y AXIS               C
C ***   (YV-Y)/EO                                                             C
C                                                                             C
CCCCCCCCCCCCCCCCCCCCCCCCCCCCCCCCCCCCCCCCCCCCCCCCCCCCCCCCCCCCCCCCCCCCCCCCCCCC
      DIMENSION XO(1000),YO(1000),T(1000),Y(1000),H(200)
      DIMENSION XS(3),YS(3)
      DATA XS/0.0,0.0,10.0/,YS/1.0,0.0,0.0/
C INITIALIZE DATA: CALCULATIONS VALID FOR ALL BO DUE TO NON-DIMENSIONAL
C    CALCULATIONS
      EO=3.534
      NPT=1000
      TMAX=10.
      DT=TMAX/FLOAT(NPT)
C   PLOT INITIALIZATION
C     CALL TEK 618
      CALL CCMERS
      CALL PAGE(14.,10.)
      CALL NOFRDR
      CALL AREA2D(9.,7.)
      CALL MX1ALF('L/CSTD','*')
      CALL MX2ALF('STANDARD','*')
      CALL MX3ALF('INSTRU','*')
      CALL HEIGHT(.24)
      CALL XFRVTK
      CALL YFRVTK
      CALL XINTAX
      CALL YINTAX
      CALL TAXANG(0.)
      CALL THKCRV(.01)
      CALL YNAME('(Y!L.5*V!I.0*-Y) / B!L.5*O!L.0*$',100)
      CALL XNAME('#V!L.5*O!I.0*T / B!L.5*O!L.0*$',100)
      SCL=DOBO/10.
      CALL GRAF(0.0,1.,TMAX,0.0,0.1,1.0)
      DO 88 IT=2,6
      DOBO=FLOAT(IT)
C CALCULATE VORTEX POSITIONS
      CALL XYTIM(TMAX,NPT,XO,YO,DOBO,BO,T)
      Y(1)=IOEO
```

```
      DO 20 I=2,NET
C CALCULATE MARKER PARTICLE POSITION
      R1=1./(X0(I-1)**2+(Y0(I-1)-Y(I-1))**2)
      R2=1./(X0(I-1)**2+(Y0(I-1)+Y(I-1))**2)
      Y1P=2.*X0(I-1)*(R2-R1)
      Y1=Y(I-1)+Y1P*DT
      R1P=1./(X0(I)**2+(Y0(I)-Y1)**2)
      R2P=1./(X0(I)**2+(Y0(I)+Y1)**2)
      Y2P=2.*X0(I)*(R2-R1)
      Y(I)=Y(I-1)+(Y1P+Y2P)*DT/2
20    CONTINUE
      DO 30 J=1,NET
      I1=(J-1)/5
      X1=FLOAT(J-1)/5.
      T1=X1-FLOAT(I1)
      IF(ABS(T1).LT..0001) GO TO 25
      GO TO 30
C *****
25    H(I1+1)=(Y0(J)-Y(J))
      T(I1+1)=T(J)
30    CONTINUE
C  PLOT RESULTS
      CALL CURVE(T,H,200,0)
      CALL CURVE(XS,YS,3,0)
88    CONTINUE
      CALL ENDPL(0)
50    CALL DONEPL
      STOP
      END
CCCCCCCCCCCCCCCCCCCCCCCCCCCCCCCCCCCCCCCCCCCCCCCCCCCCCCCCCCCCCCCCCCCCCC
C                                                                    C
C SUBROUTINE TO COMPUTE X0/B0 AND Y0/B0 AS A FUNCTION OF NON-DIM     C
C     TIME, VOT/B0                                                   C
C                                                                    C
C     INPUT PARAMETERS:                                              C
C           TMAX          MAX TIME DESIRED                           C
C           NECINT        TOTAL # OF POINTS OF INTEREST (MAX=1000)   C
C           DOBO          D0/B0                                      C
C           BO            B0                                         C
C                                                                    C
C     OUTPUT PARAMETERS:                                             C
C           XBO            ARRAY OF X0/B0                            C
C           YBO            ARRAY OF Y0/B0                            C
C           T             ARRAY OF NON-DIM TIME VOT/B0               C
C                                                                    C
CCCCCCCCCCCCCCCCCCCCCCCCCCCCCCCCCCCCCCCCCCCCCCCCCCCCCCCCCCCCCCCCCCCCCC
```

```
      SUBROUTINE XYTIM(TMAX,NPOINT,XEO,YBO,DOBO,BO,T)
      DIMENSION T(1000),YBO(1000),XBO(1000)
      T(1)=0.
      XM=2.*DOBO
      XA=XM**2/(1.+XM**2)
      XB=(XM**2-1.)/XM
      XC=1.+XM**2
      A=2.+(T(1)*2./XA**2-XE)**2
      Y1=SQRT(1./XC+(A+SQRT(A**2-4.))/2./XC)
      Y2=SQRT(1./XC+(A-SQRT(A**2-4.))/2./XC)
      IF (ABS(Y1*DOBO-DOBO).LT.0.01) GO TO 5
      YBO(1)=Y2*DOBO
      IXL=0
      GO TO 6
    5 IXL=1
      YBO(1)=Y1*DOBO
    6 CONTINUE
      IL=0
      IF((Y1-Y2)/DOBO.GE.0.02) IL=1
      XX1=Y1-Y2
      NTRANS=NPOINT
      IL2=IL
      XBO(1)=.5
      DO 10 I=2,NPOINT
      T(I)=TMAX/FLOAT(NPOINT)*FLOAT(I-1)
      A=2.+(T(I)*2./XA**2-XE)**2
      Y1=SQRT(1./XC+(A+SQRT(A**2-4.))/2./XC)
      Y2=SQRT(1./XC+(A-SQRT(A**2-4.))/2./XC)
      XX2=Y1-Y2
      IF((XX2.GE.XX1).AND.(I.LT.NTRANS)) GO TO 18
      GO TO 19
   18 IL2=IABS(IL2-1)
      NTRANS=I
   19 CONTINUE
      IF(IL.EQ.IL2) GO TO 15
      IXL=IABS(IXL-1)
      IL=IABS(IL-1)
   15 CONTINUE
      YBO(I)=Y1*DOBO
      IF (IXL.EQ.0) YBO(I)=Y2*DOBO
      XX1=XX2
      XBO(I)=XEO(I)/SQRT((4.+1./DOBO**2)*YBO(I)**2-1.)
   10 CONTINUE
      RETURN
      END
```

APPENDIX E: COMPUTER CODE FOR CALCULATING POSITION OF TOP OF RECIRCULATION CELL

```
CCCCCCCCCCCCCCCCCCCCCCCCCCCCCCCCCCCCCCCCCCCCCCCCCCCCCCCCCCCCCCCCCCCCCCCCCCCC
C                                                                            C
C     PROGRAM TO CALCULATE POSITION OF FLUID PARTICLE ON Y AXIS              C
C      HEIGHT SCALED ON DOBO:                                                C
C        (I.E. H CORRESPONDS TO THE POSITION OF THE TOP OF THE               C
C           RECIRCULATION CELL AFTER SMALL TIMES)                            C
C                                                                            C
CCCCCCCCCCCCCCCCCCCCCCCCCCCCCCCCCCCCCCCCCCCCCCCCCCCCCCCCCCCCCCCCCCCCCCCCCCCC
      DIMENSION XC(1000),YO(1000),T(1000),Y(1000),H(200),AA(2),BB(2)
C  INITIALIZES PARAMETERS. NOTE EVEN THOUGH VO,BO SPECIFIED,
C   NON-DIMENSIONALIZING IN PROGRAM MAKES CODE VALID FOR ALL GEOMETRIES
      VO=.05
      BO=3.534
      NPT=1000
      TMAX=10.
      DT=TMAX/FLOAT(NPT)
      AA(1)=0.
      AA(2)=TMAX
C   PLOT INITIALIZATION
      CALL TEK 618
      CALL PAGE(14.,10.)
      CALL NOBORD
      BB(1)=1.0
      BB(2)=1.0
      CALL AREA2D(9.,7.)
      CALL MIXALF('L/STD','*')
      CALL MIX2ALF('STANDARD','*')
      CALL MIX3ALF('INSTRU','!')
      CALL HEIGHT(.24)
      CALL XNEVTK
      CALL YNEVTK
      CALL XINTAX
      CALL YINTAX
      CALL YAXANG(0.)
      CALL THKCRV(.01)
      CALL YNAME('H / B!L.5*O!L.0*$',100)
      CALL XNAME('#V!L.5*O!I.0*T / B!L.5*O!L.0*$',100)
      CALL GRAF(0.0,1.,TMAX,0.0,1.0,8.0)
      DO 777 ITN=2,7
      DOBO=FLOAT(ITN)
```

```
      SCL=DOBO/10.
C ****CALCULATE VORTEX POSITIONS
      CALL XYTIE(TMAX,NPT,XO,YO,DOBO,BO,T)
      Y(1)=DOEO
C     CALCULATE POSITION OF PARTICLE
      DO 20 I=2,NPT
      R1=1./(XO(I-1)**2+(YO(I-1)-Y(I-1))**2)
      R2=1./(XO(I-1)**2+(YO(I-1)+Y(I-1))**2)
      Y1P=2.*XO(I-1)*(R2-R1)
      Y1=Y(I-1)+Y1P*DT
      R1P=1./(XO(I)**2+(YO(I)-Y1)**2)
      R2P=1./(XO(I)**2+(YO(I)+Y1)**2)
      Y2P=2.*XO(I)*(R2-R1)
      Y(I)=Y(I-1)+(Y1P+Y2P)*DT/2
20    CONTINUE
      DO 30 J=1,NPT
      I1=(J-1)/5
      X1=FLOAT(J-1)/5.
      T1=X1-FLOAT(I1)
      IF(ABS(T1).LT..0001) GO TO 25
      GO TO 30
C
25    H(I1+1)=DOBO-Y(J)
      T(I1+1)=T(J)
30    CONTINUE
C PLOT
      CALL CURVE(T,H,200,0)
777   CONTINUE
      CALL ENDPL(0)
50    CALL DONEPL
      STOP
      END
CCCCCCCCCCCCCCCCCCCCCCCCCCCCCCCCCCCCCCCCCCCCCCCCCCCCCCCCCCCCCCCCCCCCCCCCCCC
C SUBROUTINE TO COMPUTE XO/EO AND YO/BO AS A FUNCTION OF NON-DIM
C     TIME, VOT/BO
C
C     INPUT PARAMETERS:
C           TMAX          MAX TIME DESIRED
C           NPOINT        TOTAL # OF POINTS OF INTEREST (MAX=1000)
C           DOBO          DO/BO
C           EO            BO
C
C     OUTPUT PARAMETERS:
C           XEO            ARRAY OF XO/BO
C           YBO            ARRAY OF YO/BO
C           T             ARRAY OF NON-DIM TIME VOT/BO
C
CCCCCCCCCCCCCCCCCCCCCCCCCCCCCCCCCCCCCCCCCCCCCCCCCCCCCCCCCCCCCCCCCCCCCCCCCCC
```

```
      SUBROUTINE XYTIM(TMAX,NPOINT,XEO,YBO,DOBO,BO,T)
      DIMENSION T(1000),YBO(1000),XBO(1000)
      T(1)=0.
      XM=2.*DOEO
      XA=XM**2/(1.+XM**2)
      XB=(XM**2-1.)/XM
      XC=1.+XM**2
      A=2.+(T(1)*2./XA**2-XE)**2
      Y1=SQRT(1./XC+(A+SQRT(A**2-4.))/2./XC)
      Y2=SQRT(1./XC+(A-SQRT(A**2-4.))/2./XC)
      IF (ABS(Y1*DOBO-DOBO).LT.001) GO TO 5
      YBO(1)=Y2*DOBO
      IXL=0
      GO TO 6
    5 IXL=1
      YBO(1)=Y1*DOBO
    6 CONTINUE
      IL=0
      IF((Y1-Y2)/DOBO.GE.0.02) IL=1
      XX1=Y1-Y2
      NTRANS=NPOINT
      IL2=IL
      XBO(1)=.5
      DO 10 I=2,NPOINT
      T(I)=TMAX/FLOAT(NPOINT)*FLOAT(I-1)
      A=2.+(T(I)*2./XA**2-XE)**2
      Y1=SQRT(1./XC+(A+SQRT(A**2-4.))/2./XC)
      Y2=SQRT(1./XC+(A-SQRT(A**2-4.))/2./XC)
      XX2=Y1-Y2
      IF((XX2.GE.XX1).AND.(I.LT.NTRANS)) GO TO 18
      GO TO 19
   18 IL2=IABS(IL2-1)
      NTRANS=I
   19 CONTINUE
      IF(IL.EQ.IL2) GO TO 15
      IXL=IABS(IXL-1)
      IL=IABS(IL-1)
   15 CONTINUE
      YBO(I)=Y1*DOBO
      IF (IXL.EQ.0) YBO(I)=Y2*DOBO
      XX1=XX2
      XBO(I)=YBO(I)/SQRT((4.+1./DOBO**2)*YBO(I)**2-1.)
   10 CONTINUE
      RETURN
      END
```

APPENDIX F: TABULATED DATA

DELTA-2R d_o/b_o= 2.0 B= 5.02

α=12° V_o/U= 0.0450 b_o= 3.700

U= 3.51

$V_o t/b_o$	s/b_o
1.72	0.93*
2.23	1.40*
2.79	1.60
3.36	1.86
3.82	2.11
4.33	2.26
4.79	2.47

U= 3.53

$V_o t/b_o$	s/b_o
1.31	0.93*
2.19	1.43*
2.65	1.49*
3.12	1.81
3.79	2.01
4.05	2.24
4.36	2.46
4.87	2.52
5.23	2.72

U= 3.55

$V_o t/b_o$	s/b_o
1.53	0.84*
1.84	1.34*
2.62	1.51
2.88	1.68
3.81	2.18
4.17	2.35

U= 3.55

$V_o t/b_o$	s/b_o
1.48	0.50*
1.68	0.95*
2.67	1.61
2.93	1.77
3.81	2.24
4.12	2.37

U= 3.99

$V_o t/b_o$	s/b_o
1.45	0.97*
1.74	1.25*
2.97	2.00
3.26	2.06
4.36	2.51
4.65	2.63

U= 4.03

$V_o t/b_o$	s/b_o
1.20	0.93*
1.43	1.29*
2.43	1.73
2.78	1.90
3.84	2.40
4.25	2.57
4.72	2.68

* CORRESPONDS TO STRIATION MODE

DELTA-2R d_o/b_o= 2.0 B= 5.02

α=12° V_o/U= 0.0450 b_o= 3.700

U= 3.59		U= 3.59		U= 3.63	
$V_o t/b_o$	s/b_o	$V_o t/b_o$	s/b_o	$V_o t/b_o$	s/b_o
1.62	0.96*	1.68	0.90*	1.75	0.96*
1.83	1.20*	2.36	1.74	2.65	1.62
2.67	1.50*	2.67	1.80	2.81	1.68
3.25	1.75	3.72	2.22	3.71	2.04
3.41	1.89	3.93	2.34	3.87	2.10
4.77	2.40	4.77	2.57	4.82	2.40
4.35	2.22	5.29	2.64	5.03	2.46
5.50	2.64			5.56	2.64

* CORRESPONDS TO STRIATION MODE

DELTA-2R d_o/b_o- 3.0 B- 5.02

α-12° V_o/U- 0.0450 b_o- 3.700

U- 3.53

$V_o t/b_o$	s/b_o
2.73	0.94*
3.30	1.39*
3.76	1.55
4.23	1.86
4.64	1.99
5.05	2.24
5.82	2.34
6.28	2.60

U- 3.53

$V_o t/b_o$	s/b_o
2.73	0.92*
3.35	1.55
4.02	1.63
4.38	1.83
5.41	2.27
5.72	2.34

U- 3.53

$V_o t/b_o$	s/b_o
2.58	0.61*
3.09	1.30*
4.43	1.95
5.87	2.24

U- 3.59

$V_o t/b_o$	s/b_o
2.55	0.79*
2.92	1.17*
3.65	1.59
4.01	1.75
4.96	2.23
5.27	2.39

U- 3.55

$V_o t/b_o$	s/b_o
2.25	0.42*
2.62	0.74*
3.03	1.27*
3.70	1.51
3.85	1.65
4.16	1.81
4.58	2.02
5.26	2.23
5.72	2.60

U- 3.55

$V_o t/b_o$	s/b_o
2.77	0.99*
2.93	1.35*
3.34	1.56
3.76	1.69
4.27	1.88
4.84	2.10
5.36	2.33
5.83	2.42
6.35	2.56
6.55	2.74

* CORRESPONDS TO STRIATION MODE

DELTA-2R d_o/b_o- 3.0 B- 5.02

α-12° V_o/U- 0.0450 b_o- 3.700

U- 3.59

$V_o t/b_o$	s/b_o
2.38	0.89*
2.80	1.42*
3.33	1.63
3.85	1.90
4.37	2.04
5.48	2.47
6.05	2.62
5.53	2.51

* CORRESPONDS TO STRIATION MODE

DELTA-2R d_o/b_o = 4.0 B = 5.02°

α = 12° V_o/U = 0.0450 b_o = 3.700"

U = 3.55		U = 3.55		U = 3.51	
$V_o t/b_o$	s/b_o	$V_o t/b_o$	s/b_o	$V_o t/b_o$	s/b_o
4.04	1.01 *	3.67	0.78 *	3.49	0.25 *
4.61	1.12 *	3.73	1.02 *	3.53	0.97 *
5.33	1.80	5.18	1.85	4.51	1.46 *
6.01	1.99	6.32	2.33	5.02	1.78
6.38	2.22	6.73	2.48	5.43	1.90
6.79	2.33			5.78	2.09
7.83	2.53			6.20	2.28
				6.55	2.38

U = 3.55		U = 3.55		U = 3.51	
$V_o t/b_o$	s/b_o	$V_o t/b_o$	s/b_o	$V_o t/b_o$	s/b_o
3.67	0.65 *	4.09	0.75 *	3.43	0.49 *
4.04	0.75 *	4.65	1.50 *	3.89	1.02 *
4.55	1.35 *	5.28	1.70	4.30	1.51
5.28	1.65	5.69	1.90	5.18	1.70
5.69	1.85	6.16	2.15	5.63	2.02
6.06	2.00	6.88	2.30	6.51	2.48
				6.97	2.67

* CORRESPONDS TO STRIATION MODE

DELTA-2R d_o/b_o= 4.0 B= 5.02

α=12° V_o/U= 0.0450 b_o= 3.700

U= 3.51		U= 3.59		U= 3.59	
$V_o t/b_o$	s/b_o	$V_o t/b_o$	s/b_o	$V_o t/b_o$	s/b_o
3.74	0.90*	3.72	0.70*	3.46	0.83*
4.51	1.50*	4.03	1.14*	3.93	1.12*
4.97	1.75	5.13	1.74	4.30	1.50*
5.78	2.20	5.82	2.06	4.93	1.56
5.38	1.90	6.76	2.40	5.45	1.90
6.82	2.60			5.87	2.16
7.12	2.70			6.18	2.21
				7.02	2.40

* CORRESPONDS TO STRIATION MODE

DELTA-2R d_o/b_o= 5.0 B= 5.02

α=12° V_o/U= 0.0450 b_o= 3.700

U= 3.55

$V_o t/b_o$	s/b_o
4.53	0.76*
5.09	1.11*
6.65	1.83
7.06	2.05
7.48	2.22
7.89	2.40
8.51	2.56

U= 3.55

$V_o t/b_o$	s/b_o
5.05	0.81*
5.11	0.85*
5.93	1.49*
6.40	1.56
6.82	1.82
7.33	2.06
7.39	2.27
8.21	2.40

U= 3.55

$V_o t/b_o$	s/b_o
4.74	0.89*
5.05	1.16*
6.25	1.78
6.36	1.87
7.28	2.05

U= 3.55

$V_o t/b_o$	s/b_o
4.83	0.92*
5.09	0.96*
5.87	1.27*
6.38	1.50*
6.96	1.71
7.11	1.77
7.53	1.80

U= 3.51

$V_o t/b_o$	s/b_o
4.78	0.66*
5.29	1.17*
5.85	1.46*
6.01	1.50*
6.78	1.88
6.82	1.88
7.55	2.02

U= 3.55

$V_o t/b_o$	s/b_o
4.87	0.83*
5.13	0.99*
5.60	1.71
5.91	1.74
6.42	1.85
6.99	1.96
7.15	2.20
7.98	2.42
7.56	2.26
8.34	2.48

* CORRESPONDS TO STRIATION MODE

DELTA-2R d_o/b_o= 5.0 B= 5.02'

α=12° V_o/U= 0.0450 b_o= 3.700'

U= 3.59

$V_o t/b_o$	s/b_o
4.78	0.66*
5.29	1.17*
5.85	1.46*
6.01	1.50*
6.78	1.88
6.82	1.88
7.55	2.02

* CORRESPONDS TO STRIATION MODE

DELTA-2R d_o/b_o- 6.0 B- 5.02

α-12° V_o/U- 0.0450 b_o- 3.700

U- 3.55

$V_o t/b_o$	s/b_o
6.00	0.60*
7.70	1.65
8.47	2.05

U- 3.55

$V_o t/b_o$	s/b_o
5.89	0.77*
6.30	1.07*
6.71	1.41*
7.28	1.58
7.49	1.80
7.90	1.84
8.27	1.97

U- 3.63

$V_o t/b_o$	s/b_o
5.83	0.90*
6.10	1.08*
7.02	1.80
7.68	2.02
8.35	2.47
8.61	2.36

U- 3.62

$V_o t/b_o$	s/b_o
5.58	0.67*
6.04	0.81*
6.86	1.93
7.27	2.16
8.09	2.52

* CORRESPONDS TO STRIATION MODE

DELTA-2R d_o/b_o = 2.0 B = 5.02'

$\alpha = 10^o$ V_o/U = 0.0400 b_o = 3.700'

U = 3.67		U = 3.50		U = 3.53	
$V_o t/b_o$	s/b_o	$V_o t/b_o$	s/b_o	$V_o t/b_o$	s/b_o
1.62	0.84*	1.27	0.69*	1.51	0.68*
1.81	1.05*	1.54	1.05*	1.65	0.89*
3.05	1.83	2.45	1.67	2.79	1.73
4.09	2.43	2.63	1.80	2.98	1.80
		3.81	2.48	3.89	2.29
				4.17	2.35

* CORRESPONDS TO STRIATION MODE

DELTA-2R d_o/b_o= 3.0 B= 5.02°

α=10° V_o/U= 0.0400 b_o= 3.700'

U= 3.51

$V_o t/b_o$	s/b_o
2.82	0.81*
3.19	1.03*
4.05	1.62
4.28	1.78
4.78	2.11
5.60	2.32
6.19	2.65

U= 3.51

$V_o t/b_o$	s/b_o
3.01	0.74*
3.23	0.78*
4.14	1.57
4.37	1.68
5.42	2.08
5.56	2.18

U= 3.50

$V_o t/b_o$	s/b_o
2.59	0.62*
2.72	0.99*
3.18	1.44*
3.54	1.67
4.27	1.82
5.13	2.25
5.72	2.42

U= 3.55

$V_o t/b_o$	s/b_o
2.46	0.68*
2.79	1.24*
3.06	1.55
3.43	1.60
3.89	1.79
4.26	1.86
4.77	2.06
5.18	2.25
5.64	2.41

U= 3.60

$V_o t/b_o$	s/b_o
2.48	0.88*
3.13	1.35*
3.88	1.55
4.44	2.00
5.00	2.35
5.79	2.47

U= 4.00

$V_o t/b_o$	s/b_o
2.34	0.52*
2.65	1.11*
3.17	1.59
3.68	1.70
3.89	2.00
4.31	2.19
4.72	2.41
5.24	2.57
5.76	2.68
6.33	2.94

* CORRESPONDS TO STRIATION MODE

DELTA-2R d_o/b_o- 4.0 B- 5.02

α-10° V_o/U- 0.0400 b_o- 3.700

U- 3.59		U- 3.59	
$V_o t/b_o$	s/b_o	$V_o t/b_o$	s/b_o
3.91	0.87*	4.01	0.84*
4.38	1.33*	4.47	1.41*
4.84	1.66	4.84	1.65
5.31	1.77	5.31	1.80
5.73	1.98	5.77	2.04
6.19	2.15	6.19	2.17
6.61	2.52	6.71	2.40
7.08	2.63	7.17	2.57
		7.64	2.69

* CORRESPONDS TO STRIATION MODE

DELTA-2R d_o/b_o- 5.0 B- 5.02

α-10° V_o/U- 0.0400 b_o- 3.700

U- 3.59		U- 3.52		U- 3.55	
$V_o t/b_o$	s/b_o	$V_o t/b_o$	s/b_o	$V_o t/b_o$	s/b_o
5.82	0.99*	4.89	0.66*	5.11	0.66*
6.01	1.27*	5.16	0.99*	5.11	0.83*
6.47	1.82	5.89	1.77	5.48	1.38*
6.94	2.19	6.26	1.88	6.22	1.77
8.15	2.54	6.99	2.04	6.49	1.99
8.71	2.93	6.62	1.93	6.95	2.13
		7.40	2.26	7.46	2.32
		7.72	2.54	7.93	2.62
				8.70	2.76

* CORRESPONDS TO STRIATION MODE

DELTA-2R d_o/b_o= 6.0 B= 5.02'

α=10° V_o/U= 0.0400 b_o= 3.700'

U= 3.52

$V_o t/b_o$	s/b_o
6.31	0.77*
6.68	1.09*
7.51	1.43*
7.92	1.55
8.20	1.67
8.98	1.82
8.61	1.76
9.40	1.87
10.41	2.25
11.01	2.41

U= 3.55

$V_o t/b_o$	s/b_o
7.18	1.39*
7.55	1.50*
7.83	1.66
8.24	1.73
9.12	2.01
9.58	2.14
9.95	2.32
10.32	2.46

U= 3.55

$V_o t/b_o$	s/b_o
6.36	1.28*
6.82	1.80
7.28	1.87
7.74	1.92
8.20	2.12
8.66	2.27
9.03	2.41
9.49	2.63

U= 3.55

$V_o t/b_o$	s/b_o
6.49	0.73*
6.86	0.98*
7.46	1.47*
7.92	1.92
8.06	2.01
8.43	2.25
8.89	2.44
9.26	2.46
9.63	2.67
10.22	2.83
10.64	2.97

* CORRESPONDS TO STRIATION MODE

DELTA-2S d_o/b_o- 2.0 B- 5.02

α-10° V_o/U- 0.0330 b_o- 3.700

U- 4.06		U- 4.06		U- 4.06	
$V_o t/b_o$	s/b_o	$V_o t/b_o$	s/b_o	$V_o t/b_o$	s/b_o
1.74	0.68*	1.17	0.63*	1.30	0.87*
1.78	0.86*	1.61	1.17*	1.74	1.39*
2.17	1.57	1.87	1.47*	1.91	1.59
2.65	1.63	2.31	1.71	2.52	1.62
3.18	1.86	2.74	1.77	2.78	1.83
3.48	2.10	2.91	1.83	3.13	2.08
3.83	2.28	3.18	2.01	3.48	2.13
4.13	2.33	3.52	2.25	3.83	2.37
4.87	2.63	4.22	2.53	4.09	2.55
				4.44	2.61

* CORRESPONDS TO STRIATION MODE

DELTA-2S d_o/b_o= 3.0 B= 5.02

α=10° V_o/U= 0.0330 b_o= 3.700

U= 4.06		U= 4.06	
$V_o t/b_o$	s/b_o	$V_o t/b_o$	s/b_o
2.61	0.82*	2.35	0.68*
3.00	1.57	2.52	0.04*
3.44	1.63	3.57	1.68
3.87	1.77	3.31	1.51
4.05	1.98	4.39	1.98
4.74	2.28	4.52	2.04
5.22	2.45	5.26	2.39
5.83	2.57	5.79	2.45
6.05	2.69	6.26	2.69
		6.70	2.81

* CORRESPONDS TO STRIATION MODE

DELTA-2S d_o/b_o- 4.0 B- 5.02

α-10° V_o/U- 0.0330 b_o- 3.700

U- 4.06		U- 4.06	
$V_o t/b_o$	s/b_o	$V_o t/b_o$	s/b_o
3.18	0.78*	3.44	0.47*
3.35	0.98*	3.78	0.81*
3.78	1.31*	4.00	0.98*
4.05	1.37*	4.35	1.37*
4.57	1.70	4.65	1.69
4.83	1.76	4.96	1.81
5.52	2.23	5.22	1.93
5.87	2.37	5.83	2.32
6.13	2.48	6.09	2.37
6.48	2.65	6.70	2.60
		6.96	2.68
		7.31	2.71

* CORRESPONDS TO STRIATION MODE

DELTA-2S d_o/b_o- 5.0 B- 5.02

α-10° V_o/U- 0.0330 b_o- 3.700

U- 3.51		U- 3.55	
$V_o t/b_o$	s/b_o	$V_o t/b_o$	s/b_o
4.81	0.68*	5.05	0.85*
5.11	0.76*	5.28	1.12*
5.37	1.01*	5.59	1.39*
5.68	1.28*	5.85	1.72
5.94	1.34*	6.12	1.94
6.20	1.45*	6.38	2.10
6.73	1.61	6.65	2.21
6.88	1.66	6.92	2.26
7.07	1.77	7.18	2.37
7.29	1.81	7.45	2.54
7.55	1.94	7.71	2.59
		8.05	2.65

* CORRESPONDS TO STRIATION MODE

RP2 d_o/b_o= 2.0 B= 4.50

α=12° V_o/U= 0.0285 b_o= 3.534

U= 3.63

$V_o t/b_o$	s/b_o
1.12	0.74*
1.37	0.87*
1.62	1.38*
1.90	1.58
2.18	1.64
2.53	1.77
2.88	2.03
2.95	2.21
3.23	2.39
3.48	2.48
4.00	2.67
3.97	2.67

U= 3.67

$V_o t/b_o$	s/b_o
1.38	0.71*
1.74	1.19*
2.10	1.64
2.45	1.77
2.81	1.83
3.09	2.03
3.52	2.22
3.80	2.41
4.26	2.48
4.62	2.60

U= 3.55

$V_o t/b_o$	s/b_o
1.45	0.60*
1.78	1.12*
2.05	1.37*
2.68	1.60
3.01	1.99
3.55	2.09
3.97	2.36

U= 3.55

$V_o t/b_o$	s/b_o
0.97	0.72*
1.25	0.94*
1.75	1.36*
2.20	1.50*
2.63	1.79
3.04	1.98
3.25	2.12
3.61	2.39
3.91	2.54
4.14	2.65

U= 3.55

$V_o t/b_o$	s/b_o
1.26	0.77*
1.50	0.94*
1.79	1.25*
2.03	1.31*
2.27	1.45*
2.54	1.62
2.81	1.76
3.08	1.86
3.29	2.00
3.56	2.12

* CORRESPONDS TO STRIATION MODE

RP2 d_o/b_o = 3.0 B = 4.50

$\alpha = 12^o$ V_o/U = 0.0285 b_o = 3.534

U = 3.63

$V_o t/b_o$	s/b_o
2.21	0.91 *
2.35	0.84 *
2.63	0.91 *
2.92	1.16 *
3.20	1.66
3.41	1.72
3.69	1.85
3.97	1.97
4.25	2.15
4.46	2.22
4.74	2.47
5.02	2.59
5.37	2.66

U = 3.63

$V_o t/b_o$	s/b_o
2.07	0.52 *
2.42	0.78 *
2.60	0.88 *
2.99	1.16 *
3.13	1.60
3.41	1.75
3.69	1.85
4.32	2.10
4.53	2.22
4.81	2.35
5.09	2.50
5.45	2.72

U = 3.60

$V_o t/b_o$	s/b_o
2.65	0.79 *
3.21	1.41 *
3.80	1.76
3.87	1.80
4.46	2.09
4.60	2.26
4.95	2.42

U = 3.60

$V_o t/b_o$	s/b_o
2.96	1.35 *
3.38	1.62
3.55	1.71
4.29	2.09
4.98	2.26
5.12	2.39

U = 3.99

$V_o t/b_o$	s/b_o
3.40	1.49 *
3.82	1.74
4.09	1.80
4.83	2.14
5.10	2.26
5.48	2.42
5.52	2.48

* CORRESPONDS TO STRIATION MODE

RP2 d_o/b_o= 4.0 B= 4.50

$\alpha = 12^o$ V_o/U= 0.0285 b_o= 3.534

U= 3.63

$V_o t/b_o$	s/b_o
3.37	0.69*
3.65	0.72*
3.93	0.84*
4.36	1.44*
4.92	1.77
4.71	1.68
5.23	1.95
5.41	2.01
5.97	2.19
6.39	2.38
6.74	2.62
6.92	2.74

U= 3.61

$V_o t/b_o$	s/b_o
3.70	0.75*
4.05	1.17*
4.30	1.47*
4.54	1.65
4.82	1.71
5.10	1.83
5.59	2.07
5.80	2.13
6.15	2.31
6.50	2.56
6.64	2.62
6.85	2.74

U= 3.55

$V_o t/b_o$	s/b_o
3.50	0.85*
4.03	1.07*
4.30	1.49*
4.57	1.54
4.78	1.65
5.05	1.81
5.26	2.03
5.53	2.19
5.77	2.24
6.16	2.39
6.28	2.48

U= 3.55

$V_o t/b_o$	s/b_o
3.00	0.69*
3.45	0.83*
3.69	0.96*
3.93	1.36*
4.20	1.47*
4.23	1.54
4.50	1.64
4.86	1.75
5.33	1.97
5.46	2.14
5.84	2.24
6.23	2.42

* CORRESPONDS TO STRIATION MODE

RP2 d_o/b_o = 5.0 B = 4.50

$\alpha = 12^\circ$ V_o/U = 0.0285 b_o = 3.534

U = 3.63

$V_o t/b_o$	s/b_o
4.71	0.73*
4.85	0.79*
5.13	1.03*
5.41	1.44*
5.69	1.50*
6.15	1.79
6.29	1.79
6.53	1.91
6.82	1.97
7.10	2.20
7.31	2.26
7.66	2.44
7.87	2.50

U = 3.61

$V_o t/b_o$	s/b_o
4.51	0.79*
4.79	0.91*
5.07	0.97*
5.35	1.03*
5.56	1.62
5.83	1.85
6.11	1.97
6.60	2.08
6.88	2.26
7.16	2.32
7.44	2.50
7.65	2.61
7.93	2.67
8.21	2.79

U = 3.63

$V_o t/b_o$	s/b_o
3.86	0.80*
4.41	1.08*
4.96	1.12*
5.11	1.36*
5.39	1.71
6.19	2.01
6.70	2.16

U = 3.60

$V_o t/b_o$	s/b_o
4.28	0.60*
4.34	0.65*
4.73	0.95*
5.04	1.02*
5.22	1.48*
5.41	1.51
5.77	1.79
5.86	1.86
6.28	1.99
6.40	2.09
6.83	2.21
7.04	2.31

U = 3.60

$V_o t/b_o$	s/b_o
4.13	0.70*
4.56	0.78*
4.71	1.02*
4.92	1.10*
5.32	1.47*
5.52	1.51
5.83	1.69
5.95	1.81
6.38	1.93
6.68	1.95
6.83	2.26
6.89	2.26

* CORRESPONDS TO STRIATION MODE

RP2 d_o/b_o= 6.0 B= 4.50'

α=12° V_o/U= 0.0285 b_o= 3.534'

U= 3.99

$V_o t/b_o$	s/b_o
5.08	0.77*
5.29	1.03*
5.99	1.41*
6.33	1.79
6.43	1.92
6.73	2.06
6.97	2.16
7.24	2.25
7.51	2.34
7.81	2.48

* CORRESPONDS TO STRIATION MODE

INITIAL DISTRIBUTION LIST

	No. Copies
Dr. Arthur J. Bruckheim DARPA/TTO 1400 Wilson Blvd. Arlington, VA 22209	2
Chief of Naval Operations OP-95T, Room 5D616 The Pentagon Washington, DC 20350	
Attn: Dr. Jack Breedlove	1
Attn: Dr. A. Andreassen	1
Commander Department of the Navy Strategic Systems Project Office Washington, DC 20376	
Attn: Dr. Philip Selwyn (SP2023)	1
Chief of Naval Operations OP-021, Room 4D544 The Pentagon Washington, DC 20350	
Attn: Dr. Ed Harper	1
Dr. Irwin E. Alber Arete Associates P.O. Box 350 Encino, CA 91316	1
Dr. Steve Crow Poseidon Research 1299 Ocean Avenue Suite 821 Santa Monica, CA 90401	1
Dr. Wasyl Wasylkiwskyj Physical Dynamics, Inc. Suite 1620 1300 N. 17th Street Arlington, VA 22209	1
Dr. Richard Hoglund ORI, Inc. 1400 Spring Street Silver Spring, MD 70910	1

Dr. Denny Ko
Dynamics Technology, Inc.
22939 Hawthorne Blvd.
Suite 200
Torrance, CA 90505 — 1

Dr. C. D. Donaldson
Aeronautical Research Associates of Princeton, Inc.
1800 Old Meadow Road
Suite 114
McLean, VA 22102 — 1

Applied Physics Laboratory
The John Hopkins University
Johns Hopkins Road
Laurel, MD 20810
Attn: Dr. L. Crawford — 1
Attn: Dr. H. Gilreath — 1
Attn: Dr. G. Merritt — 1
Attn: Dr. Gary Smith — 1
Attn: Dr. Tom Taylor — 1
Attn: Dr. D. Wenstrand — 1

Dr. Dennis Holliday
R&D Associates
4640 Admiralty Way
Marina del Rey, CA 90291 — 1

Dr. Don LeVine
JASON Program Office
The MITRE Corporation
1820 Dolley Madison Blvd.
McLean, VA 22102 — 1

Flow Research
21414 68th Ave. South
Kent, WA 98031
Attn: Peter Liu — 1

Continuum Dynamics
P. O. Box 3073
32 Nassau St.
Princeton, NJ 08540
Attn: Alan Bilanin — 1

Defense Technical Information Center
Attn: DTK-DDA-2
Building 5
Cameron Station
Alexandria, VA 22314 — 2

Dr. Thomas Taylor 1
Applied Physics Laboratory
The John Hopkins University
Johns Hopkins Road
Laurel, MD 20810

Dr. Bruce Lake 1
TRW Space & Technology Group
R-1/1008
1 Space Park
Redondo Beach, CA 90278

Dr. Robert Shuchman 1
Environmental Research Institute
of Michigan
P. O. Box 8618
Ann Arbor, Michigan 48107

Dr. T. Sarpkaya 10
Code 69SL
Mechanical Engineering
Naval Postgraduate School
Monterey, CA 93943

Office of Research Administration 1
Code 012A
Naval Postgraduate School
Monterey, CA 93943

Library, Code 0142 4
Naval Postgraduate School
Monterey, CA 93943

Chairman, Mechanical Engineering 1
Code 69
Naval Postgraduate School
Monterey, CA 93943